CENTRO DE INVESTIGACIÓN Y ESTUDIOS AVANZADOS DEL INSTITUTO POLITÉCNICO NACIONAL

UNIDAD ZACATENCO
DEPARTAMENTO DE CONTROL AUTOMÁTICO

Seguimiento robusto como optimización utilizando la versión de subgradiente promedio del método de modo deslizante integral

Tesis que Presenta

Alejandra Hernandez Sanchez

Para obtener el grado de
Doctorado en Ciencias

En la especialidad de
Control Automático

Director de tesis:

Dr. Alexander Pozniak

Ciudad de México Septiembre del 2022

CENTRO DE INVESTIGACIÓN Y ESTUDIOS AVANZADOS DEL INSTITUTO POLITÉCNICO NACIONAL

UNIDAD ZACATENCO
DEPARTAMENTO DE CONTROL AUTOMÁTICO

Robust Tracking as Optimization Using Averaged Subgradient Version of Integral Sliding Mode Method

Thesis presented by

Alejandra Hernandez Sanchez

To obtain the degree of

Doctorate of science

In the speciality

Automatic control

Thesis director:

Dr. Alexander Pozniak

Ciudad de México Septiembre del 2022

Acknowledgment

"Genius is often synonymous with perseverance"

- Thomas Alva Edison

Thanks, mom, for everything. Thanks for all the lessons and for always being by my side. Thanks for always taking care of me. Thank you for all the love, dedication, time and effort you put into me. Thank you that despite everything, you are by my side, and you never leave me alone. Thank you for being my mom and for all your love. I love you. Dad, I have no words to thank you all my life because thanks to you, I had by my side the most valuable thing I could have. Thank you for giving me all the possible tools that have opened many doors for me. Thank you for teaching me by example what it is to love and responsibility. Thank you for loving me so much and caring for me in bad times. Thank you for being my hero, and thank you for not leaving me alone. I love you, dad.

Thanks to my family and all of them who were always by my side and never left me through the good, the bad and the worst, who were in my darkest moments. Thanks for encouraging me to continue and get up. Thanks to the love of my loves, who takes care of and pampers me, is by my side with all his affection and love and is with me even seeing my worst side. Thanks to my sun that illuminates my darkest moments, that is always to my side and changes my day with many laughs. To my crazy man, without him, the master's degree and the doctorate would not have been the same: he has guided and fed me many times, he did not leave me alone in my ugliest moment, and he is always there for me with his big hugs. To all I have met along the way, thank you for the laughs, the help, the good talks and the excellent food. From heart, thank you.

To Dr. Alexander Poznyak for giving me a hand in my worst moments for guiding and encouraging me. Thanks for all your support and understanding. Thank you for everything you have taught me. Thank you for the trust placed in me. It is a great example for me.

To Dr. Isaac Chairez for helping me. Thank you for considering me not only for the work done but also for other projects. Thank you for always solving all my doubts and for your patience and your pleasure in teaching. Thank you for guiding me on the path of an investigator and teaching me that research does not remain in theory. Thank you for your example as a researcher and especially as a teacher.

To the Centro de Investigación y Estudios Avanzados del Instituto Politécnico Nacional, for all the facilities, supports and education during my doctorate.

Thanks to my friends in Russia and the virtual reality team at the Lomonosov Institute in Moscow, Russia. For receiving me in your country, letting me get to know you, welcoming me with open arms, and allowing me to have the experience of working with you. Thanks for the talks and laughs and especially for the food and beer. Спасибо от души.

To the CONACyT, for the scholarship awarded (CVU 789283) to be able to carry out my doctoral studies.

Abstract

Unmanned vehicles are robotic devices that have increased interest due to the significant number of applications they may have. The potential applications of unmanned vehicles include commercial, industrial, and military areas. These vehicles are of different kinds depending the task to that must be done and easily adaptable to different environments, operating conditions and working tasks. These vehicles are relevant because they could be used to carry out tasks in places of difficult access or a risk to human life.

The efficient management of these devices requires the design of controllers under conditions of uncertainties, which include perturbations, variations in the parameters, and modelling errors. Using a mathematical model generalisation and unknown working conditions implies the necessity of robust formulations for the control designs. A possible situation with unmanned vehicles is the lack of continuous measures of all the states and variables; hence it may requires some complementary designs that can work with the state estimates. Additionally, the control design may require to consider certain optimal regimes with the aim of increasing the autonomous operation or reducing the power needed to complete the task. These characteristics seem to enforce a class of robust optimal control design. Usually, the solution at the same time to problems of robustness and optimisation is challenging.

Recent studies introduce the application of the integral sliding modes control to stabilise systems modelled by Lagrange equations. Based on this idea, this dissertation proposes to reformulate the tracking trajectory control problem for unmanned vehicles as an optimisation control design problem of a not strictly convex cost functional, that depends on the tracking trajectory error. This work proposes to solve the optimisation problem related to trajectory tracking using

the average subgradient algorithm and the integral sliding mode control technique. The primary objective is to solve the optimisation problem by giving a robust solution to the presence of external disturbances and modelling uncertainties. This work develops four solutions for solving the tracking trajectory problem: a state feedback form, a back-stepping formulation, an output feedback approach, and considering the optimisation of the integral of the tracking error.

The state feedback approach solves the problem of trajectory tracking optimisation for the general model of the unmanned vehicle. The employed control technique is an integral sliding mode control, where the integral sliding variable is a function of the tracking error, its derivative, and the average sub-gradient of the functional with respect to the tracking error. The formal proofs of the gains design of the controller and the optimal region are provided using the standard second method of stability of Lyapunov. In the corresponding chapter, numerical evaluations presented in the MATLAB/Simulink platform solve an unmanned quadrotor tracking trajectory problem with modelling uncertainties.

The approach based on the back-stepping method that solves the optimisation for the functional related to tracking problem is obtained by defining three sequential optimisation auxiliary problems. The design technique employed at each stage is the integral sliding mode control and the averaged subgradient with the corresponding integral sliding variable. This part of the thesis presents a general proof for designing the control actions at each stage using the standard second method of stability of Lyapunov. Also, the corresponding chapter presents the numerical evaluations to solve an unmanned underwater´s trajectory tracking problem with modelling uncertainties and perturbations.

The approach based on the output feedback method solves the problem of tracking trajectory optimisation for the case when just a part of the state can be measured. The design technique employed is the integral sliding mode control and the average subgradient with the estimated variable obtained with the application of the super-twisting differentiator. This part of the thesis presents a formal proof of the gains design of the controller provided using the standard second method of stability of Lyapunov. Numerical evaluations with MATLAB/Simulink platform are developed to illustrate the tracking trajectory solution of an unmanned submarine with modelling uncertainties.

The problem of trajectory tracking for the general model of the unmanned vehicle is reformulated as an optimisation problem of the integral of the tracking error and the tracking error. The approach is based on the back-stepping that may solves the optimisation for the functional related to the integral of the tracking error and defines three sequential optimisation auxiliary problems. The design technique employed at each stage is the integral sliding mode control and the averaged subgradient with the corresponding integral sliding variable which is redefined at each stage. This section of the thesis presents two general proofs for designing the control gains at each stage and the optimal region using the standard second method of stability of Lyapunov. Also, a numerical evaluation depicts the tracking trajectory of an underactuated unmanned submarine with modelling uncertainties.

The approach based on the back-stepping method solves the optimisation for the functional related to the integral of the tracking error of a terrestrial unmanned vehicle. The approach based on the back-stepping defines three sequential optimisation auxiliary problems. The design technique employed at each stage is the integral sliding mode control and the averaged subgradient with the corresponding integral sliding variable. This section presents numerical evaluations to solve an unmanned terrestrial trajectory tracking problem and results over a physical platform.

With the development of this thesis, an amount of 8 papers were published. One paper was published at an international congress conference. Seven papers were published in international journals. Also, an international stay at Lomonosov University Institute (Московский государственный университет имени М. В. Ломоносова - МГУ) was realized based on this thesis.

Resumen

Los vehículos no tripulados son dispositivos robóticos en los que se ha incrementado su interés debido a la importante cantidad de aplicaciones que pueden tener. Las aplicaciones potenciales de los vehículos no tripulados incluyen áreas comerciales, industriales y militares. Estos vehículos son de diferentes tipos dependiendo de la tarea que se deba realizar y fácilmente adaptables a diferentes entornos, condiciones de operación y tareas de trabajo. Estos vehículos son relevantes porque podrían ser utilizados para realizar tareas en lugares de difícil acceso o que impliquen un riesgo para la vida humana.

La gestión eficiente de estos dispositivos requiere el diseño de controladores en condiciones de incertidumbre, que incluyen perturbaciones, variaciones en los parámetros y errores de modelado. El uso de un modelo matemático generalizado y condiciones de trabajo desconocidas implica la necesidad de formulaciones robustas para los diseños de control. Una posible situación con los vehículos no tripulados es la falta de medidas continuas de todos los estados y variables; por lo tanto, puede requerir algunos diseños complementarios que puedan funcionar con las estimaciones de estado. Además, el diseño de control puede requerir considerar ciertos regímenes óptimas con el objetivo de aumentar la operación autónoma o reducir la potencia necesaria para completar la tarea. Estas características parecen imponer una clase de diseño de control óptimo robusto. Por lo general, la solución al mismo tiempo a los problemas de robustez y optimización es un desafío.

Estudios recientes introducen la aplicación del control integral de modos deslizantes para estabilizar sistemas modelados por ecuaciones de Lagrange. Partiendo de esta idea, esta tesis propone reformular el problema de control de trayectoria de seguimiento para vehículos no tripulados como un problema de diseño de control de optimización de un funcional de costo no estrictamente convexo, que depende del error de trayectoria de seguimiento. Este trabajo

propone resolver el problema de optimización relacionado con el seguimiento de la trayectoria utilizando el algoritmo de subgradiente medio y la técnica de control de modo deslizante integral. El objetivo principal es resolver el problema de optimización dando una solución robusta a la presencia de perturbaciones externas y modelizando incertidumbres. Este trabajo desarrolla cuatro soluciones para resolver el problema de la trayectoria de seguimiento: una formulación de retroalimentación de estado, una formulación de cascada, un enfoque de retroalimentación de salida, y considerando la optimización de la integral del error de seguimiento.

El enfoque de retroalimentación de estado resuelve el problema de la optimización del seguimiento de trayectoria para el modelo general del vehículo no tripulado. La técnica de control empleada es un control de modo de deslizamiento integral, donde la variable deslizante integral es una función del error de seguimiento, su derivada y el subgradiente promedio del funcional con respecto al error de seguimiento. Las pruebas formales del diseño de ganancias del controlador y la región óptima se proporcionan utilizando el segundo método estándar de estabilidad de Lyapunov. En el capítulo correspondiente, las evaluaciones numéricas presentadas en la plataforma MATLAB/Simulink resuelven el problema de trayectoria de seguimiento de un cuadrotor no tripulado con incertidumbres de modelado.

El enfoque basado en el método back-stepping resuelve la optimización para el problema funcional relacionado con el seguimiento de trayectoria, se obtiene definiendo tres problemas auxiliares de optimización secuencial. La técnica de diseño empleada en cada etapa es el control de modo de deslizamiento integral y el subgradiente promedio con la variable deslizante integral correspondiente. Esta parte de la tesis presenta una prueba general para diseñar las acciones de control en cada etapa utilizando el segundo método estándar de estabilidad de Lyapunov. Además, el capítulo correspondiente presenta las evaluaciones numéricas para resolver el problema de seguimiento de trayectoria de un submarino no tripulado con incertidumbres y perturbaciones de modelado.

El enfoque basado en el método de retroalimentación de salida resuelve el problema de la optimización de la trayectoria de seguimiento para el caso en que solo se puede medir una parte del estado. La técnica de diseño empleada es el control integral del modo de deslizamiento y el subgradiente promedio con la variable estimada obtenida con la aplicación del diferenciador

de super-twisting. Esta parte de la tesis presenta una prueba formal del diseño de ganancias del controlador proporcionado utilizando el segundo método estándar de estabilidad de Lyapunov. Se desarrollan evaluaciones numéricas con la plataforma MATLAB/Simulink para ilustrar la solución de seguimiento de la trayectoria de un submarino no tripulado con incertidumbres de modelado.

El problema del seguimiento de trayectoria para el modelo general del vehículo no tripulado se reformula como un problema de optimización de la integral del error de seguimiento y del mismo error de seguimiento. El enfoque se basa en el back-stepping que puede resolver la optimización para el funcional relacionado con la integral del error de seguimiento y define tres problemas auxiliares de optimización secuencial. La técnica de diseño empleada en cada etapa es el control de modo de deslizamiento integral y el subgradiente promediado con la variable deslizante integral correspondiente que se redefine en cada etapa. Esta sección de la tesis presenta dos pruebas generales para diseñar las ganancias de control en cada etapa y la región óptima utilizando el segundo método estándar de estabilidad de Lyapunov. Además, una evaluación numérica representa la trayectoria de seguimiento de un submarino no tripulado poco actuado con incertidumbres de modelado.

El enfoque basado en el método back-stepping resuelve la optimización para la funcional relacionada con la integral del error de seguimiento de un vehículo terrestre no tripulado. El enfoque basado en el back-stepping define tres problemas auxiliares de optimización secuencial. La técnica de diseño empleada en cada etapa es el control de modo de deslizamiento integral y el subgradiente promedio con la variable deslizante integral correspondiente. Esta sección presenta evaluaciones numéricas para resolver un problema de seguimiento de trayectoria terrestre no tripulado y resultados a través de una plataforma física.

Con el desarrollo de esta tesis, se publicaron una cantidad de 8 artículos. Un artículo fue publicado en una conferencia de congreso internacional. Siete artículos fueron publicados en revistas internacionales. Además, se realizó una estancia internacional en el Instituto Universitario Lomonosov (Московский государственный университет имени М. В. Ломоносова - МГУ) en base a esta tesis.

Contents

List of Figures

List of Tables

Chapter 1

Introduction

1.1 Unmanned Vehicles

Unmanned Vehicles (UV) are devices that can move in water, air or land; they have different designs, structures, sizes, and tools. Much writing exists on their designing, modelling and control [20, 42, 47]. UV's main objective is to realise tasks outside humans' limitations to simplify human life. Some of these activities that can develop include reconnaissance, surveillance, sampling, search, rescue, security reinforcement, and others. The realisation of some investigations is with the use of UV [13, 21, 39]. These activities are usually performed remotely through manual controls. One way to make these activities more efficient is by automating them.

To carry out the automation of the UV implies some aspects to consider. One of them is that the UV's working conditions are variable and unknown, implying disturbances of different natures and magnitudes. In consequence, the control design must be robust, not just to disturbances but also to modelling errors. Many works adopt highly simplified models in UV modelling that deteriorate the control's performance. In most cases, the robust solution implies the consumption of high amounts of energy. However, the critical aspect is the limited operation time by the fuel/battery life. Consequently, it implies the necessity of optimal solutions that realise the UV manipulation with a robust answer to disturbance but with less energy consumption.

Optimising UV with less consumption has been of interest in many kinds of research that

have proposed different solutions. One recent solution is proposed in [9] where the optimal tracking for a general class of nonlinear systems is tackled. This work uses recursive approximation theory with a sequence of linear quadratic problems; the problem with this kind of formulation requires linearisation of the model that, in most cases, implies losing the information of the dynamic and does not make the solution robust to external disturbances. Some proposals make the optimisation tracking robust to disturbances and uncertainties either through the use of information or the combination of techniques; an example is the proposed solution in [45] that uses previous data get in repetitions looks to compensate proactively recurring disturbances. However, most of the time, the force of nature cannot be anticipated, especially when the workspace is under uncertain conditions. An example of the combination of techniques is in the work [33], where it is proposed to implement a Lyapunov optimisation control with a trajectory-following optimisation technique; by solving the Hamilton–Jacobi–Bellman equation and the difficulty of solving this task is used a suboptimal solution for getting the optimisation.

1.2 Justification

The present investigation is directed at the trajectory tracking solution for UV by optimising a trajectory tracking functional through the average subgradient algorithm with a robust controller from the first instant. The reason for carrying out this research has to do with searching for optimal, easy and robust solutions for trajectory tracking with partial knowledge of the dynamic. The investigation in this research allows the development of formulations independent of the exact UV model, providing robust solutions from the first instant to modelling uncertainties, perturbations, and state estimations that can be applied to higher order systems. The research development seeks to show the qualities of implementing these controllers in different UV and compare the results obtained by the PID control. Furthermore, to validate the theory around this formulation by practical implementation.

1.3 Motivation

This research problem is significant because UVs are not only widely used devices for the simplification of human life but also for performing risky tasks or of difficult access. The resolution of problems around the displacement of UV allows extending the possibilities of use of these devices and the integration of Hardware more straightforward way. Implementing optimal robust controllers for trajectory tracking allows carrying out more complex trajectories without significant gains or drivers that damage the UV. It implies an efficient use of time and energy resources, helping develop more research and applications for these devices. Also, it will provide an optimal trajectory tracking solution for UV with structures that are difficult to model, whose dynamics are variable and partial knowledge of the state. Furthermore, obtain an optimal and robust response to disturbances, non-modelled dynamics, estimates and parameter variations from the first instant.

1.4 Objectives

Main objective: To solve the trajectory tracking problem for Unmanned Vehicles with partial knowledge of the dynamic by reformulating the tracking problem to an optimisation of the functional tracking trajectory using the Average Sub-gradient (ASG) algorithm by implementing the integral sliding mode control.

Secondary objectives

- To define an optimisation problem of a cost functional of the tracking error of Unmanned Vehicle.
- To design a State feedback technique implementing the ASG algorithm by Integral Sliding Mode control (ISMC) to optimise the position tracking error cost function.
- To design a Backstepping formulation implementing the ASG algorithm by ISMC for optimising the position tracking error cost function.

- To design an Output feedback technique implementing the ASG algorithm by ISMC for optimising the cost function of the position tracking error with the estimation of state by the super-twisting algorithm.
- To design a Backstepping formulation implementing the ASG algorithm by ISMC for optimising the cost function of the integral of the position tracking error.
- To obtain an illustration of the proposed solutions by using numerical evaluations and experimental whiled platform.

1.5 Study structure

Chapter 2 contains the model description of the UV by the Euler Lagrange equation and the actuators dynamic considering Permanent Magnet Direct Current (PMDC) motors. This part presents a model description of underwater, terrestrial, and quadrotor unmanned vehicles.

Chapter 3 encloses some theoretical frameworks for the ISMC bases. Also, some background around the Sub-gradient Descendent Method (SGDM) and some control techniques such as Back-stepping, State feedback and Output feedback are explained.

Chapter 4 presents the proposed solution for controlling the motion of UV by state feedback in combination with the ISM control using the application of the ASG of a cost function. The tracking trajectory problem is reformulated as optimising a functional tracking error. Some numerical evaluations are included to compare the performance of the proposed controller with a PD controller. The implementation is on the motion control of a Quadrotor in 3D space, optimising a cost function of the tracking error.

Given the structure of the UV model, the control motion solution can be on the Backstepping formulation in combination with the ISMC, proposed in Chapter 5, using the regular ASG to optimise a cost function. At the same time, a new guidance law by backstepping for an underwater vehicle is defined in the numerical results of this chapter for the displacement in the 3D space of an underwater UV presenting numerical evaluation by simulations in MATLAB for demonstrating the applicability of the control and its performance compared with a PID control.

Considering the case when a variable is unknown, Chapter 6 presents the development of two solutions for the control motion of UV using the output feedback approach. The first solution considers a specific variable unknown, and the second is for the case when part of the state is estimated. The proposed solution uses the technique of super twisting to estimate the missing variables. Also, numerical evaluation of the missing state case with the implementation of the proposed solution and a PID controller are included.

Chapter 7 presents the development of the proposed solution to the trajectory tracking problem for a UV. The problem is reformulated as an optimisation problem of a cost functional of the integral of the tracking error that is tackled with the backstepping approach considering the actuators' dynamic. Numerical evaluations of the proposed solution and the implementation of a PID control are also presented.

Chapter 8 presents the proposed solution for the control motion of a terrestrial UV using a back-stepping formulation with a state feedback control and the ISMC. The proposed solution and a PID controller are implemented in a numerical evaluation in the MATLAB/Simulink platform for comparison. Also, both controllers are implemented on a terrestrial device in different scenarios to force the UV position to the desired point and to compare the UV performance.

Concluding remarks and recommendations for future work are offered in Chapter 9.

Chapter 10 contains the stability analysis for the different control propositions in Chapters 4, 5, 6 and 7. It also presents the proof of the desired trajectory and zone of converges of some of these controls.

Chapter 2

Antecedents

An unmanned vehicle (UV) is a vehicle without people on board to control it, it can be remotely controlled or guided, or it can be autonomous depending on the sensors and characteristics. UV classification could be by the mission, autonomy, weight and distance they travel. For example, aerial UV can be classified as target, reconnaissance, combat, logistics, research, development, commercial and civil UAVs. The UV can be aquatic, aerial and terrestrial, designed for different tasks. The structural design of UV depends on the development task that modified the modelling considerations. The model description of these devices can be generalized. A general modelling description is in this chapter, and the same is for the motor actuators for the UV. Given the types of UV, a model description for each of these is given in the following chapter.

2.1 The model of Unmanned Vehicle

The description of the UV dynamics is by mechanical analysis based on two frameworks, the inertial (earth) frame $[a]$ and the body frame $[b]$, located at the centre of mass of the UV, as is shown in Figure (2.1).

The vector of generalized position represents the UV dynamics coordinates $\rho \in \mathbb{R}^6$, with reference to the frame $[a]$ and its corresponding velocity vector $\varphi \in \mathbb{R}^6$ with respect to the body

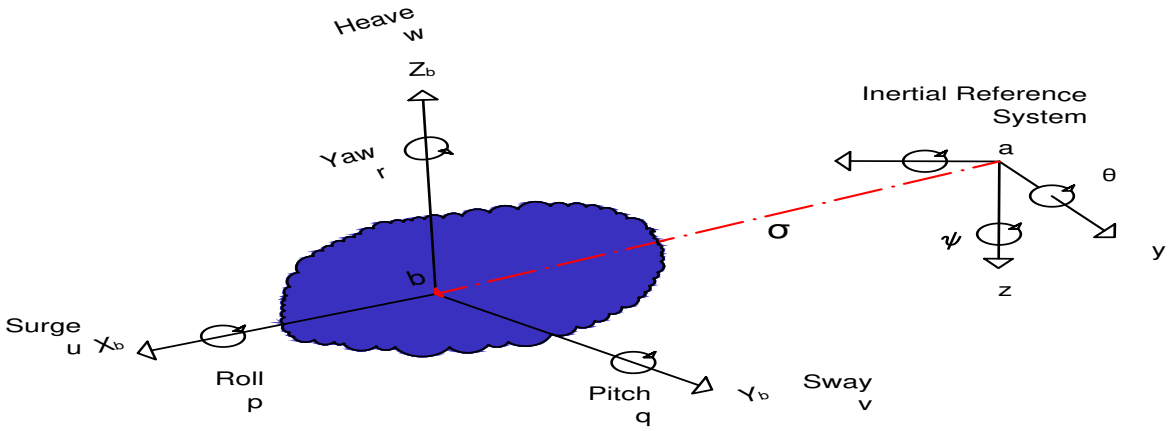

Figure 2.1: Unmanned Vehicle Frameworks

frame $[b]$. Then the position vector is given by

$$\rho = \begin{bmatrix} \rho_1^\top & \rho_2^\top \end{bmatrix}^\top, \tag{2.1}$$

where aggregates both translation $\rho_1 \in \mathbb{R}^3$, and orientation coordinates $\rho_2 \in \mathbb{R}^3$ to characterize the UV dynamics. The translational coordinates correspond to

$$\rho_1 = \begin{bmatrix} x & y & z \end{bmatrix}^\top \tag{2.2}$$

are the surge, sway and heave displacement, respectively. The orientation coordinates are given by the vector ρ_2 given by:

$$\rho_2 = \begin{bmatrix} \phi & \theta & \psi \end{bmatrix}^\top \tag{2.3}$$

are the roll angle ϕ $[rad]$, the pitch angle θ $[rad]$ and the yaw angle ψ $[rad]$. The generalized velocities vector is defined as

$$\varphi = \begin{bmatrix} \varphi_1^\top & \varphi_2^\top \end{bmatrix}^\top. \tag{2.4}$$

The translational velocity section corresponds to

$$\varphi_1 = \begin{bmatrix} u & v & w \end{bmatrix}^\top \tag{2.5}$$

where u, v, and w are the surge, sway and heave velocity, respectively. The angular velocities are described by:

$$\varphi_2 = \begin{bmatrix} p & q & r \end{bmatrix}^\top \tag{2.6}$$

where p, q and r are roll, pitch and yaw angular velocity respectively. Considering the UV as a rigid body and using the application of the Lagrange approach [17, 19, 26, 48] yield modelling the UV dynamic as follows:

$$\begin{aligned} \dot{\rho}_t &= J(\rho_t)\varphi_t \\ \mathbb{M}\dot{\varphi}_t &= F(\rho_t, \varphi_t) + G\mathbf{u}_t + \xi_t \end{aligned} \tag{2.7}$$

In the expression (2.7) the vector ρ_t, represents the time-dependent evolution of the vector ρ (that is $\rho_t = \rho(\mathbf{t})$). The kinematic modelling of UV uses Euler angles to relate the UV velocity with respect to the body frame $[b]$ in relation to the velocity in the inertial frame $[a]$. The model of UV is defined by the Jacobian $J : \mathbb{R}^6 \to \mathbb{R}^{6\times 6}$. The nonlinear (Jacobian) transformation J is defined as:

$$J(\rho_t) := \begin{bmatrix} R_b^a(\rho_t) & 0_{3\times 3} \\ 0_{3\times 3} & \mathbb{T}(\rho_t) \end{bmatrix} \tag{2.8}$$

where $R_b^a : \mathbb{R}^6 \to \mathbb{R}^{3\times 3}$ given by $R_b^a(\rho) = R_{z,\psi}R_{y,\theta}R_{x,\phi}$ defines the relative rotation matrix between the respective frame $[a]$ and $[b]$. The rotation is in the order of z, y and x with the corresponding angles ψ, θ and ϕ. The complementary transformation $\mathbb{T}(\rho)$, $\mathbb{T} : \mathbb{R}^6 \to \mathbb{R}^{3\times 3}$ is defined depending of the UV and defines the homogeneous transformation for the angular velocity with respect to the body frame $[b]$ and inertial frame $[a]$.

The vector $F : \mathbb{R}^6 \times \mathbb{R}^6 \to \mathbb{R}^6$ describes the dynamic forces acting over the UV as damping, Coriolis, centrifugal, lift, buoyancy, drag and gravity, depending on the kind of UV and their specific characteristics. Matrix $\mathbb{M} : \mathbb{R}^6 \to \mathbb{R}^{6\times 6}$ defines the inertia relation for the UV dynamics. The participation of external forces and model uncertainties over the UV is considered as perturbations in the respectively dynamic and described by vector $\xi \in \mathbb{R}^6$. The matrix $G : \mathbb{R}^6 \to \mathbb{R}^{6\times m}$ characterizes the effect of the control input vector $\mathbf{u} \in \mathbb{R}^m$ over the systems dynamic.

2.1.1 Main assumptions for UV dynamic

Considering the following main assumptions to describe UV dynamics:

A. The full vector ρ_t is available (can be measured online) and φ_t can be available or can be estimated at any time $t \geq 0$. It is a common condition considering that the UV's position and orientation can be obtained online using inertia measurement devices.

B. The inertia matrix $\mathbb{M}$ is bounded $0 < \mathbf{m}^- \leq \|\mathbb{M}\| \leq \mathbf{m}^+ < \infty$ with known positive scalars $\mathbf{m}^-, \mathbf{m}^+$.

C. The admissible set of controllers $\mathbf{u}_t \in \mathbb{R}^m$ is a collection of all partially continuous vector functions, depending on the available data ρ_t and φ_t.

D. The uncertain component $F(\rho_t, \varphi_t)$ admits the following bound ($F_t^+ > 0$):

$$\left.\begin{array}{c} \|F(\rho_t, \varphi_t)\| \leq F^+, \\ F^+ = \gamma_0 + \gamma_1 \|\rho_t\| + \gamma_2 \|\varphi_t\| \\ \gamma_j > 0, \quad j = 0,1,2 \end{array}\right\} \tag{2.9}$$

E. External disturbances and modeling uncertainties are bounded, i.e.,

$$\|\xi_t\| \leq \gamma_\xi. \tag{2.10}$$

This class of perturbations are common in studies centred on designing robust controllers under the persistent effect of external perturbations and internal modelling imprecision.

2.2 Actuators dynamics

Some studies consider the dynamics of the actuators. The dynamic of actuators depends on the nature of the UV [8, 22, 24]. This study considers that UV actuators are by independent Permanent Magnet Direct Current (PMDC) motor, each of the actuators satisfies the following dynamics, described in [46]:

$$\begin{array}{c} \mathbf{u}_t = E_f D_f \mathbf{I}_t \\ \dot{\mathbf{I}}_t = Z_L^{-1} \left[-Z_R \mathbf{I}_t - B_f E_f^\top J(\rho_t) \varphi_t + \upsilon_t \right] \end{array} \tag{2.11}$$

where $\mathbf{I} \in \mathbb{R}^m$ is the vector of the armature currents, $E_f \in \mathbb{R}^{6\times m}$, $D_f \in \mathbb{R}^{m\times m}$ and $B_f \in \mathbb{R}^{m\times m}$ are the electromotive, direct-electromotive and back-electromotive forces constants matrices respectively, $Z_L \in \mathbb{R}^{m\times m}$ and $Z_R \in \mathbb{R}^{m\times m}$ are the armature inductance and resistant respectively which are positive matrices. And $\upsilon \in \mathbb{R}^m$ is the vector of armature voltages, which is considered as the control of the actuator system.

For this study, in the cases where is abording the actuator dynamic, it is considered that υ divided into two parts: a nominal control υ_n for compensating the participation of the armature resistant and the different proposed forward control υ_d, that is

$$\upsilon_t = \upsilon_{n,t} + \upsilon_{d,t}$$

with the nominal part of the control given by:

$$\upsilon_{n,t} = Z_R \mathbf{I}_t$$

The resulting dynamics of the actuator satisfy the following expression:

$$\begin{aligned} \mathbf{u}_t &= E_f D_f \mathbf{I}_t \\ \dot{\mathbf{I}}_t &= Z_L^{-1}\left[F_I(\rho_t, \varphi_t) + \upsilon_{d,t}\right]. \end{aligned} \tag{2.12}$$

The back electromotive force is described by:

$$F_I(\rho_t, \varphi_t) = -B_f E_f^\top J(\rho_t)\varphi_t.$$

2.2.1 Main assumptions of PMDC actuators

The main assumptions of the actuator dynamic are:

A. The full vector $\mathbf{I}_t$ is available (can be measured on-line) and $\dot{\mathbf{I}}_t$ can be estimated at any time $t \geq 0$.

B. The matrix Z_L is bounded according to $0 < \mathbf{z}^- \leq \left\|Z_L^{-1}\right\| \leq \mathbf{z}^+ < \infty$ with $\mathbf{z}^-$, $\mathbf{z}^+$ known positive scalars.

C. The admissible set of controllers $\upsilon_d \in \mathbb{R}^m$ is a collection of all partially continuous vector functions, depending on the available data $\mathbf{I}_t$ and $\dot{\mathbf{I}}_t$.

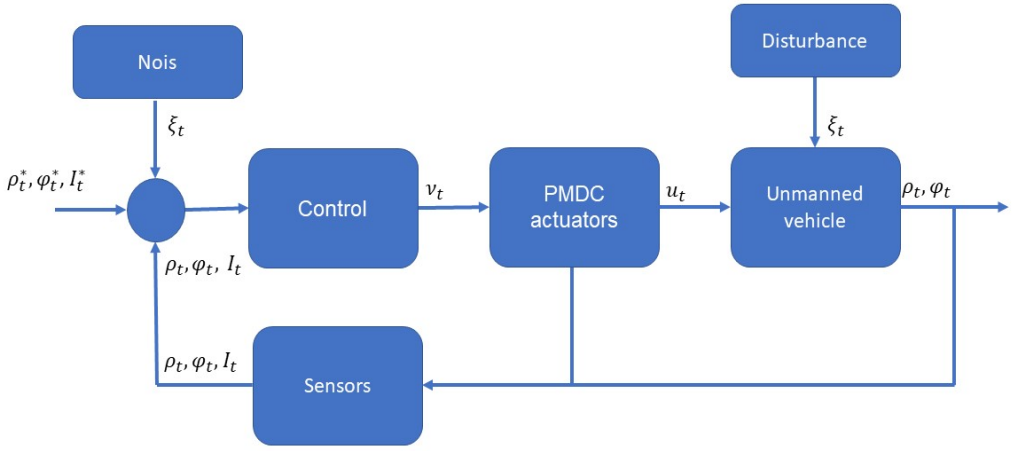

Figure 2.2: General diagram of UV

D. The uncertain component $F_I(\rho_t, \varphi_t)$ is bounded according to

$$\left.\begin{array}{c} \|F_I(\rho_t, \varphi_t)\| = F_I^+, \\ F_I^+ = \gamma_{I,0} + \gamma_{I,1}\|\rho_t\| + \gamma_{I,2}\|\varphi_t\| \\ \gamma_{I,j} > 0, \quad j = 0,1,2 \end{array}\right\}. \tag{2.13}$$

2.3 Complete dynamic (UV and PMDC actuators)

Considering the dynamics of the UV in the equation (2.7) and the model of the actuator in the expression (2.11), the complete (mobile system and actuator evolution) dynamic of the considered system is:

$$\left.\begin{array}{c} \dot{\rho}_t = J(\rho_t)\varphi_t \\ \dot{\varphi}_t = \mathbb{M}^{-1}\left[F(\rho_t, \varphi_t) + GE_f D_f \mathbf{I}_t + \xi_t\right] \\ \dot{\mathbf{I}}_t = Z_L^{-1}\left[F_I(\rho_t, \varphi_t) + \upsilon_{d,t}\right] \end{array}\right. . \tag{2.14}$$

Figure (2.2) illustrates the relation between the UV and actuators.

2.4 Different kinds of Unmanned vehicles

More specifically, a model can be given for UV according to their nature. The model of a submarine, quadrotor and land vehicle will be shown below. The specific models' election is because they are structures commonly used in various research works.

2.4.1 Underwater Unmanned Vehicle model

For the underwater UV, the components of the equation (2.7) are described in [18] and are given by:

$$\mathbb{M} = \begin{bmatrix} m_{3\times3} & 0_{3\times3} \\ 0_{3\times3} & I_0 \end{bmatrix}$$
$$F(\rho_t, \varphi_t) = -E(\varphi_t)\varphi_t - g(\rho_t)$$

where $m_{3\times3}$ is the matrix of mass and $I_0 \in \mathbb{R}^{3\times3}$, $I_0 > 0$ the matrix of moments of inertia, the forces acting over the UV consider the hydrodynamic forces and rigid body forces, that are:

$$E(\varphi_t) = C(\varphi_t) + D(\varphi_t)$$

and the forces over the underwater UV are subject to the following inequality

$$\|E(\varphi_t)\| \leq \lambda_E I_{6\times6}, \max_{i,k} \left\| \frac{d}{dt} E_{i,k}(\varphi_t) \right\| \leq E^+$$

with $0 < E^+ < +\infty$ and λ_E the maximum eigenvalue of $E(\varphi_t)$ uniformly in $t \geq 0$. Where Centrifugal and Coriolis forces are described by the matrix $C(\varphi_t) : \mathbb{R}^6 \to \mathbb{R}^{6\times6}$ and $D(\varphi_t) : \mathbb{R}^6 \to \mathbb{R}^{6\times6}$ describe the hydrodynamic damping forces. The description of the damping matrix

is given by

$$D(\varphi_t) = \begin{bmatrix} X_u & 0 & 0 & 0 & 0 & 0 \\ 0 & Y_v & 0 & 0 & 0 & Y_r \\ 0 & 0 & Z_w & 0 & Z_q & 0 \\ 0 & 0 & 0 & K_p & 0 & 0 \\ 0 & 0 & M_w & 0 & M_q & 0 \\ 0 & N_v & 0 & 0 & 0 & N_r \end{bmatrix} - \begin{bmatrix} X_{u|u|}|u| & 0 & 0 & 0 & 0 & 0 \\ 0 & Y_{v|v|}|v| & 0 & 0 & 0 & Y_{r|r|}|r| \\ 0 & 0 & Z_{w|w|}|w| & 0 & Z_{q|q|}|q| & 0 \\ 0 & 0 & 0 & K_{p|p|}|p| & 0 & 0 \\ 0 & 0 & M_{w|w|}|w| & 0 & M_{q|q|}|q| & 0 \\ 0 & N_{v|v|}|v| & 0 & 0 & 0 & N_{r|r|}|r| \end{bmatrix} \tag{2.15}$$

The last expression is negligible in low velocities.

The Coriolis and centripetal terms acting over the underwater UV are given by

$$C(\varphi_t) = \begin{bmatrix} 0_{3x3} & C_{12}(\varphi_t) \\ C_{21}(\varphi_t) & C_{22}(\varphi_t) \end{bmatrix} \tag{2.16}$$

where

$$C_{12}(\varphi_t) = \begin{bmatrix} mZ_G r_t & (m-Z_{\dot{w}})w_t & -(m-Y_{\dot{v}})v_t \\ -(m-Z_{\dot{w}})w_t & mZ_G r_t & (m-X_{\dot{u}})u_t \\ -mZ_G p_t + (m-Y_{\dot{v}})v_t & -mZ_G q_t - (m-X_{\dot{u}})u_t & 0 \end{bmatrix} \tag{2.17}$$

$$C_{21}(\varphi_t) = \begin{bmatrix} mZ_G r_t & (m-Z_{\dot{w}})w_t & mZ_G p_t - (m-Y_{\dot{v}})v_t \\ -(m-Z_{\dot{w}})w_t & mZ_G r_t & mZ_G q_t + (m-X_{\dot{u}})u_t \\ (m-Y_{\dot{v}})v_t & -(m-X_{\dot{u}})u_t & 0 \end{bmatrix} \tag{2.18}$$

$$C_{22}(\varphi_t) = \begin{bmatrix} 0 & (I_z-N_{\dot{r}})r_t & -(I_y-M_{\dot{q}})q_t \\ -(I_z-N_{\dot{r}})r_t & 0 & (I_x-K_{\dot{p}})p_t \\ (I_y-M_{\dot{q}})q_t & -(I_x-K_{\dot{p}})p_t & 0 \end{bmatrix} \tag{2.19}$$

The following expression gives the description of gravity and buoyancy over the UV

$$g(\rho_t) = \begin{bmatrix} \left(R_b^a\right)^{-1}(g_f + b_f) \\ \rho_g \times \left(R_b^a\right)^{-1} g_f + \rho_b \times \left(R_b^a\right)^{-1} b_f \end{bmatrix}.$$

Here $g_f \in \mathbb{R}^3$ is the vector force of gravity, $b_f \in \mathbb{R}^3$ is the vector force of buoyancy, described by the inertial frame, $\rho_g \in \mathbb{R}^3$ and $\rho_b \in \mathbb{R}^3$ are the position of the gravity and buoyancy centre with respect to the body frame. The control variables that participate in the dynamic are $u_u \in \mathbb{R}$, $u_q \in \mathbb{R}$ and $u_r \in \mathbb{R}$ which are the propeller velocity, horizontal fin inclination and vertical fin inclination. By defining the control vector as $\mathbf{u}_t = \begin{bmatrix} u_u & u_q & u_r \end{bmatrix}^\top$ and considering $G \in \mathbb{R}^{6\times 3}$, which is given by

$$G = \begin{bmatrix} 1 & 0 & 0 & 0 & 0 & 0 \\ 0 & 0 & 0 & 0 & 1 & 0 \\ 0 & 0 & 0 & 0 & 0 & 1 \end{bmatrix}^\top.$$

For simplicity most of the time in numerical simulations is considered a neutral buoyancy $\left(R_b^a\right)^{-1} g_f = -\left(R_b^a\right)^{-1} b_f$.

Some studies' considerations, such as taking $\phi = 0$ and slow velocities, in consequence, reduce the nonlinear dynamics of an underwater UV to a system of five degrees of freedom with a more simple dynamic. At first, the differential equation for the kinematic of the UV is

$$\begin{aligned} \dot{\rho}_{1,t} &= R_b^a(0, \theta_t, \psi_t)\, \varphi_{1,t}, \\ \begin{bmatrix} \dot{\theta}_t \\ \dot{\psi}_t \end{bmatrix} &= \begin{bmatrix} q_t \\ \dfrac{r_t}{c_\theta} \end{bmatrix}, \end{aligned} \tag{2.20}$$

where

$$R_b^a(0, \theta_t, \psi_t) = \begin{bmatrix} c_\theta c_\psi & -s_\psi & s_\theta c_\psi \\ c_\theta s_\psi & c_\psi & s_\theta s_\psi \\ -s_\theta & 0 & c_\theta \end{bmatrix}$$

where $s_\chi = \sin(\chi)$ and $c_\chi = \cos(\chi)$, $\theta \in \left(-\dfrac{\pi}{2}, \dfrac{\pi}{2}\right)$. The reduced dynamic of the underwater

UV is given by

$$\dot{\varphi}_{1,t} = \begin{bmatrix} -\frac{d_{11}}{m_{11}} & \frac{m_{22}}{m_{11}} r_t & -\frac{m_{33}}{m_{11}} q_t \\ -\frac{m_{11}}{m_{22}} r_t & -\frac{d_{22}}{m_{22}} & 0 \\ \frac{m_{11}}{m_{33}} q_t & 0 & -\frac{d_{33}}{m_{33}} \end{bmatrix} \varphi_{1,t} + \begin{bmatrix} \frac{1}{m_{11}} \mathbf{u}_{u,t} \\ 0 \\ 0 \end{bmatrix} \tag{2.21}$$

$$\begin{bmatrix} \dot{q}_t \\ \dot{r}_t \end{bmatrix} = \begin{bmatrix} \frac{m_{33} - m_{11}}{m_{55}} u_t w_t - \frac{d_{55}}{m_{55}} q_t - \frac{mghs_\theta}{m_{55}} + \frac{\mathbf{u}_{q,t}}{m_{55}} \\ \frac{m_{11} - m_{22}}{m_{66}} u_t v_t - \frac{d_{66}}{m_{66}} r_t + \frac{\mathbf{u}_{r,t}}{m_{66}} \end{bmatrix} \tag{2.22}$$

where $m_{ii} > 0$ corresponds to the mass and inertia moments of the underwater UV.

2.4.2 Quadrotor Unmanned Vehicle

The dynamic of the UV can be expressed by a differential equation of second order by a nonlinear transformation. Given the definition $\dot{\rho}$ in the kinematic UV in equation (2.7) and the nonlinear transformation matrix $J(\rho_t)$. One may justify that the following equations are valid

$$\begin{aligned} \dot{\rho}_t = J(\rho_t)\varphi_t &\iff \ddot{\rho}_t = J(\rho_t)\dot{\varphi}_t + \dot{J}(\rho_t)\varphi_t \\ \varphi_t = J(\rho_t)^{-1}\dot{\rho}_t &\iff \dot{\varphi}_t = J(\rho_t)^{-1}\left[\ddot{\rho}_t - \dot{J}(\rho_t)\varphi_t\right] \end{aligned} \tag{2.23}$$

So, by the last relations and taking variables of the dynamics of the system described in expression (2.7) as:

$$F(\rho_t, \varphi_t) := F_Q(\rho_t, \dot{\rho}_t)_{\dot{\rho}_t = J(\rho_t)\varphi_t}$$
$$G = G_Q$$

The components of the dynamic equation (2.7) following [4] are:

$$F(\rho_t, \varphi_t) = \begin{bmatrix} -mgE_z \\ -\mathbb{C}(\rho_t, \dot{\rho}_t)\dot{\rho}_t \end{bmatrix} \quad G = \begin{bmatrix} 0_{2\times 4} \\ I_{4\times 4} \end{bmatrix} \quad \mathbb{M} = \begin{bmatrix} mI_{3\times 3} & 0_{3\times 3} \\ 0_{3\times 3} & \mathbb{I}(\rho_t) \end{bmatrix}$$

In here, the inertia matrix $\mathbb{I}(\rho_t) \in \mathbb{R}^{3\times 3}$ is

$$\mathbb{I}(\rho_t) = \begin{bmatrix} \mathbb{I}_{11} & \mathbb{I}_{12} & \mathbb{I}_{13} \\ \mathbb{I}_{21} & \mathbb{I}_{22} & \mathbb{I}_{23} \\ \mathbb{I}_{31} & \mathbb{I}_{32} & \mathbb{I}_{33} \end{bmatrix}$$

The components of the inertia matrix are

$$\mathbb{I}_{11} = I_{xx}s_\theta^2 + I_{yy}c_\theta^2 s_\phi^2 + I_{zz}c_\theta^2 c_\phi^2 \qquad \mathbb{I}_{12} = \mathbb{I}_{21} = c_\theta c_\phi s_\phi \left(I_{yy} - I_{zz}\right)$$
$$\mathbb{I}_{22} = I_{yy}c_\phi^2 + I_{zz}s_\phi^2 \qquad \mathbb{I}_{13} = \mathbb{I}_{31} = -I_{zz}s_\theta$$
$$\mathbb{I}_{33} = I_{xx} \qquad \mathbb{I}_{23} = \mathbb{I}_{32} = 0$$

The inertia with respect the corresponding axes x, y, and z are I_{xx}, I_{yy} and I_{zz} respectively. In addition, $F \in \mathbb{R}^6$ represents the generalized force vector applied in the earth-fixed frame. For the Quadrotor the control vector $\mathbf{u} \in \mathbb{R}^4$, $\mathbf{u}_= \begin{bmatrix} \mathbf{u}_1 & \mathbf{u}_\psi & \mathbf{u}_\theta & \mathbf{u}_\phi \end{bmatrix}^\top$ with $u_1 = \sum_{k=1}^4 f_k$ (f_k is the thrust of each motor) is the total thrust along the Z axis, m is the vehicle mass, g is the gravity force and $E_z = [0,0,1]$ is an unitary vector. Between the forces that conforms F the Coriolis and Centripetal forces are also consider that are described by the matrix $\mathbb{C}(\rho_t, \dot{\rho}_t) \in \mathbb{R}^{3\times 3}$ satisfy the following expressions:

$$\mathbb{C}(\rho_t, \dot{\rho}_t) = \begin{bmatrix} C_{11} & C_{12} & C_{13} \\ C_{21} & C_{22} & C_{23} \\ C_{31} & C_{32} & C_{33} \end{bmatrix}$$

where

$$\begin{aligned}
C_{11} &= I_{xx}\dot{\theta}_t s_\theta c_\theta + I_{yy}\left(-\dot{\theta}_t s_\theta c_\theta s_\phi^2 + \dot{\phi}_t c_\theta^2 s_\phi c_\phi\right) - I_{zz}\left(\dot{\theta}_t s_\theta c_\theta c_\phi^2 + \dot{\phi}_t c_\theta^2 s_\phi c_\phi\right) \\
C_{12} &= I_{xx}\dot{\psi}_t s_\theta c_\theta - I_{yy}\left(\dot{\theta}_t s_\theta s_\phi c_\phi + \dot{\phi}_t c_\theta s_\phi^2 - \dot{\phi}_t c_\theta c_\phi^2 + \dot{\psi}_t s_\theta c_\theta s_\phi^2\right) \\
&+ I_{zz}\left(\dot{\phi}_t c_\theta s_\phi^2 - \dot{\phi}_t c_\theta c_\phi^2 - \dot{\psi}_t s_\theta c_\theta c_\phi^2 + \dot{\theta}_t s_\theta s_\phi c_\phi\right) \\
C_{13} &= -I_{xx}\dot{\theta}_t c_\theta + I_{yy}\dot{\psi}_t c_\theta^2 s_\phi c_\phi - I_{zz}\dot{\psi}_t c_\theta^2 s_\phi c_\phi \\
C_{21} &= -I_{xx}\dot{\psi}_t s_\theta c_\theta + i_{yy}\dot{\psi}_t s_\theta c_\theta s_\phi^2 + I_{zz}\dot{\psi}_t s_\theta c_\theta c^2\phi_t \\
C_{22} &= -I_{yy}\dot{\phi}_t s_\phi c_\phi + I_{zz}\dot{\phi}_t s_\phi c_\phi \\
C_{23} &= I_{xx}\dot{\psi}_t c_\theta + I_{yy}\left(-\dot{\theta}_t s_\phi c_\phi + \dot{\psi}_t c_\theta c_\phi^2 - \dot{\psi}_t c_\theta s_\phi^2\right) - I_{zz}\left(\dot{\psi}_t c_\theta s_\phi^2 - \dot{\psi}_t c_\theta c_\phi^2 + \dot{\theta}_t s_\phi c_\phi\right) \\
C_{31} &= -I_{yy}\dot{\psi}_t c_\theta^2 s_\phi c_\phi + I_{zz}\dot{\psi}_t c_\theta^2 s_\phi c_\phi \\
C_{32} &= -I_{xx}\dot{\psi}_t c_\theta + I_{yy}\left(\dot{\theta}_t s_\phi c_\phi + \dot{\psi}_t c_\theta s_\phi^2 - \dot{\psi}_t c_\theta c_\phi^2\right) - I_{zz}\left(\dot{\psi}_t c_\theta s_\phi^2 - \dot{\psi}_t c_\theta c_\theta^2 + \dot{\theta}_t s_\phi c_\phi\right) \\
C_{33} &= 0
\end{aligned}$$

Expressing the quadrotor UV dynamics in the equation (2.7) in a component form and omit-

ting the explicit dependence on time leads to

$$\ddot{x}_t = (c_\psi s_\theta c_\phi + s_\psi s_\phi)\frac{u_{1,t}}{m} - \frac{1}{2}C_x A \rho \dot{x}_t |\dot{x}_t| + \xi_{x,t} \tag{2.24}$$

$$\ddot{y}_t = (s_\psi s_\theta c_\phi - c_\psi s_\phi)\frac{u_{1,t}}{m} - \frac{1}{2}C_y A \rho \dot{y}_t |\dot{y}_t| + \xi_{y,t} \tag{2.25}$$

$$\ddot{z}_t = -g + (c_\theta c_\phi)\frac{u_{1,t}}{m} + \xi_{z,t} \tag{2.26}$$

$$\ddot{\phi}_t = \tilde{\tau}_{\phi,t} - mc_\phi(\rho_t, \dot{\rho}_t)\dot{\rho}_t + \xi_{\phi,t} \tag{2.27}$$

$$\ddot{\theta}_t = \tilde{\tau}_{\theta,t} - mc_\theta(\rho_t, \dot{\rho}_t)\dot{\rho}_t + \xi_{\theta,t} \tag{2.28}$$

$$\ddot{\psi}_t = \tilde{\tau}_{\theta,t} - mc_\psi(\rho_t, \dot{\rho}_t)\dot{\rho}_t + \xi_{\psi,t} \tag{2.29}$$

Here $mc_i(\rho, \dot{\rho}) \in \mathbb{R}^{1\times 3}$ is the i-th row of the matrix $\mathbb{I}(\rho)^{-1}\mathbb{C}(\rho, \dot{\rho}) \in \mathbb{R}^{3\times 3}$. The terms $-\frac{1}{2}C_x A\rho\dot{x}|\dot{x}|$ and $-\frac{1}{2}C_y A\rho\dot{y}|\dot{y}|$ are introduced in equations (2.24) and (2.25) to consider the effect of the drag forces in the X and Y axes, respectively. The perturbance vector $\xi = \begin{bmatrix} \xi_x & \xi_y & \xi_z & \xi_\phi & \xi_\theta & \xi_\psi \end{bmatrix}^\top$ consider the parameter uncertainties as well as the external disturbances (including wind gusts) that modify the performance of the studied quadrotor device.

2.5 Wheel Unmanned Vehicle

The position and orientation of a wheel UV can be described by the vector $\rho = \begin{bmatrix} X & Y & \theta \end{bmatrix}^\top$ with respect to the inertial frame work $[a]$. Where X and Y correspond to the coordinates in the horizontal plane, and the value for θ is the angle measured with respect to the horizontal axis, as is shown in Figure 2.3.

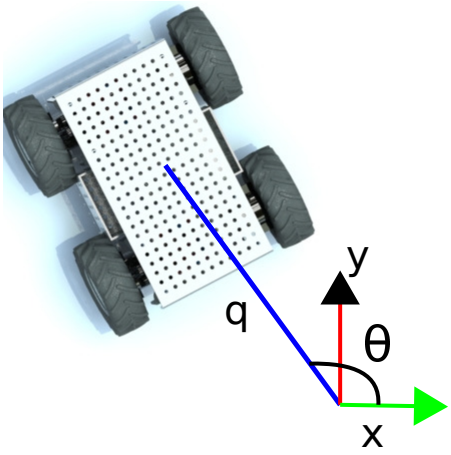

Figure 2.3: Inertial framework

The variables in the (2.7) are described in the article [7] and are given by :

$$\mathbb{M} = \begin{bmatrix} m & 0 & 0 \\ 0 & m & 0 \\ 0 & 0 & I \end{bmatrix}$$

$$F(\rho_t, \dot{\rho}_t) = \begin{bmatrix} R_x c_\theta - F_y s_\theta \\ R_x s_\theta - F_y c_\theta \\ M_r \end{bmatrix}$$

$$G(\rho) = \frac{1}{r} \begin{bmatrix} c_\theta & c_\theta \\ s_\theta & s_\theta \\ l & -l \end{bmatrix}$$

where m and I correspond to the mass and inertia, r is the radius of the wheels, l is the distance from the centre of mass to the sides, R_x is the total longitudinal resisting force, F_y is total lateral force and M_r is the resisting moment, and are given by:

$$R_x = f_r \frac{mg}{2} \left[sign\left(\dot{x}_{1,t}\right) + sign\left(\dot{x}_{2,t}\right) \right]$$

$$F_y = \kappa \frac{mg}{a+b} \left[sign\left(\dot{y}_{1,t}\right) + sign\left(\dot{y}_{3,t}\right) \right]$$

$$M_r = \kappa \frac{abmg}{a+b} \left[sign\left(\dot{y}_{1,t}\right) - sign\left(\dot{y}_{3,t}\right) \right] + f_r \frac{lmg}{2} \left[sign\left(\dot{x}_{2,t}\right) + sign\left(\dot{x}_{1,t}\right) \right]$$

where κ is the lateral friction coefficient, f_r is the coefficient of rolling resistance, g corresponds to the gravity, the letters a and b are the distance from the centre of mass to the front wheel and

the rear wheel, and x_i, y_i corresponds to the longitudinal and transversal displacement for i-wheel.

The vector $\xi \in \mathbb{R}^3$ describes the perturbations over the wheel UV dynamic and are subjects to:

$$\|\xi_t\| \leq \xi^+$$
$$\left\|\dot{\xi}_t\right\| \leq \dot{\xi}^+$$

The control vector $\mathbf{u} \in \mathbb{R}^2$ that is given by $\mathbf{u} = \begin{bmatrix} \mathbf{u}_1 & \mathbf{u}_2 \end{bmatrix}^\top$, where $\mathbf{u}_1$ and $\mathbf{u}_2$ the torque produced by the left and right side motors.

Considering a pseudo velocity left and right, the kinematic can be described as follow:

$$\dot{\rho}_t = S(\rho_t)\eta_t \tag{2.30}$$

where

$$S(\rho_t) = \begin{bmatrix} c_\theta & s_\theta & 0 \\ -s_\theta & c_\theta - \dfrac{1}{d_0} & \end{bmatrix}^\top$$

where d_0 is a restriction in the relation of $\dot{y}$ the velocity in the lateral displacement and the angular velocity $\dot{\theta}$ and is given by the expression

$$\dot{y}_t + d_0\dot{\theta}_t = 0 \tag{2.31}$$

that is an operative constraint with $0 < d_0 < a$. Considering the relation in equation (2.30) the complete dynamic can be expressed as:

$$\begin{aligned} \dot{\rho}_t &= S(\rho_t)\eta_t \\ \dot{\eta}_t &= \left(S^\top(\rho_t)\mathbb{M}S(\rho_t)\right)^{-1} S^\top(\rho_t)\left(G_C(\rho_t)\mathbf{u}_{n,t} - \mathbb{M}\dot{S}(\rho_t)\eta_t - F_C(\rho_t,\dot{\rho}_t) - \xi_t\right) \end{aligned} \tag{2.32}$$

To simplify the dynamic of the wheel UV, the control vector $\mathbf{u}$ is proposed as

$$\mathbf{u}_{n,t} = \left(S^\top G_C(\rho_t)\right)^{-1}(S^\top(\rho_t)\mathbb{M}\dot{S}(\rho_t)\eta_t + S^\top(\rho_t)F_C(\rho_t,\dot{\rho}_t) + S^\top(\rho_t)\mathbb{M}S(\rho_t)u_t) \tag{2.33}$$

in consequence, the dynamic is given by

$$\begin{aligned} \dot{\rho}_t &= S(\rho_t)\eta_t \\ \dot{\eta}_t &= u_t - \left(S^\top(\rho_t)\mathbb{M}S(\rho_t)\right)^{-1} S^\top(\rho_t)\xi_t \end{aligned} \tag{2.34}$$

For linearizing the dynamic, the auxiliary vector is defined:

$$z = \begin{bmatrix} X + d_0 c_\theta \\ Y + d_0 s_\theta \end{bmatrix}. \tag{2.35}$$

Also, the auxiliary variable is defined as

$$\begin{aligned} u_{1,t} &= \zeta_t \\ \dot{\zeta}_t &= v_{1,t} \\ u_{2,t} &= v_{2,t} \end{aligned}$$

Considering the dynamic expression in (2.32) the third time variation for variable z is expressed as:

$$\dddot{z}_t = A(\eta_t) + B(\eta_t)\mathbf{u}_t + C(\eta_t)\xi_t + D(\rho_t)\dot{\xi}_t$$

where

$$A(\eta_t) = \begin{bmatrix} -\dfrac{\eta_{1,t}\eta_{2,t}^2}{d_0^2}c_\theta + \dfrac{2}{d_0}\zeta_t\eta_{2,t}s_\theta \\ -\dfrac{\eta_{1,t}\eta_{2,t}^2}{d_0^2}s_\theta + \dfrac{2}{d_0}\zeta_t\eta_{2,t}c_\theta \end{bmatrix}, \; B(\eta_t) = \begin{bmatrix} c_\theta & \dfrac{\eta_{1,t}}{d_0}s_\theta \\ s_\theta & \dfrac{\eta_{1,t}}{d_0}c_\theta \end{bmatrix}$$

$$C(\eta_t) = \begin{bmatrix} C_{11} & C_{12} & C_{13} \\ c_{21} & c_{22} & c_{23} \end{bmatrix}$$

where the components of $C(\eta_t)$ are

$$\begin{aligned} C_{11} &= \left(\frac{\eta_{1,t}d_0 s_\theta}{md_0^2 + I} - \frac{2\eta_{2,t}c_\theta}{d_0 m} - \frac{c_\theta}{m}\right)s_\theta \\ C_{12} &= \left(-\frac{\eta_{1,t}d_0 c_\theta}{md_0^2 + I} - \frac{2\eta_{2,t}s_\theta}{d_0 m}\right)s_\theta + \frac{c_\theta^2}{m} \\ C_{13} &= -\frac{\eta_{1,t}}{md_0^2 + I}s_\theta \\ C_{21} &= \left(\frac{2\eta_{2,t}c_\theta}{d_0 m} - \frac{\eta_{1,t}d_0 s_\theta}{md_0^2 + I}\right)c_\theta + \frac{s_\theta^2}{m} \\ C_{22} &= \left(\frac{\eta_{1,t}d_0 c_\theta}{md_0^2 + I} + \frac{2\eta_{2,t}s_\theta}{d_0 m} - \frac{s_\theta}{m}\right)c_\theta \\ C_{23} &= -\frac{\eta_{1,t}}{md_0^2 + I}c_\theta \end{aligned}$$

$$D(\rho_t) = \frac{1}{m}\begin{bmatrix} c_\theta^2 & s_\theta c_\theta & 0 \\ c_\theta s_\theta & s_\theta^2 & 0 \end{bmatrix}$$

The auxiliary dynamic of z is summarized in :

$$\dot{z}_t = \begin{bmatrix} c_\theta \\ s_\theta \end{bmatrix} \eta_{1,t}$$
$$\ddot{z}_t = \begin{bmatrix} s_\theta \\ -c_\theta \end{bmatrix} \frac{\eta_{2,t}}{d_0}\eta_{1,t} + \begin{bmatrix} c_\theta \\ s_\theta \end{bmatrix} u_{1,t}$$
$$\dddot{z}_t = A(\eta_t) + B(\eta_t)\mathbf{u}_t + C(\eta_t)\xi_t + D(\rho_t)\dot{\xi}_t$$

Now defining the variables $z_1 = z$, $z_2 = \dot{z}$ and $z_3 = \ddot{z}$ the auxiliary dynamic of z can be expressed as:

$$\begin{aligned} \dot{z}_{1,t} &= z_{2,t} \\ \dot{z}_{2,t} &= z_{3,t} \\ \dot{z}_{3,t} &= A(\eta_t) + B(\eta_t)\mathbf{u}_t + C(\eta_t)\xi_t + D(\rho_t)\dot{\xi}_t \end{aligned} \tag{2.36}$$

Chapter 3

Fundamentals of Gradient Descendent Integral Sliding Mode Control

3.1 Sliding Mode

The Sliding Mode (SM) is all system with a discontinuous state function as control [54]. The SM control is considered as an on-off control [14, 40, 54, 57]. The SM control can be described as follows.

For system given by

$$\dot{x}_t = f(x_t, u_t, \zeta_t), \qquad x, \zeta \in \mathbb{R}^n, \;\; u \in \mathbb{R}^m \tag{3.1}$$

where $\|\zeta_t\| \leq \zeta^+$ with ζ^+ is a positive constant.

With the control of the form

$$u_t = -k_t sign(s_t) \tag{3.2}$$

where $s \in \mathbb{R}^m$ is denominated as the sliding variable and defined as

$$s_t = F_s(x_t) \tag{3.3}$$

where $F_s : \mathbb{R}^n \to \mathbb{R}^m$, and the gain k_t in most of the cases is denominated as a constant taking the control between extremum.

The control objective is to force the system dynamic to the switching line, that is, $s = 0$, by the use of the *sign* function defined as

$$sign(x) = \begin{cases} sign(x) = 1 & if \quad x > 0 \\ sign(x) \in [-1, 1] & if \quad x = 0 \\ sign(x) = -1 & if \quad x < 0 \end{cases} \tag{3.4}$$

the convergence to the switching line is in finite time $t_0 \geq t$. For the existence of SM, the sliding variable must to satisfies the following condition

$$s_t^\top \dot{s}_t < 0 \tag{3.5}$$

Given the form of the control, some remarkable advantages are easy implementation in the systems, high efficiency, convergence in finite time, applicability in linear and nonlinear systems, decoupled high dimensional design in independent sub-problems of low dimension and robust to disturbances and noise in measurements. Some of the features to consider are: high frequencies (chattering) that can affect the systems' hardware, high gains and the SM control is not robust in the reaching phase. Given the characteristics of this control exist a high level of research and publications around this.

Publications as for the mechanical problems like flexible bar [14]. For electromechanical systems such as DC motors, permanent magnet synchronous motors, induction motors, power converters, and robots [54]. Furthermore, for math problems such as the numerical solution of constrained ODEs, the real-time differentiation, and the problem of finding the zeroes of nonlinear algebraic systems [40].

3.2 Integral Sliding Mode

Given the existence of a reaching phase by SM controllers where the control needs high gains to be robust and to force the dynamic to the sliding surface, a technique denominated as Integral Sliding Mode was proposed to eliminate this disadvantage in the SM approach. Defined by Utkin as:

Definition 1. ***Integral Sliding Mode***

A sliding mode is said to be an integral sliding mode if it is motion equation is of the same order as the original system [54] (pg. 118).

The ISM consist of adding an extra degree of freedom by an integral term added to the sliding surface.

An affine system without perturbations described as

$$\dot{x}_t = f(x_t) + B(x_t)u_t \tag{3.6}$$

exist $u = u_0$ which stabilises the system. The close loop system is given by

$$\dot{x}_{0,t} = f(x_{0,t}) + B(x_{0,t})u_{0,t} \tag{3.7}$$

in an ideal case without perturbations. Considering perturbation by the vector Ξ in the dynamic of the system described in equation (3.6) the expression becomes in:

$$\dot{x}_t = f(x_t) + B(x_t)u_t + \Xi \tag{3.8}$$

The control problem is to find a control such that $x_t = x_{0,t}$ at the initial time $x_0 = x_{0,0}$. Adding a term to the control u_0 and defining a sliding manifold given by

$$s_t = s_0(x_t) + z_t \tag{3.9}$$

where $s_0(x)$ is a function of the states of the system that could be similar to the sliding variable defined for the SM. The term z introduce an integral to the sliding surface, defined in a form that the dynamic of the sliding surface s is $\dot{s} = 0$. The sliding dynamic is defined as

$$\dot{s}_t = \frac{\partial s_0(x_t)}{\partial x}\dot{x}_t + \dot{z}_t \tag{3.10}$$

$$= \frac{\partial s_0(x_t)}{\partial x}\left[f(x_t) + B(x_t)u_t + \Xi_t\right] + \dot{z}_t \tag{3.11}$$

considering $u = u_0 + u_1$ where u_1 is equivalent to the perturbations in the system $u_1 = B(x)^{-1}\Xi$ the dynamic can be defined as

$$\dot{s}_t = \frac{\partial s_0(x_t)}{\partial x}\left[f(x_t) + B(x_t)u_{0,t} + B(x_t)u_{1,t} + \Xi_t\right] + \dot{z}_t \tag{3.12}$$

$$= \frac{\partial s_0(x_t)}{\partial x}\left[f(x_t) + B(x_t)u_{0,t}\right] + \dot{z}_t \tag{3.13}$$

defining z as

$$\dot{z}_t = -\frac{\partial s_0(x_t)}{\partial x}\left[f(x_t) + B(x_t)u_{0,t}\right] \tag{3.14}$$

with initial conditions $z(0) = s_0(x(0))$ then the dynamic of the sliding surface satisfies $\dot{s}_0 = 0$ since $t = 0$ [1, 54, 55].

This approach has the advantages that the sliding regimen starts at the beginning of the process, makes the control robust to parameter variation, non-modelled dynamics and external disturbances for all t, and gives the system an extra degree of freedom.

The ISM has been applied to different devices: as for the controller of underwater UV using integral of the tracking error in the sliding surface as is shown in [27]. Also, in a small radio control helicopter, for reduction of the chattering generated by the control in [37]. Alternatively, in a power converter like in [52] where an ISM is applied in the hysteresis modulation with a double integral to alleviating the steady-state error.

3.3 Super twisting algorithm

In most cases, some derivatives are not available by measure. So a finite time exact differentiator based on the super twisting algorithm (a second-order sliding mode algorithm [30]) was introduced in [31]. The algorithm of super twisting [16] can be used in combination with a variable gain, as the proposed in [5, 11, 56] .

The estimation of the derivative for a variable χ_t is given by

$$\begin{aligned} \dot{\hat{\chi}}_t &= \hat{x}_{1,t} - \tilde{k}_t(\hat{x}_{2,t})\hat{x}_{2,t} \\ \dot{\hat{x}}_{1,t} &= \chi_t - \beta_\chi \operatorname{sign}(\hat{\chi}_t - \chi_t) \\ \hat{x}_{2,t} &= |\chi_t - \hat{\chi}_t|^{1/2}\operatorname{sign}(\hat{\chi}_t - \chi_t) \end{aligned} \tag{3.15}$$

with $\beta_\chi > 0$ and the variable gain described by:

$$\begin{gathered} \dot{\tilde{k}}_t(\hat{x}_{2,t}) = \rho_k \tilde{k}_t \operatorname{sign}(\Phi_t) - \bar{M}\left[\tilde{k}_t - k^+\right]_+ + \bar{M}\left[\chi_t - \tilde{k}_t\right]_+, \\ \Phi_t := \left|\left[\operatorname{sign}(\hat{x}_{2,t})\right]_{eq}\right| - \alpha_k, \quad \alpha_k \in (0,1), \\ \bar{M} > \rho_k k^+,\ k^+ > \sup_{t\geq 0}|\dot{\chi}_t|, \\ \rho_k > 0,\ \chi > 0. \end{gathered}$$

The convergence conditions and how to select the differentiator parameters can be analysed in [56].

This derivative has been used in other studies. As in [16] for a nonlinear system, multiple inputs and outputs are weakly observable, proposing a hierarchical observer for state estimation and reconstruction of unknown inputs. In [35] the super twisting algorithm modified with nonlinear gains is used for the state estimation of a particular type of aerobic bioreactor system with only the measure of dissolved oxygen. Furthermore, in [44] the state estimation of a second-order mechanical system in discrete time despite the fact that the presence of noise and parametric uncertainties is analysed.

3.4 The regular gradient descendent method

Define the optimization (minimization) of a smooth convex functional $H = H(\delta_t)$,
$H : \mathbb{R}^n \to \mathbb{R}^+$ given by:

$$H(\delta_t) \to \min_{u\mathbb{R}^m}.$$

A solution to the optimisation problem can be obtained by using the Sub-Gradient Descent (SGD) algorithm.:

$$\frac{d}{dt}\delta_t = -\kappa \partial H(\delta_t), \quad 0 < \kappa < +\infty,\ \kappa \in \mathbb{R}, \quad t \geq 0 \tag{3.16}$$

The initial conditions for δ_0 are known. The analysis of the optimization algorithm (3.16) for a strictly convex or not functional $H(\delta_t)$ is presented below.

3.4.1 C1: Strictly convex functions

If $H(\delta_t)$ is strictly convex, the following properties hold (considering that $\partial H = \nabla H$) for all $\delta_t \in \mathbb{R}^n$:

$$\left.\begin{array}{c} \delta_t^\top \nabla H(\delta_t) \geq \lambda \left\|\delta_t\right\|^2, \\ \left\|\nabla H(\delta_t)\right\|^2 \geq \lambda (H(\delta_t) - H^*), \quad \lambda > 0,\ \lambda \in \mathbb{R} \end{array}\right\} \tag{3.17}$$

where $H^* = H(\delta_t^*)$ with $\delta_t^* = \arg\min_{\delta_t \in \mathbb{R}^n} H(\delta_t)$ is a unique extreme point of H and, considering as the ideal case, it should be $\delta_t^* = 0$. Considering the properties of the functional (3.17), it can be proven that the argument and functional converge simultaneously to their optimal values and estimate the rate of convergence for the SGD algorithm (3.16).

1. **Argument convergence**: Consider the candidate Lyapunov function $V(\delta_t) = 0.5\,\|\delta_t\|^2$ (which is positive definite and radially unbounded). The derivative of V on the trajectories of (3.16), yields

$$\dot{V}(\delta_t) = \delta_t^\top \dot{\delta}_t = -\kappa \delta_t^\top \partial H(\delta_t). \tag{3.18}$$

   Given $\partial H = \nabla H$, the last expression leads to

$$\dot{V}(\delta_t) = -\kappa \delta_t^\top \nabla H(\delta_t). \tag{3.19}$$

   Using the first property in (3.17) results into $\dot{V}(\delta_t) \leq -\kappa\lambda\,\|\delta_t\|^2 = -2\kappa\lambda V(\delta_t)$, implying the argument's exponential convergence to the origin with the rate $e^{-2\kappa\lambda t}$, namely $V(\delta_t) \leq V(\delta_0)e^{-2\kappa\lambda t} \to 0$

2. **Functional convergence**: Consider the Lyapunov function $V_H(\delta_t) = H(\delta_t) - H^*$, $V_H > 0$, $V_H(\mathbf{0}) = 0$. The time derivative of V_H on the trajectories of the SGD-algorithm (3.16) leads to

$$\dot{V}_H(\delta_t) = \partial H(\delta_t)\dot{\delta}_t = -\kappa\,\|\partial H(\delta_t)\|^2. \tag{3.20}$$

   By the second property in (3.17), one gets $\dot{V}_H(\delta_t) \leq -\kappa\lambda(H(\delta_t) - H^*) = -\kappa\lambda V_H(\delta_t)$. In consequence, the functional converges exponentially to its optimal value with the rate $e^{-\kappa\lambda t}$, that is

$$H(\delta_t) - H^* \leq (H(\delta_0) - H^*)e^{-\kappa\lambda t} \underset{t\to\infty}{\to} 0.$$

3.4.2 C2: Non-strictly convex functions

For some classes of convex functions, the constant λ in (3.17) is equal to 0, i.e., $\lambda = 0$. Therefore, both inequalities (3.18) and (3.20) are trivially confirmed, providing the properties

$\dot{V}(\delta_t) \leq 0$ and $\dot{V}_H(\delta_t) \leq 0$, which guarantees only boundedness for δ_t and $H(\delta_t)$. Nevertheless, for general convex functional, the following inequality, Known as Jensen's inequality, is valid:

$$\delta_t^\top \partial H(\delta_t) \geq H(\delta_t) - H^*, \quad \delta_t \in \mathbb{R}^n. \tag{3.21}$$

Remark 1. *Consider $\tilde{\delta}_t$ as the averaged estimation of δ_t*

$$\tilde{\delta}_t = \frac{1}{t+\mu} \int_0^t \delta_\tau d\tau, \quad t > 0, \quad \tilde{\delta}_0 = 0, \quad \mu > 0. \tag{3.22}$$

With the application of the Jensen´s inequality (3.21)*, leads to the following upper bound for $H(\tilde{\delta}_t) - H^*$*

$$\left.\begin{aligned} H(\tilde{\delta}_t) - H^* &\leq \frac{1}{t+\mu} \int_0^t (H(\delta_\tau) - H^*)\, d\tau \\ &\leq \frac{1}{t+\mu} \int_0^t \delta_\tau^\top \partial H(\delta_\tau) d\tau \end{aligned}\right\}. \tag{3.23}$$

Taking $V_H(\delta_t) = H(\delta_t) - H^*$

$$\begin{aligned} H(\tilde{\delta}_t) - H^* &\leq -\frac{1}{\kappa(t+\mu)} \int_0^t \dot{V}(\delta_\tau) d\tau \\ &\leq \frac{1}{\kappa(t+\mu)} \left[H(\delta_0) - H^*\right]. \end{aligned}$$

The last inequality implies that if $t \to \infty$ then $H(\tilde{\delta}_t) \to H^*$. This functional convergence results in an averaged algorithm as described in the equation (3.16) *using the averaging strategy of the equation* (3.22)*.*

For the cases considered in this study, the average of the states is not an input in the UV dynamics, so this is not applicable in our study.

3.5 Automatic Feedback control

The automatic feedback control is considered to use a system's output in this one's input to shape the process's behaviour; this can be by state feedback and output feedback control.

3.5.1 State Feedback Control

The control by state feedback consists of designing a control such that the system's dynamic is a desired dynamic, using the system's output as a variable for the designed control.

Considering a system n dimensional with the state variable $x \in \mathbb{R}^n$, described by:

$$\dot{x}_t = F(x_t) + Bu_t \tag{3.24}$$

$$y_t = Cx_t + D \tag{3.25}$$

where $F(x) \in \mathbb{R}^n$ is a nonlinear function and $B \in \mathbb{R}^{n\times m}$ is a coefficient matrix that describe the relation of the state with the control $u \in \mathbb{R}^m$. The matrix $C \in \mathbb{R}^{l\times n}$ is a coefficient for relate the state with the measurable output and $D \in \mathbb{R}^l$ is a disturbance vector.

Assuming that the differential equation in (3.24) is stabilized to the origin $x = \mathbf{0}$ by the control function u in function of the state x (i.e. $u = u(x)$). The control problem is design a control function $u(x)$ such that $x \to 0$ as $t \to 0$ [12, 25, 43].

This control technique, in combination with other methods, has been studied extensively as in [50], where a delayed state feedback control is implemented in continuous linear systems with nonlinear perturbations and time delays in the measurements for the stability problem. Also, Ningsu Luo and Manuel de la Sen, in [34], study the robust stability of uncertain internally delayed systems by state feedback with SM control, which is proportional to the state and the delayed state, considering the sign of the sliding surface. In [23] is implemented, an adaptive Neuronal Network (NN) controller for the unknown second-order nonlinear discrete system, expressed in the non-strict feedback form for the tracking error where the NN approximates the unknown parts of the dynamic. The state feedback control has been implemented in different forms and devices for UV control. Huan-Yin Zhou, Kai-Zhou Liu and Xi-Sheng Feng implement a combination of state feedback and sliding mode controllers for tracking error in underwater UV using a relation between the state feedback control parameters and the coefficients of the switching surface in [58]. Benjamas Panomrattanarug, Kohji Higuchi and Felix Mora-Camino study the state feedback control, determined by the linear quadratic regulator, for trajectory tracking for Euler angles, considering the case when all the state is measurable and when the state is estimated by an observer in [38]. In [53] S. Thorel and B. d'Andreá Novel

implement a state feedback control in the form of PID after some linearisations for the control of displacement in a 3D space for a hybrid vehicle.

Chapter 4

State Feedback Realization of Averaged Subgradient Integral Sliding Mode Control

4.1 Chapter Introduction

One of the principal problems in the control of Unmanned Vehicles (UV) is that they are of different characteristics and forms. Moreover, it is not easy to get a complete UV model. Therefore, for compensating the modelling errors, no knowledge of parameters, perturbations and environmental conditions is necessary to use robust controllers and significant gains to force the development of UV to fulfil a specific task. This chapter presents an integral sliding mode (ISM) formulation based on an average sub-gradient (ASG) for tracking a trajectory for UV. The tracking problem formulation is an optimisation problem of a cost functional of the tracking error. The proposed solution to the optimisation problem is using the average subgradient approach. In this way, the control formulation does not need a complete knowledge of the UV model to get a solution to the optimisation problem. Some simulations are presented to control quadrotor UV to demonstrate the proposed formulation.

4.2 Variables

A list of the variables used in this chapter is included in Table 4.1

$\mathbf{h}_t$	Selective vector
h_t^*	Desired reference
$\dot{h}_t^*$	Time derivative of desired reference
$\ddot{h}_t^*$	Second time derivative of desired reference
$x_{a,t}$	Position tracking error
$x_{b,t}$	Time derivative of position tracking error
u	Control vector
H	Tracking error cost functional
s	Integral sliding variable
A	Selection matrix

Table 4.1: State feedback Variables

4.3 The problem statement

Considering the structure of the UV dynamic without actuators dynamic described in equation (2.7), and all the assumptions of chapter 1, the control problem description is as follows:

To find a control law $\mathbf{u}$ that regulates the trajectory tracking error (the difference between the position of the UV and some feasible attainable reference trajectories $\mathbf{h}^* \in \mathbb{R}^n$, where $n \in \{1,2,...,6\}$), making it as small as possible without complete knowledge of the UV dynamic.

4.4 Position Tracking problem

4.4.1 Dynamics of the position tracking error

Defining a selective position vector h for the UV positioning as:

$$h_t = \mathbb{A}\rho_t \tag{4.1}$$

where $\mathbb{A} \in \mathbb{R}^{n\times 6}$ is a selection matrix, where $n \in [1,2,...6]$. Moreover, a selective position tracking error is given by:

$$\begin{aligned} \mathbf{x}_{a,t} &:= \mathbf{h}_t - \mathbf{h}_t^* \\ &= \mathbb{A}\rho_t - \mathbf{h}_t^*, \end{aligned} \tag{4.2}$$

where $\mathbf{h}^* = \begin{bmatrix} h_1^*, & h_2^*, ..., & h_n^* \end{bmatrix}^\top$, $\mathbf{h}^* \in \mathbb{R}^n$ represents the vector of a reference trajectory, where the first and second derivative vectors satisfy the following inequalities

$$\left\|\dot{\mathbf{h}}_t^*\right\| \leq \dot{h}^+, \left\|\ddot{\mathbf{h}}_t^*\right\| \leq \ddot{h}^+.$$

The time variation of the tracking error $\mathbf{x}_{a,t}$ is defined as

$$\begin{aligned} \mathbf{x}_{a,t} &= \dot{\mathbf{h}}_t - \dot{\mathbf{h}}_t^* \\ &= \mathbb{A}\dot{\rho}_t - \dot{\mathbf{h}}_t^*. \end{aligned} \tag{4.3}$$

Taking the first differential equation of (2.14), the time derivative of x_a can be expressed as

$$\dot{x}_{a,t} = \mathbb{A}J(\rho_t)\varphi_t - \dot{\mathbf{h}}_t^*. \tag{4.4}$$

Defining an auxiliary variable x_b as the time derivative of the selective position tracking error

$$x_{b,t} := \dot{x}_{a,t}, \tag{4.5}$$

the dynamic of the tracking error described in terms of the variables $\mathbf{x}_{a,t}$ and $\mathbf{x}_{b,t}$ is given by

$$\begin{aligned} \dot{\mathbf{x}}_{a,t} &= \mathbf{x}_{b,t}, \\ \dot{\mathbf{x}}_{b,t} &= F_{\mathbf{x},t} + G_{\mathbf{x},t}\mathbf{u}_{\mathbf{x},t}, \end{aligned} \tag{4.6}$$

where

$$\begin{aligned} F_{\mathbf{x},t} &:= \mathbb{A}J(\rho_t)\mathbb{M}^{-1}\left[F\left(\rho_t,\varphi_t\right)+\xi_t\right]+\ddot{\mathbf{h}}_t^* \\ G_{\mathbf{x},t} &= \mathbb{A}J(\rho_t)\mathbb{M}^{-1}G \\ u_{\mathbf{x},\mathbf{t}} &= u_t. \end{aligned} \tag{4.7}$$

The determinant of the matrix $G_{\mathbf{x}}$ satisfies the condition of $det(G_{\mathbf{x}}) \neq 0$, so $G_{\mathbf{x}}$ is invertible $\forall t \geq 0$. The function $F_{\mathbf{x}}$ is subject to the upper bound described by:

$$\left.\begin{array}{c} \left\|F_{\mathbf{x}}\left(\mathbf{x}_{a,t},\mathbf{x}_{b,t},\ddot{\mathbf{h}}_t^*\right)\right\| = F_{\mathbf{x},t}^+, \\ F_{\mathbf{x},t}^+ = \gamma_0+\gamma_1\left\|\rho_t\right\|+\gamma_2\left\|\varphi_t\right\| \\ \gamma_0 = \gamma+\gamma_\xi \\ \gamma_j > 0,\ \gamma_\xi > 0;\ \ j = 0,...,2 \\ \|G_{\mathbf{x}}\| \leq \gamma_G,\ \ \gamma_G > 0 \end{array}\right\}. \tag{4.8}$$

An optimisation problem of a tracking error cost functional is formulated to get a solution to the tracking problem.

4.4.2 Application of the averaged sub-gradient descendent technique

Define the optimization (minimization) of the smooth convex functional $H = H(\mathbf{x}_a)$, where $H : \mathbb{R}^n \to \mathbb{R}^+$ and given by

$$H(\mathbf{x}_{a,t}) \to \min_{u_{\mathbf{x}}\mathbb{R}^m}. \tag{4.9}$$

A possible solution to the optimisation problem is by the ASG algorithm by an ISM controller. The convex (non-strictly and not obligatory differentiable) function $H(\mathbf{x}_a)$, proposed in this study, is

$$H(\mathbf{x}_{a,t}) = \sum_{j=1}^{n}\left|\mathbf{x}_{a,j,t}\right|. \tag{4.10}$$

The cost function satisfies the following inequality $H(\mathbf{x}_a) \geq \min_{\mathbf{x}_a} H(\mathbf{x}_a) = H^* = 0$ (assuming that $\mathbf{x}_a$ belongs to a closed set) and the Jensen's inequality described in the expression (3.21) (valid for any convex function) given by

$$\delta_t^\top \partial H(\mathbf{x}_{a,t}) \geq H(\mathbf{x}_{a,t}) - H^*, \quad \mathbf{x}_a \in \mathbb{R}^n. \tag{4.11}$$

Desired sliding surface

Considering the usual gradient descendent method explained in Chapter 2, the auxiliary integral sliding variable s_t is described by

$$\left.\begin{aligned} s_t &= \mathbf{x}_{b,t} + \frac{\mathbf{x}_{a,t} + \eta}{t + \mu_0} + \Psi_t, \\ \Psi_t &= \frac{1}{t + \mu_0} \int_{\tau=0}^{t} \partial H(\mathbf{x}_{a,\tau}) d\tau, \end{aligned}\right\} \tag{4.12}$$

where $\mu_0 > 0$, Ψ_t is the suggested integral term, and η is a compensation term. The structure of η is going to be defined below. In expression (4.12), the term s_t is referred below as the *integral sliding variable* [54].

Integral SMC and averaged sub-gradient application to find $\mathbf{u_x}$

A. Robust controller structure

For the auxiliary dynamic, described in equation (6.13), satisfying the conditions in the expression (4.8), the control is proposed in the following theorem.

Theorem 1. *The proposed ASG-ISM controller, which solves the optimisation problem given in the expression* (4.9)*, has the following structure*

$$\mathbf{u}_{\mathbf{x},t} = -G_{\mathbf{x}}^{+} \left(k_{\mathbf{x},t} \frac{s_t}{\|s_t\| + \varepsilon_t} \right), \tag{4.13}$$

The positive function $k_{\mathbf{x},t}$ is defined as

$$k_{\mathbf{x},t} = 2 \left(\gamma_G^{-1} \mathbf{z}_{\mathbf{x},t}^{(1)} + k_0 \right) \tag{4.14}$$

where $k_0 > 0$, $\mathbf{z}_{\mathbf{x},t}^{(1)} \in \mathbb{R}$ and $\mathbf{z}_{\mathbf{x},t}^{(0)} \in \mathbb{R}^n$ and are defined as:

$$\mathbf{z}_{\mathbf{x},t}^{(1)} := F_{\mathbf{x}}^{+} + \left\| \mathbf{z}_{\mathbf{x},t}^{(0)} \right\| + |\dot{\varepsilon}_t| \tag{4.15}$$

$$\mathbf{z}_{\mathbf{x},t}^{(0)} := (t + \mu) \left[\mathbf{x}_{b,t} + \partial H(\mathbf{x}_{a,t}) - \Psi_t \right] - (t + \mu)^2 (\mathbf{x}_{a,t} + \eta) \tag{4.16}$$

Providing for all $t \geq 0$ the property

$$\|s_t\| \leq \varepsilon_t \tag{4.17}$$

Lemma 1. *For the desired variable, satisfying the condition in equation* (4.17)*, with any* $h_g > 0$ *and any* η *for* $t \geq t_0 \geq 0$ *we may guarantee that*

$$H(\mathbf{x}_{a,t}) \leq \frac{\Omega_t}{t+\mu} + \frac{h_g}{t+\mu} \int_{\tau=t_0}^{t} (\tau+\mu)\varepsilon_\tau d\tau. \tag{4.18}$$

where

$$\begin{gathered} \Omega_t = \lambda_{t_0} \left[H(\mathbf{x}_{a,t_0}) - H^*\right] - \frac{1}{2}\left\|\zeta_t + \eta\right\|^2 + \frac{1}{2}\left\|\zeta_{t_0}\right\|^2 + \frac{1}{2}\left\|\eta\right\|^2 \\ \zeta_t = \int_{\tau=0}^{t} \partial H\left(\mathbf{x}_{a,\tau}\right) d\tau \end{gathered} \tag{4.19}$$

Corollary 1. *If*

$$\varepsilon_t = \frac{\varepsilon_0}{(t+\mu)^{1+\alpha}}, \;\; \alpha \in (0,1), \; \varepsilon_0 > 0, \tag{4.20}$$

the following equality holds

$$\begin{gathered} \frac{h_g}{(t+\mu)} \int_{\tau=t_0}^{t} (\tau+\mu)\varepsilon_\tau d\tau \\ = h_g \varepsilon_0 \left[\frac{1}{(1+\alpha)(t+\mu)^\alpha} - \frac{(t_0+\mu)}{(1+\alpha)(t+\mu)}\right] \end{gathered} \tag{4.21}$$

the inequality (4.18) *becomes*

$$H(\mathbf{x}_{a,t}) \leq \frac{\Omega_t}{t+\mu} + h_g \varepsilon_0 \left[\frac{1}{(1+\alpha)(t+\mu)^\alpha} - \frac{(t_0+\mu)}{(1+\alpha)(t+\mu)}\right]. \tag{4.22}$$

Corollary 2. *For* $t_0 = 0$ *the sliding variable* s_t *satisfies*

$$0 = \mathbf{x}_{b,0} + \frac{\mathbf{x}_{a,0} + \eta}{\mu} \tag{4.23}$$

so defining

$$\eta = -\mathbf{x}_{a,0} - \mu \mathbf{x}_{b,0} \tag{4.24}$$

and taking ε_t *as in the equation* (4.20)*, finally, the inequality* (4.18) *becomes*

$$H(\mathbf{x}_{a,t}) \leq \frac{\Omega_{1,t}}{t+\mu} + \frac{h_g \varepsilon_0}{(1+\alpha)(t+\mu)^\alpha}. \tag{4.25}$$

The proof of the Theorem 1 and Lemma 1 are attached in the annexe. A diagram of the state feedback is also included in Figure (4.1).

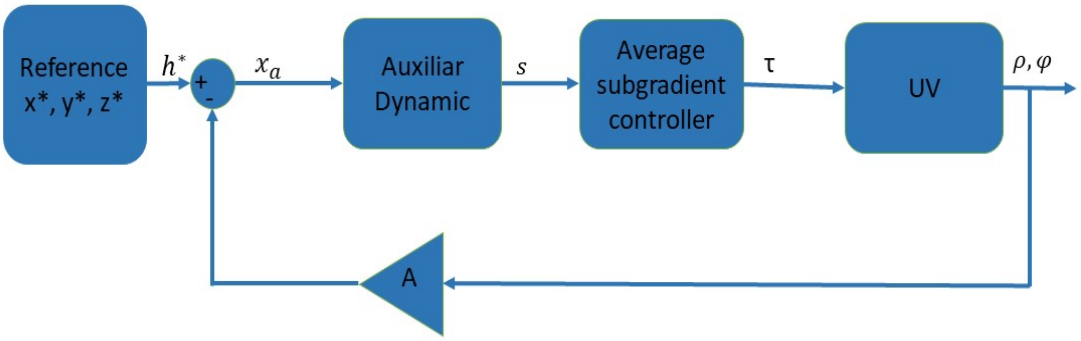

Figure 4.1: State feedback diagram

4.5 Numerical evaluations

This section presents the control motion of quadrotor UV for the tracking error in 3D-space considering the dynamic equations in the expressions (2.7). Also, considering actuators' dynamics.

4.5.1 3D Space Quadrotor

A state feedback control of PD form with model compensation implemented in the quadrotor system serves as a comparative control reference. The parameters employed are:

Table 4.2: Parameters of Quadrotor

Parameter	Parameter
$m = 0.47\text{kg}$	$g = 9.806 m/s^2$
$l = .205m$	$b = 2.9842 * 10^{-5} N/rad/s$
$d = 3.2320 + 10^{-7} N/rad/s$	$Jr = 2.8385 * 10^{-5} N$
$Ix = Iy = 3.8278 * 10^{-3} N$	$Iz = 7.1345 * 10^{-3} N$

The uncertainties considered in the dynamic are generated by a uniform random number

Table 4.3: PD and ISM control gains for quadrotor UV

Variable	K_p	K_d	Variable	K_s	K_d
x	2	1	x	2	1
y	2	1	y	2	1
z	350	25	z	55	35
θ	2	1	θ	275	0
ψ	1645	5	ψ	6245	0
ϕ	50	5	ϕ	50	5

software with a maximal magnitude equal to 0.5.

The references trajectories for the quadrotor are described by:

$$x_t^* = 2cos(0.75t)$$

$$y_t^* = 2sin(0.75t)$$

$$z_t^* = \frac{2}{1+e^{-2(t-55)}} - \left[\frac{2}{1+e^{-2(t-43)}} + \frac{2}{1+e^{-2(t-27.5)}}\right] - \left[\frac{2}{1+e^{-2(t-17.5)}} + \frac{2}{1+e^{-2(t-3)}}\right]$$

The control gains employed in this numerical evaluation are in the Table (4.3).

The controllers reduce the translation tracking errors (Figures (4.2), (4.3) and (4.4)) within the first 10 s, even though there are disturbances in the dynamics. Due to several curves, the PD controller cannot follow them as the proposed controller, and this one does not present deviations in the reference tracking. Also, the proposed control keeps bounded the cost function H as shown in Figure (4.5). The implemented controllers carry 3-dimensional path tracking in the first 10 s (Figure (4.9)). Given the nonlinear references, the controllers' magnitude variates continuously (Figure (4.7)). Due to the form of the reference on the z-axis, there is less deviation at the tracking reference (Figure (4.4)). There are oscillations in the trajectory tracking in the first 5s. The integral of the square of the control action is estimated for comparison of the controllers Figure (4.6). Given the ISM controller performance in the first 5s, the integral square

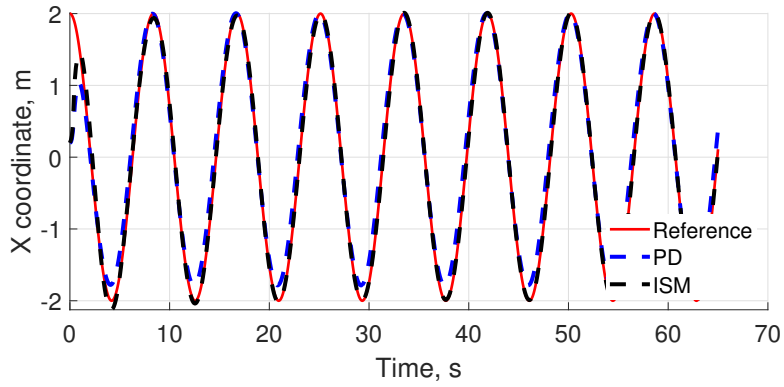

Figure 4.2: Displacement in x axes for the Quadcopter

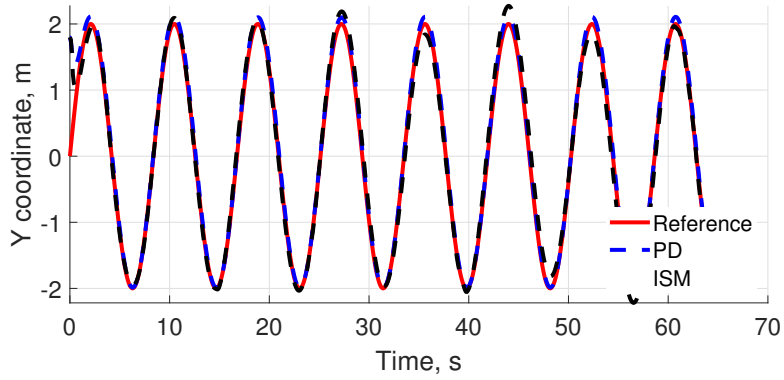

Figure 4.3: Displacement in y axes for the Quadcopter

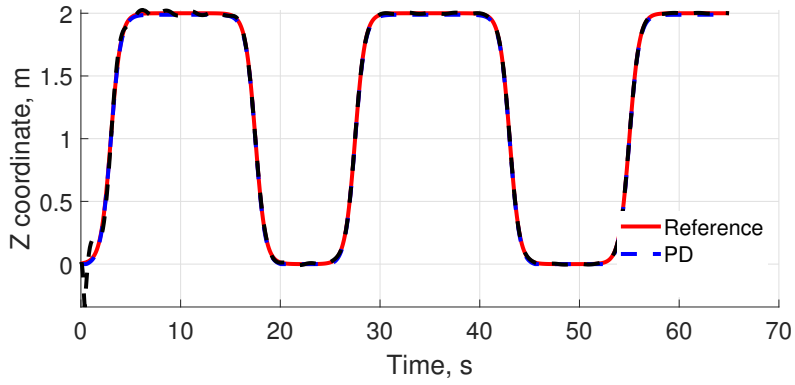

Figure 4.4: Displacement in z axes for the Quadcopter

of the control was $2.3 \cdot 10^6\ N^2m^2$. During the first 2s of numerical simulations, the norm of the

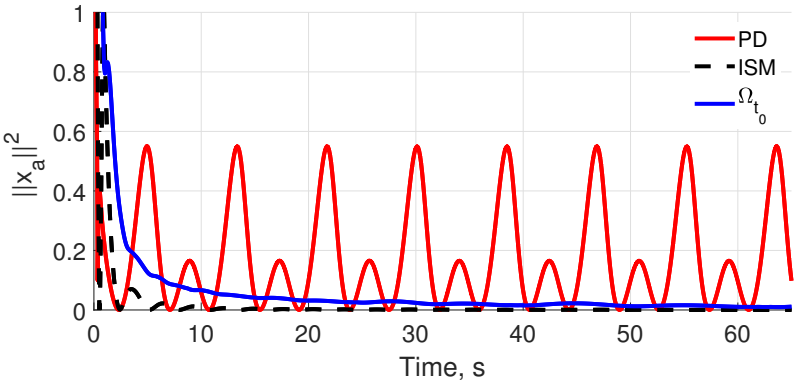

Figure 4.5: Norm of $\mathbf{x}_a$ of Quadcopter

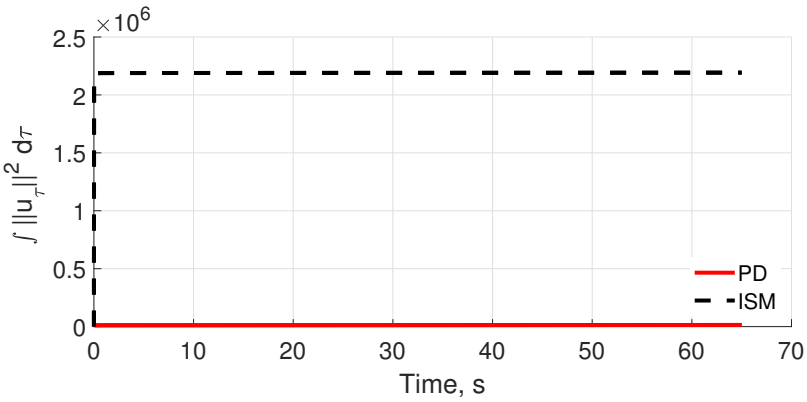

Figure 4.6: Integral of the square norm of $\mathbf{u}_t$ of the Quadcopter

ISM control was $9 \cdot 10^7$. However, along the rest of the simulation, the maximum value of the proposed ISM is near 60 (Figure (4.7)). Given the relationship between the control for x and y and the reference of ψ, θ and ϕ, the bounded uncertainties and perturbations the ISMs have high values to compensate for them. Figure (4.8) depicts the comparison of the integral square error enforced by the PD and ISM controllers over the quadrotor dynamics. The ISM controller is three times smaller than the corresponding PD controller. The integral square error of the ISM grows slowly compared to that of the PD controller, and this one keeps constantly growing (Figure (4.8)). Figure (4.9) shows the reference tracking on a 3D phase space. In the tracking by the ISM controller, no deviations are observed during the simulation, and the quadrotor reaches the desired reference trajectory. With the supposed partial knowledge of the UV model, with the

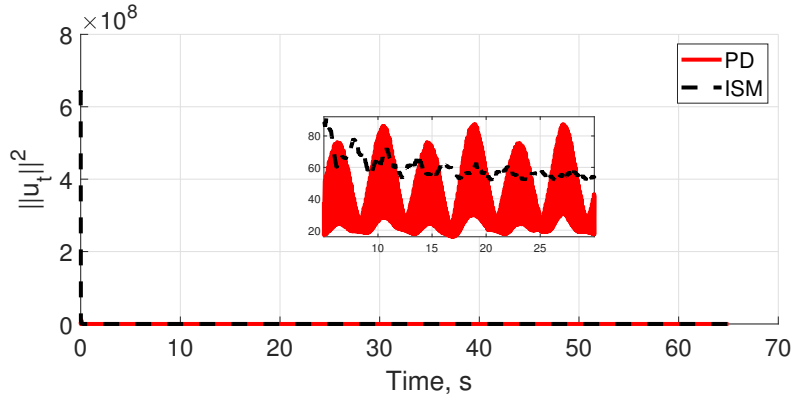

Figure 4.7: Square norm of **u** of Quadcopter

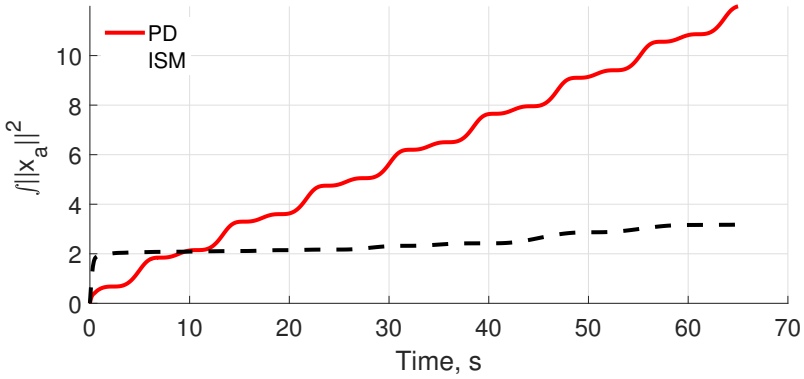

Figure 4.8: Integral of square norm of $\mathbf{x}_a$ of Quadcopter

presence of perturbations (nonlinear phenomena, external dynamics, the poor knowledge of the $\mathbb{M}$ and non-modelled dynamics), the proposed optimising controller exhibits better performance.

4.6 Pseudo-code algorithm

The algorithm steps are:

1. Define the reference trajectory ρ^*.

2. Calculate the tracking trajectory error x_a and the time derivative of the tracking error x_b.

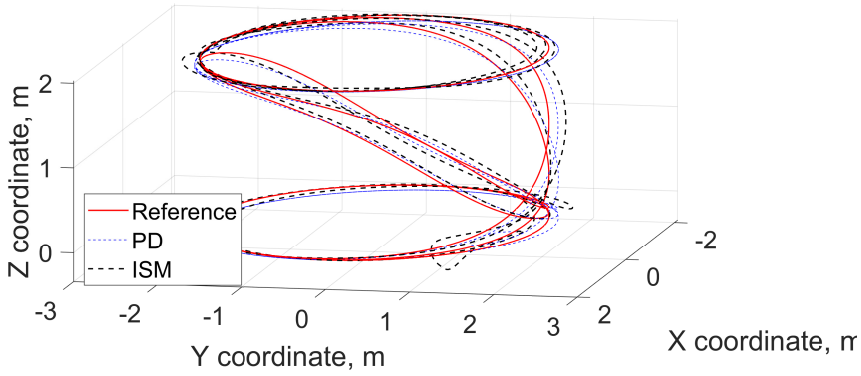

Figure 4.9: 3D-displacement of Quadcopter

3. Calculate the sliding variable s according to the definition presented in expression (4.12) using the tracking error and its first and second derivatives.

4. Implement the tracking error in the dynamic control law $u_{\mathbf{x}}$ presented in expression (4.13).

4.7 Chapter Conclusions

The present chapter presented a new proposal for solving the trajectory tracking of UV. The formulation does not require an explicit definition of the UV dynamic. The ISM-ASG controller optimises the tracking error for the position. An upper bound for the cost functional of the tracking error is established. The proposed formulation can be implemented in n dimensional tracking error and the tracking error not just for the position. The efficiency of the proposed controller in the control motion of different vehicles is demonstrated. It is important to note that this formulation was obtained for second-order dynamics. However, in the case of having a higher-order system, this formulation can also be adapted.

Chapter 5

Back-Stepping Realization of Averaged Sub Gradient Integral Sliding Mode Control

5.1 Chapter Introduction

In many cases, Unmanned Vehicles (UV) can be underactuated; consequently, it is necessary to consider auxiliary formulations to carry out UV control. It should also be noted that the actuators' dynamics are generally not considered. For these motives is required management systems of a higher order. A frequent solution is using the back-stepping or the better-known cascade formulation. Many formulations based on this approach require complete knowledge of the UV's dynamics in each stage to compensate for the forces that participate in the UV. This chapter proposes using the Back-stepping formulation and defining a tracking error in each step. Then formulate the tracking trajectory problem as an optimisation problem of a cost functional. In this way, propose pseudo-continuous controls that carry out the UV control, obtaining a formulation that does not require exact knowledge of the dynamics of each stage within the system. The design of a Back-stepping form by integral sliding mode (ISM) based on the average subgradient algorithm is presented. Some numerical evaluations by the SIMULINK/MATLAB platform

are exposed to get control of underwater UV. Also, a state-feedback formulation with a PID controller is used as a benchmark for the proposed controller. The analysis and some comments around the chapter are at the end of this one.

5.2 Problem stage

Given the complete state structure of the UV described in equation (2.14) the motion control of a UV can be aboard directly in three stages by Back-stepping combined with the technique of ASG. The description of the three stages are:

- The trajectory tracking problem for the position of the UV is as follows: to regulate position tracking error magnitude, the difference between the UV position and some feasible attainable reference trajectories $\rho^* \in \mathbb{R}^6$, making it as small as possible by the design of the referred ideal virtual continuous signal φ^* with partial knowledge of the time derived of the position.

- The tracking trajectory control problem for the velocity of the UV can be described as controlling the velocity tracking error, the difference between the velocity of the UV φ and the ideal virtual velocity φ^*, proposed for the first stage. Minimising the magnitude as much as possible by defining the referred ideal continuous signal I^* without knowledge of the parameters in the dynamic, unmodelled forces and under perturbations.

- The main problem around the UV actuators is as follows: to force the current tracking error, the difference between the current of the Permanent Magnet Direct Current (PMDC) motor and the virtual control $\mathbf{I}^* \in \mathbb{R}^m$ of the second stage (m is the number of actuators). Without a complete knowledge of the parameters of the motor and under perturbations.

To illustrate the stages, a representative diagram is shown in Figure 5.1

These three stages are for the general model of the UV, described in equation (2.14). In particular cases, the problem can be divided into more stages or less, mainly for underactuated systems.

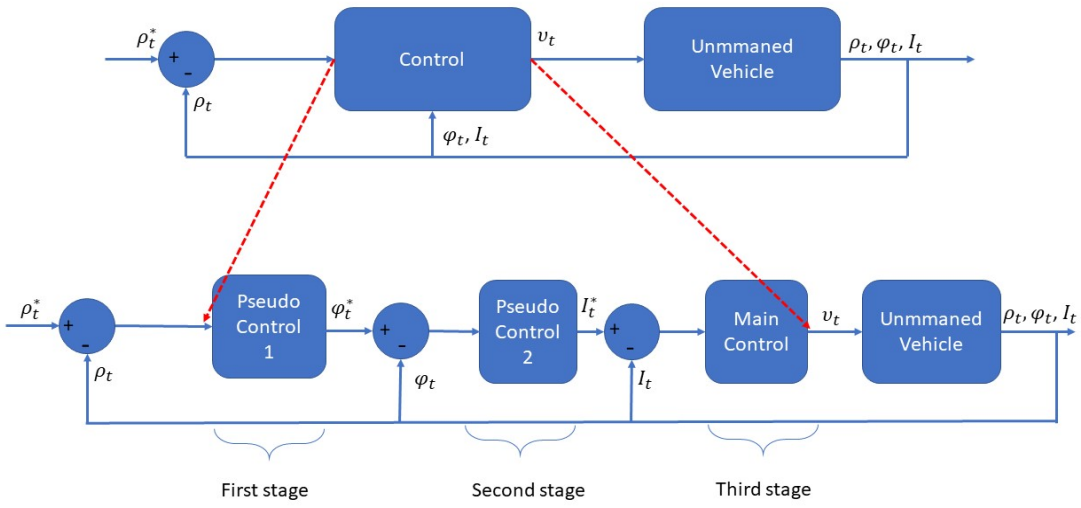

Figure 5.1: Back-stepping Diagram

5.3 Variables

A list of the variables used in this chapter is included in Table 5.1

5.4 Position Tracking problem statement

Given the position of UV by the vector $\rho \in \mathbb{R}^{n_1}$, with $n_1 = 6$, subject kinematic relation described in the equation (2.30), given by:

$$\dot{\rho}_t = J(\rho_t)\varphi_t. \tag{5.1}$$

The vector $\rho^* \in \mathbb{R}^{n_1}$, that corresponds to a desired reference trajectory in the 3-dimensional space. Where the first and second derivatives of ρ^* are subject to the following inequalities:

$$\|\dot{\rho}_t^*\| \leq \dot{\rho}^{*+}, \|\ddot{\rho}_t^*\| \leq \ddot{\rho}^{*+}. \tag{5.2}$$

The position tracking error vector $\delta_1 \in \mathbb{R}^{n_1}$ for the UV is defined as:

$$\delta_{1,t} = \rho_t - \rho_t^*, \tag{5.3}$$

where the corresponding time derivative $\dot{\delta}_1$ is given by:

$$\dot{\delta}_{1,t} := \dot{\rho}_t - \dot{\rho}_t^* \tag{5.4}$$

ρ	UV position
ρ^*	Desired UV position
$\dot{\rho}^*$	Time derivative of the desired UV position
$\ddot{\rho}^*$	Second time derivative of the desired UV position
ρ_1	Translation position
φ	UV velocity
$\dot{\varphi}^*$	Desired time derivative UV velocity
$J(\rho)$	Jacobian matrix
I^*	Desired current
δ_1	Position tracking error
δ_2	Velocity tracking error
δ_3	Current tracking error
H	Cost function
s_1	Integral sliding variable of first stage
s_2	Integral sliding variable of second stage
s_3	Integral sliding variable of third stage

Table 5.1: Back stepping Variables

Considering the dynamics of the UV, given by the expression (2.30), the differential equation (5.4) can be expressed as

$$\dot{\delta}_{1,t} = F_{1,t} + G_{1,t}\mathbf{u}_{1,t}, \tag{5.5}$$

where

$$\left.\begin{array}{c} F_{1,t} := \dot{\rho}_t^* \\ G_{1,t} := J(\rho_\mathbf{t}) \end{array}\right\}. \tag{5.6}$$

Where $G_1 \in \mathbb{R}^{n_1 \times m_1}$ and satisfy $\det(G_1) \neq 0$, in consequence G_1 is invertible all the time. The upper bounds for the functions F_1 and G_1 are described according to the following expressions:

$$\left.\begin{array}{c} \|F_1\| = F_1^+, \;\; F_1^+ = \dot{\rho}^{*+} \\ \left\|G_{1,t}\right\| \leq g_1^+, \;\; g_1^+ > 0, \;\; g_1^- = (g_1^+)^{-1} \end{array}\right\}. \tag{5.7}$$

A Back-stepping formulation [2] is used for get the stabilization of δ_1. The vector $\mathbf{u}_1 \in \mathbb{R}^{m_1}$ that corresponds to the control in this stage is defined as $\mathbf{u}_1 := \varphi$, where φ is considered as a pseudo auxiliary controller. The trajectory problem is reformulated as an optimisation problem to obtain the stabilisation δ_1. Let's consider that $\mathbf{u}_1$ must minimise a cost function depending on the position tracking error. The solution for the optimisation problem is based on the average sub-gradient algorithm. This technique has been successfully applied for controlling systems modelled by the Euler- Lagrange equations with uncertain models [41]. The proposed smooth convex cost function is:

$$H(\delta_1) = \sum_{i=1}^{n_1} \left|\delta_{1,i}\right|, \tag{5.8}$$

where $\delta_{1,i}$ corresponds to the i-th component of δ_1.

The control problem formulation for this first stage consists of designing a reference vector $\mathbf{u}_1^* = \varphi^*$ such that:

$$\begin{array}{c} H(\delta_1) \rightarrow \min\limits_{u_1 \in \mathbb{R}^{m_1}}, \\ u_{1,t}^* = \arg\min\limits_{u_{1,t} \in \mathbb{R}^{m_1}} H(\delta_{1,t}). \end{array} \tag{5.9}$$

According to the ASG method previously used in [41], the optimisation problem can be solved with the suitable definition of a sliding surface $s_{1,t}$ and the application of the ISM. The *integral sliding variable* $s_{1,t}$ satisfies [54],

$$\left.\begin{array}{c} s_{1,t} = \dot{\delta}_{1,t} + \mu_t \left[\delta_{1,t} + \eta_1\right] + \Psi_{1,t}, \\ \Psi_{1,t} = \mu_t \int\limits_{\tau=0}^{t} \partial H(\delta_{1,\tau}) d\tau, \\ \mu_t = (t+\mu)^{-1}, \;\; \mu > 0 \end{array}\right\} \tag{5.10}$$

with Ψ_1 the temporal average of the gradient for the cost function $H(\delta_1)$. To solve this, it was formulated the following theorem.

Theorem 2. *The proposed ASG-ISM controller, which solves the optimisation problem given in the expression* (5.9)*, has the following structure*

$$u_{1,t} = -\beta_{1,t} \frac{s_{1,t}}{\left\|s_{1,t}\right\| + \varepsilon_{1,t}}, \tag{5.11}$$

The positive function $\beta_{1,t}$ *is defined as*

$$\beta_{1,t} = 2\left(g_1^- \mathbf{z}_{1,t}^{(1)} + \lambda_{1,}\right) \tag{5.12}$$

where

$$\begin{aligned} \mathbf{z}_{1,t}^{(1)} &:= F_1^+ + \left\|\mathbf{z}_{1,t}^{(0)}\right\| + \left|\dot{\varepsilon}_{1,t}\right| \\ \mathbf{z}_{1,t}^{(0)} &:= \dot{\delta}_{1,t} + \partial H(\delta_{1,t}) - \Psi_{1,t} \\ \varepsilon_{1,t} &= \mu_t^{-(1+\alpha)} \varepsilon_{1,0}, \;\; \varepsilon_{1,0} > 0, \lambda_1 > 0. \end{aligned} \tag{5.13}$$

Then the integral sliding surface s_1 *proposed as in expression* (5.10) *converges to a desired regimen in a finite time* $t_0 = \dfrac{2\sqrt{2}}{\lambda_1}\left\|s_{1,0}\right\|$.

$$\|s_{1,t}\| \leq \varepsilon_{1,t} \tag{5.14}$$

Where s_{1,t_0} *the sliding surface evaluated over the trajectory of* $\delta_{1,t}$ *with* $t = t_0$

Lemma 2. *The control law* (5.11) *with* $\mathbf{s}_{1,t}$*, generated by* (5.10) *with* η_1 *as* $\eta_1 = \delta_{1,0}$*, guarantees the following inequality*

$$\|H(\delta_{1,t})\| \leq \mu_t d_i \|\delta_{1,t}\| + \mu_t \left(1 + t + \mu\right) d_i \|\eta_1\| + \mu^{-(1+\alpha)}(1 + t + \mu) d_i \varepsilon_{1,0} \tag{5.15}$$

The stability analysis and the proof of the corollary are in the Appendix.

5.5 Velocity tracking problem

Given the desired reference proposed in the expression (5.11) and remembering the equivalence:

$$u_{1,t} = \varphi_t^* \tag{5.16}$$

The second stage is to tackle the velocity trajectory tracking problem. For this is defined the velocity tracking error δ_2 for the UV as:

$$\delta_{2,t} := \varphi_t - \varphi_t^*, \tag{5.17}$$

where $\varphi^* \in \mathbb{R}^{n_2}$, with $n_2 = m_1$, $m_1 = 6$. The time derivative of the velocity tracking error δ_2 is:

$$\dot{\delta}_{2,t} := \dot{\varphi} - \dot{\varphi}^* \tag{5.18}$$

Now given the complete dynamic of the UV, given by the expression (2.14), the equation (5.18) can be expressed as:

$$\dot{\delta}_{2,t} = F_{2,t} + G_2 \mathbf{u}_{2,t}, \tag{5.19}$$

where

$$\left.\begin{aligned} F_{2,t} &:= \mathbb{M}^{-1}\left[F\left(\rho_t, \varphi_t\right) + \xi_t\right] - \dot{\varphi}_t^* \\ G_2 &:= G E_f D_f. \end{aligned}\right\} \tag{5.20}$$

Where $G_2 \in \mathbb{R}^{n_2 \times m_2}$ and exist $G_2^+ = (G_2^\top G_2)^{-1} G_{\delta,2}^\top$ defined as the pseudo-inverse of G_2. The upper bound for the function $F_{2,t}$ satisfies the following expression:

$$\left.\begin{aligned} \left\|F_{2,t}\right\| &\leq F_{2,t}^+, \\ F_{2,t}^+ &= \gamma_{2,0} + \gamma_{2,1}|\rho_t| + \gamma_{2,2}|\varphi_t| \\ \gamma_0^{(2)} &> 0; \\ \left\|G_2^\top G_2\right\| &\leq g_2^+, \;\; g_2^+ > 0, \;\; g_2^- = (g_2^+)^{-1}. \end{aligned}\right\}. \tag{5.21}$$

In a similar form as in the previous stage, a pseudo-control action is considered. For the velocity stage, the control action is given by the vector $\mathbf{u}_2 := I$ where $\mathbf{u}_2 \in \mathbb{R}^{m_2}$ and $\mathbf{m}_2$ depends of the number of actuators in the UV. The proposition of $\mathbf{u}_2^* = I^*$ will be defined below. The variable I^* is the reference of current for actuators.

Continue with the Back-stepping formulation [2] to obtain the stabilisation in this stage of δ_2. As in the previous stage, the stabilisation problem of δ_2 is reformulated as an optimisation problem. The main objective of $\mathbf{u}_2$ is to obtain the minimum value of a cost function depending on the velocity tracking error. The proposed algorithm is based on the averaged sub-gradient to solve the optimisation problem. The proposed smooth convex cost function is:

$$H(\delta_{2,t}) = \sum_{i=1}^{n_2} \left|\delta_{2,i,t}\right|, \tag{5.22}$$

where $\delta_{2,i}$ corresponds to the i-th component of δ_2.

In the second stage, the control problem formulation consists of designing a reference vector $\mathbf{u}_2^* = I^*$ such that:

$$\begin{aligned} H(\delta_{2,t}) &\rightarrow \min_{u_2 \in \mathbb{R}^{m_2}}, \\ u_{2,t}^* &= \arg\min_{u_{2,t} \in \mathbb{R}^{m_2}} H(\delta_{2,t}). \end{aligned} \tag{5.23}$$

Using the same average sub-gradient formulation used in the previous stage and based on the formulation in [41] defines the integral sliding surface $s_{2,t}$ to solve the optimisation problem and considering the ISM approach. The *integral sliding variable* $s_{2,t}$ satisfies [54], and is given by:

$$\left.\begin{aligned} s_{2,t} &= \dot{\delta}_{2,t} + \mu_t \left[\delta_{2,t} + \eta_2\right] + \Psi_{2,t}, \\ \Psi_{2,t} &= \mu_t \int_{\tau=0}^{t} \partial H(\delta_{2,\tau}) d\tau, \\ \mu_t &= (t+\mu)^{-1}, \;\; \mu > 0 \end{aligned}\right\} \tag{5.24}$$

with $\Psi_{\mathbf{2}}$ the temporal average of the gradient for the cost function $H(\delta_2)$.

The following theorems were formulated to solve this stage, based on the previous stage theorem,

Theorem 3. *The formulated ASG-ISM controller, for the optimisation problem given in the expression* (5.23)*, satisfies*

$$u_{2,t} = -\beta_{2,t} \frac{s_{2,t}}{\left\|s_{2,t}\right\| + \varepsilon_{2,t}}, \tag{5.25}$$

The positive function $\beta_{2,t}$ *is defined as*

$$\beta_{2,t} = 2\left(g_2^- \mathbf{z}_{2,t}^{(1)} + \lambda_{2,}\right) \tag{5.26}$$

where

$$\begin{aligned} \mathbf{z}_{2,t}^{(1)} &:= F_2^+ + \left\|\mathbf{z}_{2,t}^{(0)}\right\| + \left|\dot{\varepsilon}_{2,t}\right| \\ \mathbf{z}_{2,t}^{(0)} &:= \dot{\delta}_{2,t} + \partial H(\delta_{2,t}) - \Psi_{2,t} \\ \varepsilon_{2,t} &= \mu_t^{-(1+\alpha)} \varepsilon_{2,0}, \;\; \varepsilon_{2,0} > 0, \lambda_2 > 0. \end{aligned} \tag{5.27}$$

Then the integral sliding surface $s_{2,t}$ *proposed as in expression* (5.24) *converges to a desired regimen in a finite time* $t_0 = \dfrac{2\sqrt{2}}{\lambda_2}\left\|s_{2,0}\right\|$.

$$\left\|s_{2,t}\right\| \leq \varepsilon_{2,t} \tag{5.28}$$

Where s_{2,t_0} the sliding surface evaluated over the trajectory of $\delta_{2,t}$ with $t = t_0$

Lemma 3. *The control law* (5.25) *with* $\mathbf{s}_{2,t}$, *generated by expression* (5.24) *with* η_2 *as* $\eta_2 = \delta_{2,0}$, *guarantees the following inequality*

$$\|H(\delta_{2,t})\| \leq \mu_t d_i \|\delta_{2,t}\| + \mu_t (1+t+\mu) d_i \|\eta_1\| + \mu^{-(1+\alpha)}(1+t+\mu) d_i \varepsilon_{2,0} \tag{5.29}$$

The stability analysis and the proof of the corollary are in the Appendix.

5.6 Actuator control problem

Considering the desired reference for I in the expression (5.25) is defined the current tracking error δ_3 as:

$$\delta_{3,t} = I_t - I_t^*, \tag{5.30}$$

where $I \in \mathbb{R}^{n_3}$ with $n_3 = m_2$. The dynamic of tracking error δ_3 is described as:

$$\dot{\delta}_{3,t} := \dot{I}_t - \dot{I}_t^* \tag{5.31}$$

Considering the dynamics of the actuators on the UV, described by the expression (2.14), the equation (5.31) is equivalent to

$$\dot{\delta}_{3,t} = F_{3,t} + G_3 \mathbf{u}_{3,t}, \tag{5.32}$$

where

$$\left.\begin{array}{c} F_3 := -E_f D_f Z_L^{-1} F_I(\rho_t, \varphi_t) - \dot{I}_t^* \\ G_3 := Z_L^{-1}. \end{array}\right\} \tag{5.33}$$

where $G_3 \in \mathbb{R}^{m_2 \times m_2}$ and for $\det(G_3)$ the non singularity condition is satisfied $\det(G_3) \neq 0$, the upper bound for the function F_3 is given according to the following expression:

$$\left.\begin{array}{c} \|F_3\| = F_3^+, \\ F_3^+ = \gamma_{3,0} + \gamma_{3,1}|\rho_t| + \gamma_{3,2}|\varphi_t| \\ \gamma_0^{(3)} > 0 \\ \|G_3\| \leq g_3^+, \;\; g_3^+ > 0, \;\; g_3^- = (g_3^+)^{-1}. \end{array}\right\} \tag{5.34}$$

The real control action over UV system and for the third stage of the Backstepping formulation is $\mathbf{u}_3 = \upsilon_d$ where $\mathbf{u}_3 \in \mathbb{R}^{m_3}$and $m_3 = m$. The optimal control $\mathbf{u}_3^* = \upsilon_d^*$ will be defined below

Finally, the last part of the Back-stepping formulation [2] consist of forcing the stabilisation of δ_3. The tracking trajectory problem is expressed as an optimisation problem to solve this problem. Defining the objective of $\mathbf{u}_3$ as obtain the minimum value of a cost functional of the current tracking error. The optimal solution for the problem is getting by the algorithm of averaged sub-gradient. The proposed smooth convex cost function is:

$$H(\delta_{3,t}) = \sum_{i=1}^{n_3} \left|\delta_{3,i,t}\right|, \tag{5.35}$$

where $\delta_{3,i}$ corresponds to the i-th component of δ_3.

The control problem is designing an optimal control vector $\mathbf{u}_3^* = v^*$ such that:

$$\begin{aligned} H(\delta_{3,t}) &\rightarrow \min_{u_3 \in \mathbb{R}^{m_3}}, \\ u_{3,t}^* &= \arg\min_{u_{3,t} \in \mathbb{R}^{m_3}} H(\delta_{3,t}). \end{aligned} \tag{5.36}$$

To solve the optimisation problem in the last stage, a integral sliding variable is defined, following the formulation in [41] and based on the algorithm of average sub-gradient, as in the first stages. The sliding surface s_3 formulated for solve the optimization problem called *integral sliding variable* s_3 satisfies [54], and is given by:

$$\left.\begin{aligned} s_{3,t} &= \dot{\delta}_{3,t} + \mu_t \left[\delta_{3,t} + \eta_3\right] + \Psi_{3,t}, \\ \Psi_{3,t} &= \mu_t \int_{\tau=0}^{t} \partial H(\delta_{3,\tau}) d\tau, \\ \mu_t &= (t+\mu)^{-1}, \;\; \mu > 0 \end{aligned}\right\} \tag{5.37}$$

where the average partial derivative of the cost function $H(\delta_3)$ corresponds to $\Psi_{\mathbf{3}}$.

For the considered dynamic in the final stage, described in the equation (5.32), satisfying the conditions given in (5.34), the real control action of the UV is proposed in the following theorem

Theorem 4. *The proposed ASG-ISM controller, which solves the optimisation problem given in the expression* (5.36)*, for the tracking error* δ_3 *has the following structure*

$$u_{3,t} = -\beta_{3,t} \frac{s_{3,t}}{\left\|s_{3,t}\right\|}, \tag{5.38}$$

The positive function β_3 is defined as β_3 is selected as

$$\beta_{3,t} = F_3^+ + \left\| \mathbf{z}_{3,t}^{(0)} \right\| + \frac{\varepsilon_3}{\eta_3} \tag{5.39}$$

where

$$\mathbf{z}_{3,t}^{(0)} := (t+\mu)^{-1} \left[\partial H(\delta_{3,t}) - \Psi_{3,t} \right] \tag{5.40}$$

then the sliding surface $\mathbf{s}_3$ proposed as in expression (5.37) *converges to the origin in a finite-time $t_0 = (\frac{\sqrt{2}}{\lambda_3} g_3^-) \left\| \mathbf{s}_{3,t_0} \right\|$. Where $\mathbf{s}_{3,t_0}$ is the integral sliding surface evaluated over the trajectories of δ_3 with $t = t_0$.*

5.7 Numerical Evaluation

5.7.1 Backstepping formulation for underwater UV

Tackling the case of an underwater UV was considered the situation in which $\phi = 0$ with the reduced kinematic given in the equation (2.20) and the equations of translation and orientation in the expressions (2.21) and (2.22) respectively. As was mentioned before, the Back-stepping formulation described can be formulated in different ways as it is convenient for the UV device and circumstances. For this particular case, the number of stages is four. The cost functional considered in this example was the same as for each stage in the previous description in the equations (5.8), (5.22) and (5.35). The integral sliding variables are described in similar way as before in the expressions (5.10), (5.24) and (5.37). The relation between the steps can be considered as guidance laws by control.

5.7.2 First stage-Position tracking

For this stage the reference trajectory is given by $\rho_1^* = \begin{bmatrix} x^* & y^* & z^* \end{bmatrix}^\top$ with the corresponding dynamic given by $\dot{\rho_1}_t^* = F(t)$. Taking the position tracking error as $\delta_1 := \rho_1 - \rho_1^*$. The components of the tracking error dynamic are

$$f_{1,t} = -F(t), \quad G_{1,t} = R_b^a(0, \theta_t, \psi_t)$$

for this stage, the vector of translation velocity φ_1 acts as the control action over the position tracking error δ_1, renaming the control variable as $\mathbf{u}_1$. The ideal virtual control φ_1^* is defined using the expression (5.11).

5.7.3 Second stage- Traslational Velocity tracking

The second stage consists of the control of the translation velocity tracking. The tracking error δ_2 is defined as

$$\delta_{2,t} := \varphi_{2,t}^* - \varphi_{2,t}$$

The form of the dynamic is as the equation (2.21) with the components given by

$$F_{2,t} = \begin{bmatrix} -\frac{d_{11}u_t}{m_{11}} \\ -\frac{d_{22}v_t}{m_{22}} \\ -\frac{d_{33}w_t}{m_{33}} \end{bmatrix} - \dot{\varphi}_{1,t}^*,\ G_{\delta_2} = \begin{bmatrix} \frac{1}{m_{11}} & -\frac{m_{33}w_t}{m_{11}} & +\frac{m_{22}v_t}{m_{11}} \\ 0 & 0 & -\frac{m_{11}u_t}{m_{22}} \\ 0 & \frac{m_{11}u_t}{m_{33}} & 0 \end{bmatrix}$$

The control action over the dynamic of $\delta_{2,t}$ corresponds to $\mathbf{u}_2 = \begin{bmatrix} \mathbf{u}_u & \omega \end{bmatrix}^\top$, where ω corresponds to the angular velocity of pitch and yaw, $\omega = \begin{bmatrix} q & r \end{bmatrix}^\top$. The ideal virtual control $\mathbf{u}_2^*$ is described in a similar way as in the expressions (5.11) and (5.25).

5.7.4 Third Stage- Angular Velocity Tracking

The third control step is defined as the solution of angular velocity tracking. It is defined the tracking error δ_3 as

$$\delta_{3,t} := \omega_t^* - \omega_t$$

where the control action corresponds to the vector $\mathbf{u}_3 = \begin{bmatrix} \mathbf{u}_r & \mathbf{u}_q \end{bmatrix}^\top$. The dynamic of δ_3 is described in a similar form as in the expression (5.5), (5.19) and (5.32). The components are given by

$$F_{3,t} = \begin{bmatrix} \frac{m_{33}-m_{11}}{m_{55}}u_t w_t - \frac{d_{55}}{m_{55}}q_t - \frac{mghs_\theta}{m_{55}} \\ \frac{m_{11}-m_{22}}{m_{66}}u_t v_t - \frac{d_{66}}{m_{66}}r_t \end{bmatrix} - \begin{bmatrix} \dot{r}_t^* \\ \dot{q}_t^* \end{bmatrix}, \quad G_3 = \begin{bmatrix} \frac{1}{m_{55}} & 0 \\ 0 & \frac{1}{m_{66}} \end{bmatrix}$$

The ideal control $\mathbf{u}_3^*$ is formulated in a similar form as in the expressions (5.11) and (5.25).

5.7.5 Fourth Stage - Torque Tracking

In the last stage, the tracking error is as in the form in the expression (5.30). Taking the tracking error δ_4 as

$$\delta_{4,t} := \mathbf{u}_t^* - \mathbf{u}_t$$

where $\mathbf{u}^\top = \begin{bmatrix} \mathbf{u}_u & \mathbf{u}_q & \mathbf{u}_r \end{bmatrix}$ where $\mathbf{u}_u$ is defined in the second stage and $\mathbf{u}_q$ and $\mathbf{u}_r$ are defined in the previous stage. The components of the tracking error dynamic, considering the structure in the equation (5.32), are

$$F_4 = Z_E \begin{bmatrix} g_u \\ g_q \\ g_r \end{bmatrix} - \begin{bmatrix} \dot{\mathbf{u}}_{u,t}^* \\ \dot{\mathbf{u}}_{q,t}^* \\ \dot{\mathbf{u}}_{r,t}^* \end{bmatrix}, \quad G_4 = Z_E$$

The control vector is $v = \begin{bmatrix} v_u & v_q & v_r \end{bmatrix}^\top$ is given the equation (5.38).

5.7.6 Evaluation

This section describes the numerical results evaluated in the MATLAB/Simulink platform for the previous case described. The simulation algorithm uses the Runge-Kutta integration algorithm with a step size of $1 * 10^{-4}$ s. The parameters used in the dynamic of the underwater UV are as follows in the Table (5.2)

Parameter	Value	Parameter	Value	Parameter	Value
m_{11}	1116	d_{11}	25.5	m	1089.9
m_{22}	2133	d_{22}	138	g	9.81
m_{33}	2133	d_{33}	138	h	0.0065
m_{55}	4061	d_{55}	490		
m_{66}	4061	d_{66}	490		

Table 5.2: Simulation Parameters underwater vehicle

First stage

The tracking of the position of the UV is in the three-dimensional space x-y-z. The proposed reference is a circle in the horizontal plane, and a bell function gives the heave displacement. The desired trajectory is described by:

$$x_t^* = 15sin(0.02t)$$
$$y_t^* = 15cos(0.02t)$$
$$z_t^* = -5\left[\frac{1}{1+|0.01t-2|^8}\right]$$

In a similar form for each stage, a state feedback formulation (proportional-integral-derivative or PID form) with model compensation is formulated for the UV system, with the main objective to serve as a benchmark for the proposed controller in all the stages. For the position tracking in the initials 20s. both controllers force the system to a zone near the desired trajectory (Figures (5.2), (5.3) and (5.4)), and the observed oscillations correspond to the disturbances in the kinematic of the system. The displacement in the three-dimensional space can be observed in Figure (5.5).

As the tracking error is reduced (Figure (5.6)), in consequence, the proposed controller keeps bounded the cost function Ψ_1 as can be noticed in the same figure.

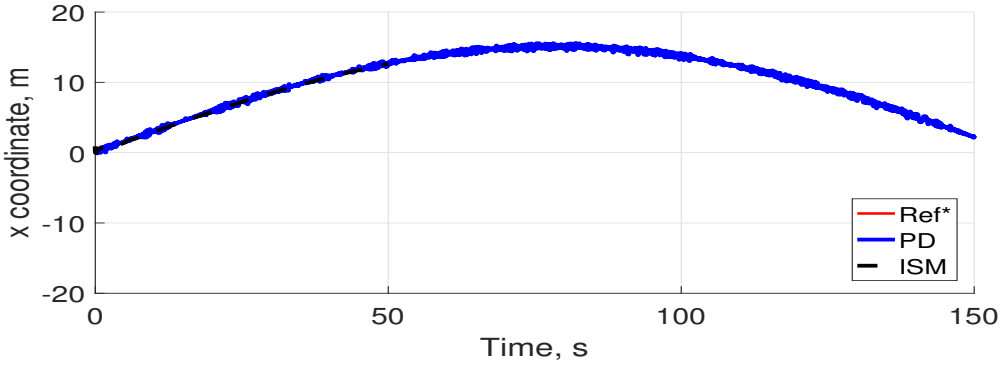

Figure 5.2: Surge displacement "x" by state feedback and integral sliding mode

Second stage

In the same first 20 seconds for the second stage, both controllers force the velocities states to the desired trajectory as is shown in Figures (5.7), (5.8) and (5.9), showing just the first 20

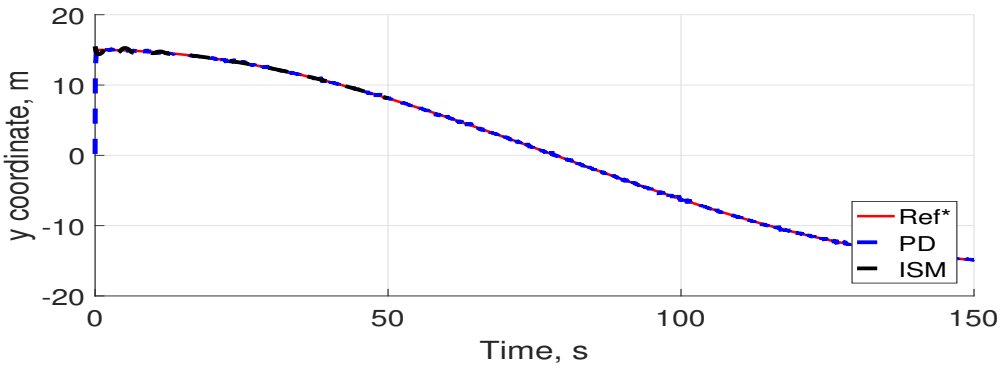

Figure 5.3: Sway displacement "y" by state feedback and integral sliding mode

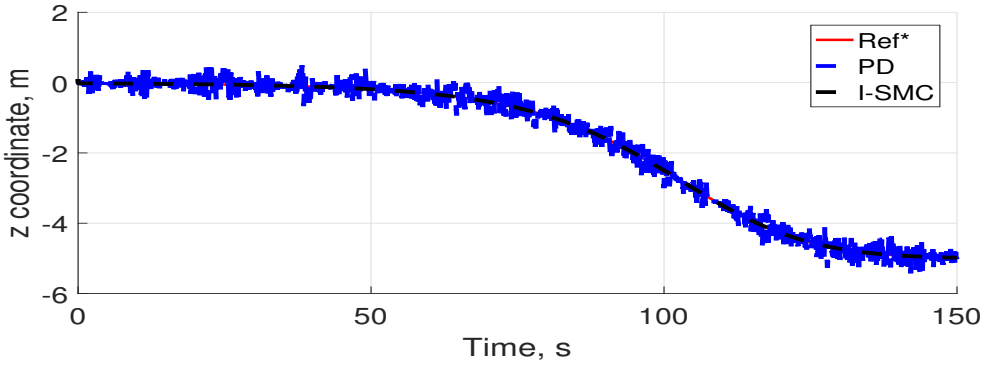

Figure 5.4: Heave displacement "z" by state feedback and integral sliding mode

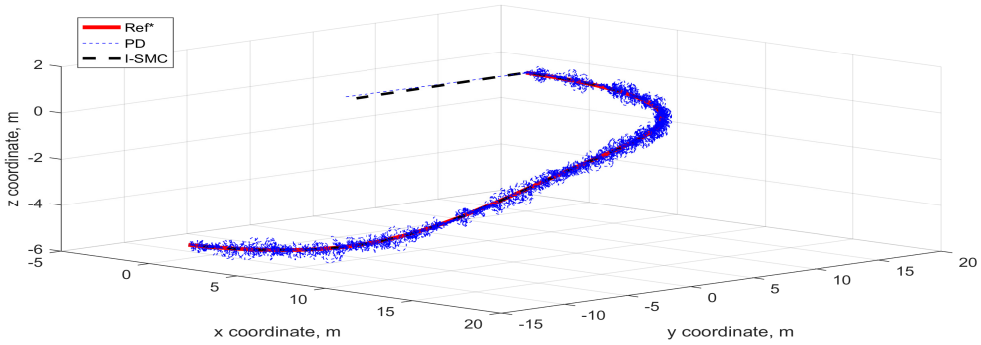

Figure 5.5: 3D space "$x-y-z$" by state feedback and integral sliding mode

seconds of simulation. As can be observed in the tracking error development in Figure (5.10) the ISM controller obtain a smaller magnitude of the tracking error as obtained by the state feedback formulation. The magnitude obtained by the ISM controller is .5 timeless than by the

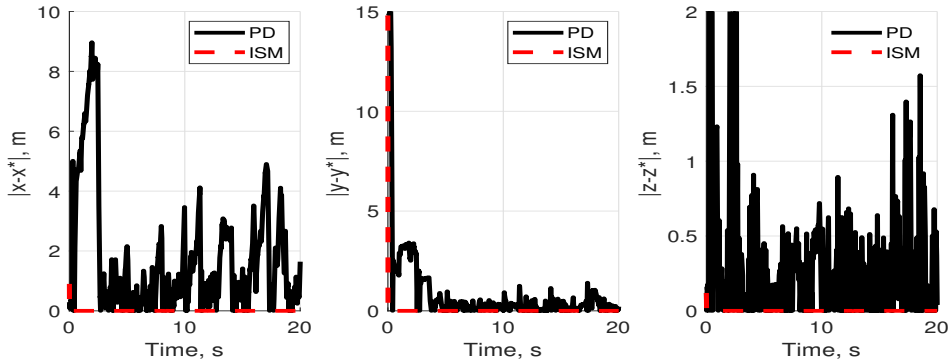

Figure 5.6: Position tracking error "$\delta_{1,t}$" by state feedback and integral sliding mode

PID controller.

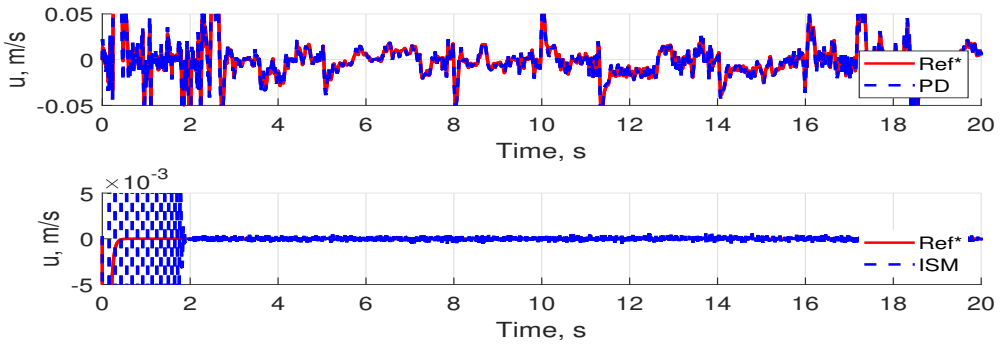

Figure 5.7: Surge velocity "u" by state feedback and integral sliding mode

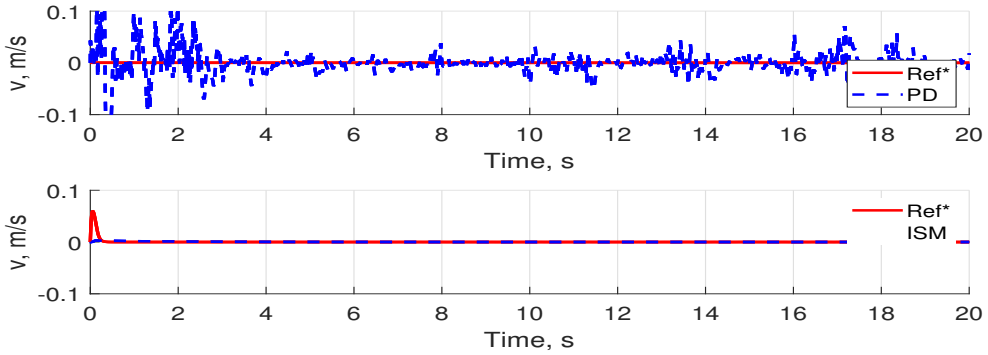

Figure 5.8: Sway velocity "v" by state feedback and integral sliding mode

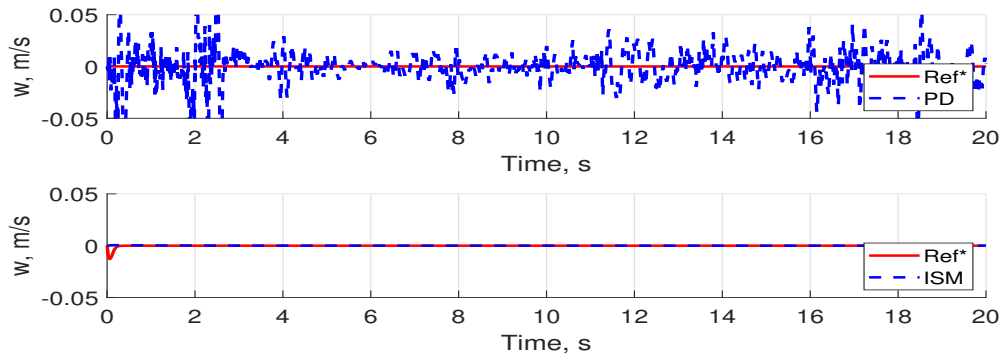

Figure 5.9: Heave velocity "w" by state feedback and integral sliding mode

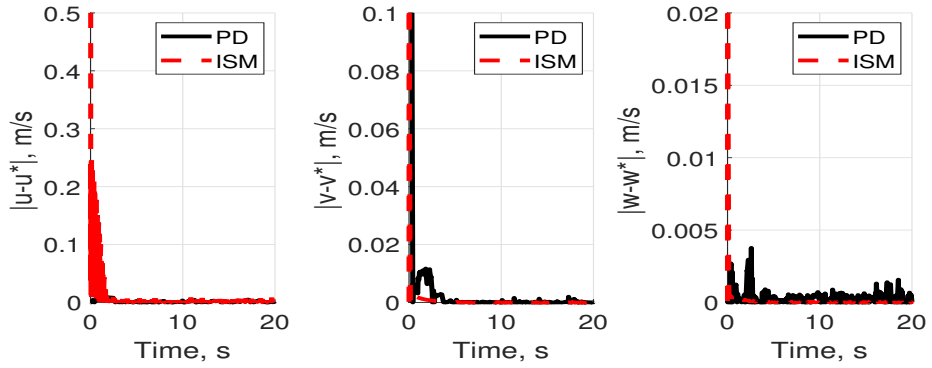

Figure 5.10: Velocity tracking error "$\delta_{2,t}$" by state feedback and integral sliding mode

Third stage

Following the angular velocity tracking, both controllers force the state to the desired trajectory as shown in figures (5.11), and (5.12). Evaluating the magnitude of the tracking error obtained by the controllers can be observed that the results obtained by the ISM controller are less than those obtained by the state feedback formulation, as can be seen in Figure (5.13).

Fourth stage

In the actuators stage, both formulations are applied, suc ceeding in forcing the actuators' development to the desired reference closing in this form of the Back-stepping formulation. In the first instant of the simulation the actuators development is the same as the reference as shown in Figures (5.14), (5.15) and (5.16). On average, in the simulations, the truster magnitude ob-

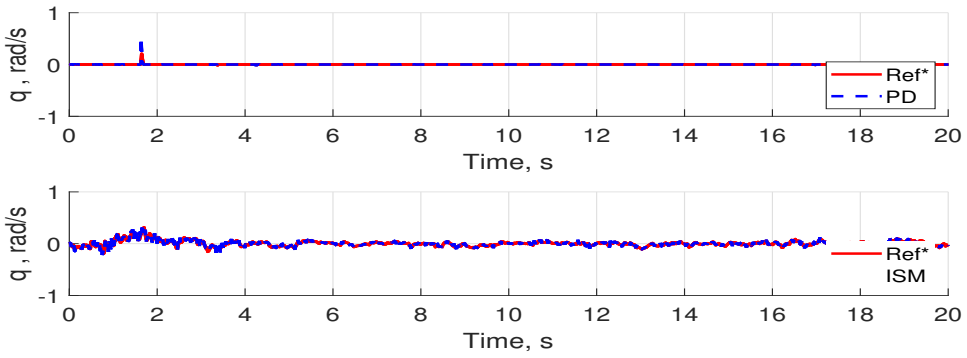

Figure 5.11: Pitch angular velocity "q" by state feedback and integral sliding mode

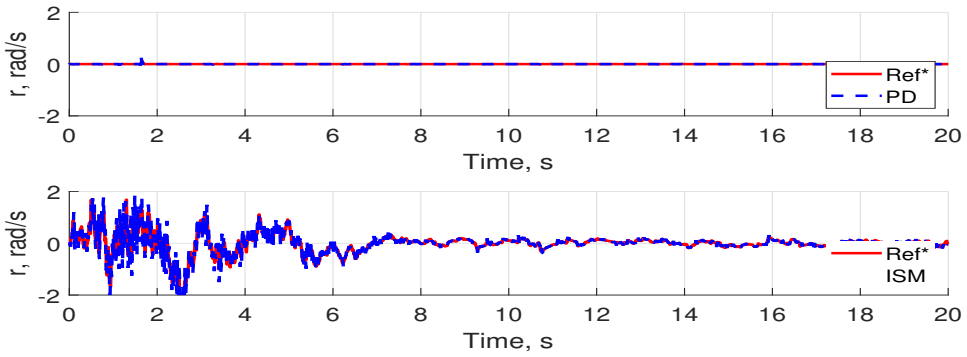

Figure 5.12: Yaw angular velocity "r" by state feedback and integral sliding mode

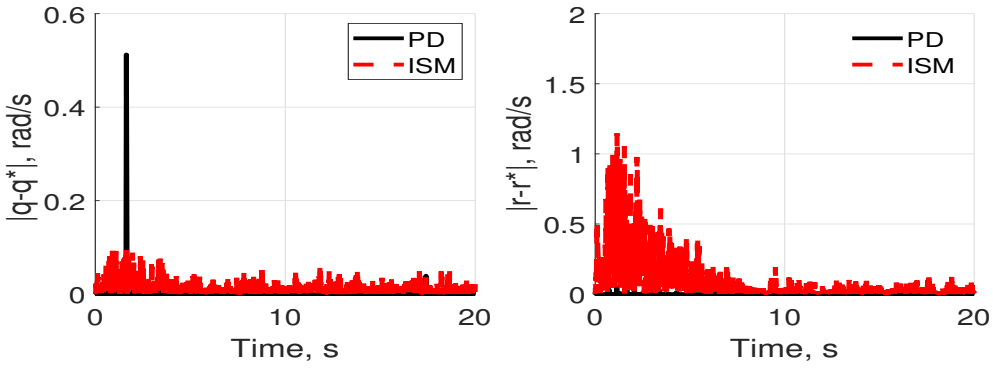

Figure 5.13: Angular velocity tracking error "$\delta_{3,t}$" by state feedback and integral sliding mode

tained by the state feedback is 100 times greater than the obtained by the ISM. The magnitude of the real controllers are presented in Figures (5.17), (5.18) and (5.19), where can be observed overdrafts in different times. The power used by the PID controller is 2.65 times higher than the

voltage used by the proposed controller. The ISM controller presents better trajectory tracking, as seen in the error norm where the ISM controller norm is less than that of the PID controller, as shown in Figure (5.20).

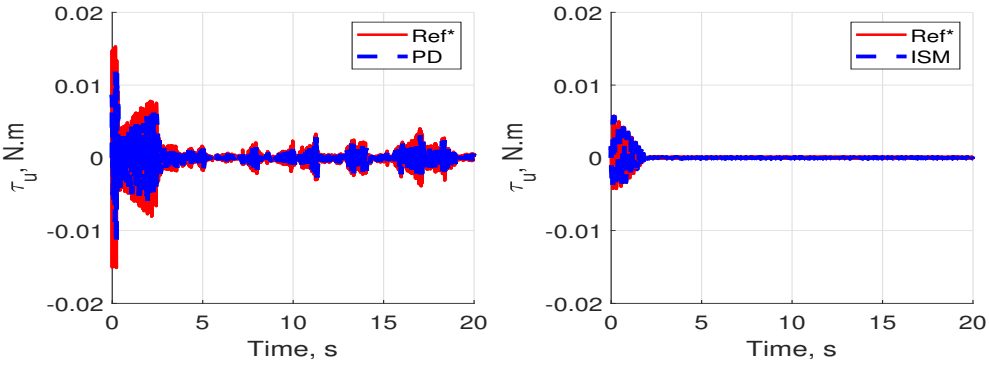

Figure 5.14: Surge torque "τ_u" by state feedback and integral sliding mode

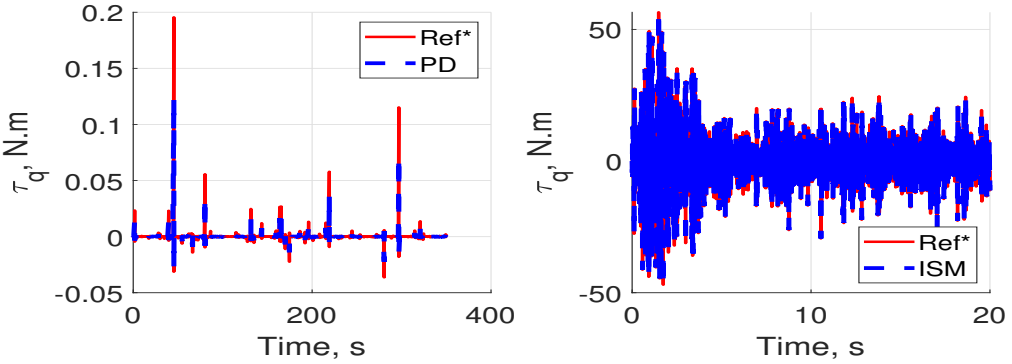

Figure 5.15: Pitch torque "τ_q" by state feedback and integral sliding mode

The gains employed in each stage are in Table (5.3).

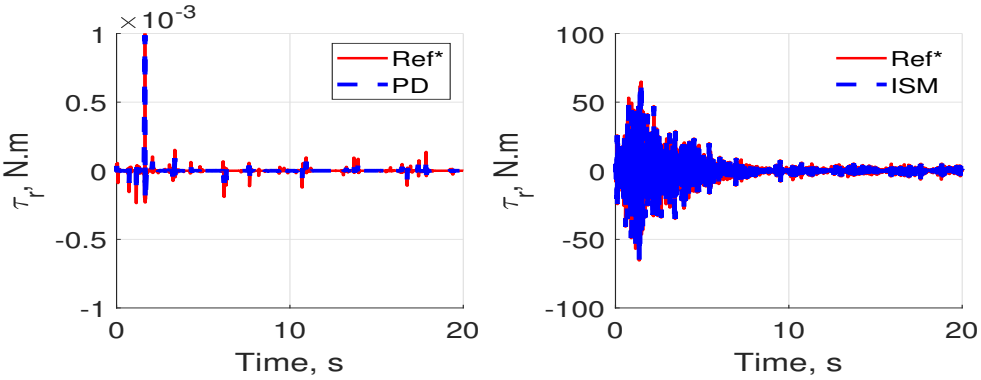

Figure 5.16: Yaw torque "τ_r" by state feedback and integral sliding mode

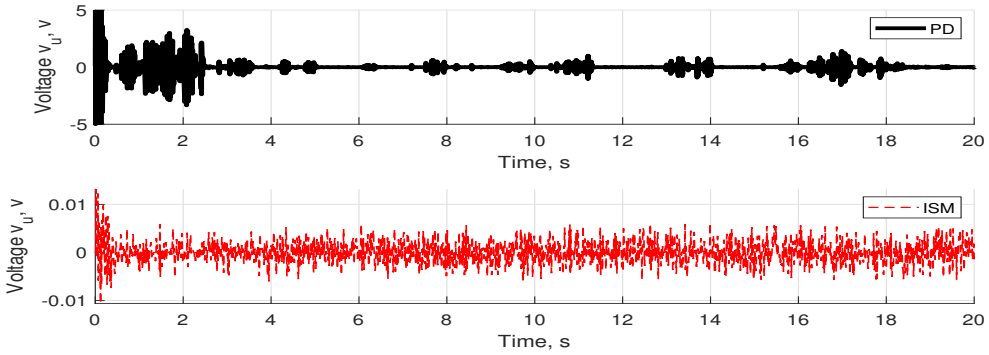

Figure 5.17: Surge voltage "v_u" by state feedback and integral sliding mode

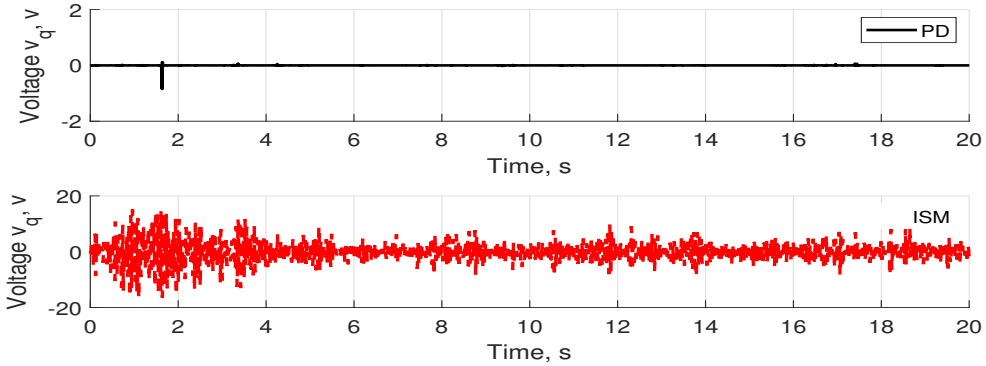

Figure 5.18: Pitch voltage "v_q" by state feedback and integral sliding mode

5.8 Pseudo-code algorithm

The algorithm steps for each stage are:

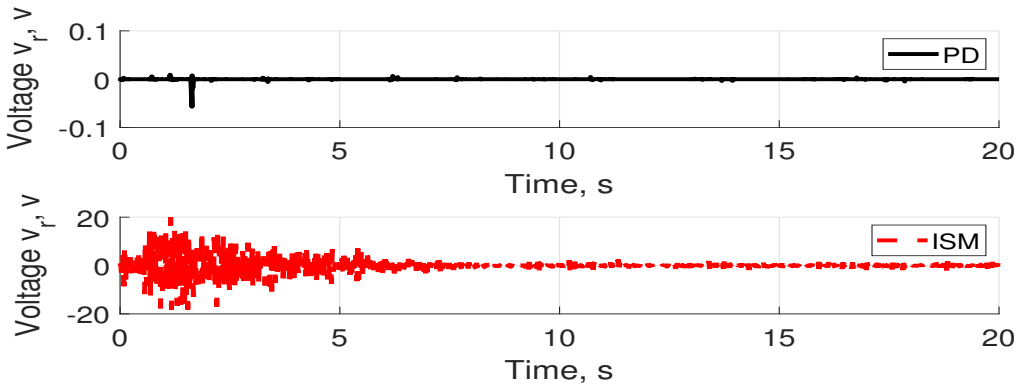

Figure 5.19: Surge voltage "v_r" by state feedback and integral sliding mode

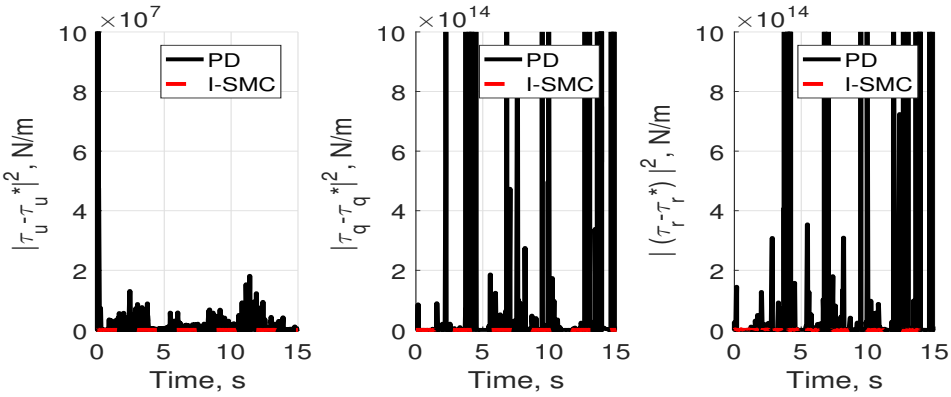

Figure 5.20: Actuator tracking error "$\delta_{4,t}$" by state feedback and integral sliding mode

1. Define the reference trajectory ρ^*.

2. Calculate the tracking trajectory error δ_1.

3. Estimate the first and second derivatives of the tracking error applying the robust exact differentiator over δ_1.

4. Calculate the first sliding surface s_1 according to the definition presented in (5.10) using the estimates of the tracking error and its first and second derivatives.

5. Implement the tracking error in the dynamic control law u_1 presented in (5.11).

6. Fix the desired velocity φ^* to the result gotten for the first back-stepping stage: $\varphi^* = u_1$

Table 5.3: Table of gains used for evaluating ISM and PID controllers.

Stage	ASG-**ISM**	**PID**
First	$\gamma_{1,0}$ $\gamma_{1,1}$ $\gamma_{1,2}$ $\gamma_{1,3}$ $B^{+}_{\varphi 1}$ 8 7 6 .7 1	$K_p = diag([\ -30 \quad 40 \quad -40\ ])$ $K_d = 0$ $K_i = 0$
Second	$\gamma_{2,0}$ $\gamma_{2,1}$ $\gamma_{2,2}$ $\gamma_{2,3}$ $B^{+}_{\varphi 2}$ $1*10^4$ $5*10^7$ 50 5 1	$K_p = 2\mathbb{I}_2$ $K_d = \mathbb{I}_2$ $K_i = 0.3\mathbb{I}_2$
Third	$\gamma_{3,0}$ $\gamma_{3,1}$ $\gamma_{3,2}$ $\gamma_{3,3}$ $B^{+}_{\varphi 3}$ 10^2 10^2 10^2 10^{-4} 1 10^9 10^{11} 10^{11} 10^{-6} .5 10^9 10^{11} 10^{11} 10^{-6} .5	$K_p = diag([\ -5 \quad -2 \quad -2\ ])$ $K_d = diag([\ -2 \quad 0.5 \quad -2\ ])$ $K_i = diag([\ -4 \quad 2 \quad -2\ ])$
Fourth	$\gamma_{4,0}$ $\gamma_{4,1}$ $\gamma_{4,2}$ $\gamma_{4,3}$ $B^{+}_{\varphi 4}$ 50 $5*10^6$ $7*10^3$ 7 .5	K_p $20\mathbb{I}_3$ K_d $\mathbb{I}_3$ K_i $diag([\ 12 \quad 12 \quad 7\ ])$

7. Calculate the first and second-time derivatives of φ^* using a robust exact differentiator such as a super-twisting algorithm for each component of φ^*

8. Calculate the second sliding surface s_2 according to the definition presented in (5.24) using the estimates of the error between φ and φ^* and its first and second derivatives.

9. Implement the tracking error in the dynamic control law u_2 presented in (5.25).

10. Fix the desired current I^* to the result for the second back-stepping stage depending on the estimation of u_2.

11. Calculate the first and second-time derivatives of I^* using a robust exact differentiator such as a super-twisting algorithm.

12. Calculate the third sliding surface s_3 according to the definition presented in expression

(5.37) using the estimates of the error between I and I^* and its first and second derivatives.

13. Implement the tracking error in the dynamic control law u_3 presented in (5.38)

5.9 Chapter Conclusions

This chapter obtained the complete formulation of Back-stepping in general form for UV. With this formulation is possible to get new ways to solve the trajectory tracking for underactuated systems. In this form is possible to formulate a robust reference to the unacknowledged dynamic and variation of parameters in each stage of the formulation. A numerical example for the tracking trajectory of an underwater UV was presented, showing an example for underactuated systems. The proposed controllers' implementation in underwater vehicles' dynamics was presented, demonstrating greater efficiency than the PID controller.

Chapter 6

Output Feedback Realisation of Averaged Subgradient Integral Sliding Mode Control

6.1 Chapther Introduction

In UV control, the ignorance of some variables and parameters on the UV dynamic can increase the number of uncertainties to be resolved and increases the energy demand in the controller to compensate for unknown disturbances. In practice, some variables are impossible to measure, so the use of estimations is common to obtain information about variables and parameters. Therefore, this section proposes two solutions to the optimal tracking problem: integrating variables and parameter estimation through an observer formulation by super twisting. Integrating these formulations allows us to reduce the robustness demand of the previously presented controller, and a more precise controller is made by reasonably estimating the variables and parameters. This chapter presents the theoretical control formulation estimating the parameter ε_t and using the estimation of UV velocities. Also, this section presents numerical evaluations in an underwater vehicle through the numerical evaluation in the Matlab/Simulink platform for the case with the estimation of the UV velocities.

6.2 Variables

A list of the variables used in this chapter is included in Table 6.1

$U_{\mathbf{x}}$	Control vector
$s_{\mathbf{x}}$	Integral sliding variable
ε	Sliding converge zone
$G_{\mathbf{x}}^{+}$	Bound of control matrix
x_a	Tracking error vector
x_b	Time derivative of tracking error vector
$F_{\mathbf{x}}$	Forces in the UV dynamic
$k_{\mathbf{x}}$	Control gains
$\hat{\varepsilon}_{\mathbf{x}}$	Estimation of integral sliding converge zone
z_1	Auxiliary variable
z_2	Time derivative of z_1
Δ_1	Estimation error of z_1
Δ_2	Estimation error of z_2
$\hat{x}_a$	Estimation of tracking error x_a
$\hat{x}_b$	Estimation of time derivative of the tracking error x_b
$e_{\mathbf{x}}$	Estimation error of the tracking error
$\hat{s}$	Estimation of sliding variable
H	Cost functional of the tracking error
A	Projection matrix

Table 6.1: Output feedback Variables

6.3 Output feedback with ε estimation

6.3.1 The problem statement in descriptive form

Given the proposed solution in chapter 4 by the State feedback form and considering that the derivative of the parameter ε_t is unknown, the stages of the problem are the following:

- The error estimation of ε_t: design of the dynamic of the estimator that reduces the error estimation $\tilde{\varepsilon}_t$.

- The description of the tracking trajectory control problem for the UV is as follows: to regulate the trajectory tracking error, making it as small as possible, and by the use of the ideal continuous signal $\mathbf{u}_{\mathbf{x},t}$ (in the function of the estimated ε_t) using the ASG formulation.

The control law for state feedback is described in chapter 4 in expression (4.13) for the state feedback by the tracking error.

$$\mathbf{u}_{\mathbf{x},t} = G_x^+ k_{\mathbf{x},t} \frac{s_{\mathbf{x},t}}{||s_{\mathbf{x},t}|| + \varepsilon_t} \tag{6.1}$$

Defining the estimated control $\hat{u}$ as

$$\hat{\mathbf{u}}_{\mathbf{x},t} \quad = \quad G_x^+ \hat{k}_{\mathbf{x},t} \frac{s_t}{||s_t|| + \varepsilon_t} \tag{6.2}$$

The dynamic in the close loop for the tracking error is given by:

$$\begin{aligned} \dot{\mathbf{x}}_{b,t} &= F_{\mathbf{x},t} - \hat{k}_{\mathbf{x},t} \frac{s_t}{||s_t|| + \varepsilon_t} \\ &= F_{\mathbf{x},t} - k_{\mathbf{x},t} S_s(s_t) - \left(\hat{k}_{\mathbf{x},t} - k_{\mathbf{x},t}\right) S_s(s_t) \end{aligned}$$

where the function $S_s(\bullet)$

$$S_s(s_t) := \frac{s_t}{||s_t|| + \varepsilon_t} \tag{6.3}$$

Defining the error estimation of $k_{\mathbf{x},t}$ as

$$\begin{aligned}
\tilde{k}_{\mathbf{x},t} &= \hat{k}_{\mathbf{x},t} - k_{\mathbf{x},t} \\
&= 2\left(\gamma_G^{-1}\mathbf{z}_{\mathbf{x},t}^{(1)} + k_0\right) - 2\left(\gamma_G^{-1}\mathbf{z}_{\mathbf{x},t}^{(1)} + k_0\right) \\
&= 2\left(\gamma_G^{-1}F_{\mathbf{x}}^{+} + \left\|\mathbf{z}_{\mathbf{x},t}^{(0)}\right\| + \left|\dot{\hat{\varepsilon}}_t\right| + k_0\right) \\
&\quad -2\left(\gamma_G^{-1}F_{\mathbf{x}}^{+} + \left\|\mathbf{z}_{\mathbf{x},t}^{(0)}\right\| + \left|\dot{\varepsilon}_t\right| + k_0\right) \\
&= 2\left(\left|\dot{\hat{\varepsilon}}_t\right| - \left|\dot{\varepsilon}_t\right|\right)
\end{aligned} \tag{6.4}$$

In consequence, the close loop equation (6.3) can be described as

$$\begin{aligned}
\dot{\mathbf{x}}_{b,t} &= F_{\mathbf{x},t} - k_{\mathbf{x},t}S_s(s_t) - \tilde{k}_{\mathbf{x},t}S_s(s_{\mathbf{x},t}) \\
&= F_{\mathbf{x},t} - k_{\mathbf{x},t}S_s(s_{\mathbf{x},t}) - 2\left(\left|\dot{\hat{\varepsilon}}_t\right| - \left|\dot{\varepsilon}_t\right|\right)S_s(s_t)
\end{aligned} \tag{6.5}$$

New variables are defined $z_1 = \varepsilon$ and $z_2 = \dot{\varepsilon}$ with dynamic described by

$$\begin{aligned}
\dot{z}_{1,t} &= z_{2,t} \\
\dot{z}_{2,t} &= \ddot{\varepsilon}_t
\end{aligned} \tag{6.6}$$

the defining estimated variables of ε as

$$\begin{aligned}
\hat{\varepsilon}_t &:= \hat{z}_1 \\
\dot{\hat{\varepsilon}}_t &:= \hat{z}_{2,t} + l_1|\Delta_{1,t}|^{1/2}sign(\Delta_{1,t})
\end{aligned} \tag{6.7}$$

where the corresponding estimation error as $\Delta_1 := \hat{z}_1 - z_1$ with dynamic given by

$$\begin{aligned}
\dot{\Delta}_{1,t} &= \hat{z}_{2,t} + l_1|\Delta_{1,t}|^{1/2}sign(\Delta_{1,t}) - z_{2,t} \\
&= \hat{z}_{2,t} - z_{2,t} + l_1\|\Delta_{1,t}\|^{1/2}sign(\Delta_{1,t}) \\
&= \Delta_{2,t} + l_1|\Delta_{1,t}|^{1/2}sign(\Delta_{1,t}) \\
\dot{\Delta}_{2,t} &= l_2 sign(\Delta_{1,t}) - \ddot{\varepsilon}_t
\end{aligned} \tag{6.8}$$

The complete state is given by

$$\begin{aligned}
\dot{\mathbf{x}}_{a,t} &= \dot{\mathbf{x}}_{b,t} \\
\dot{\mathbf{x}}_{b,t} &= F_{\mathbf{x},t} - k_{\mathbf{x},t}S_s(s_t) - 2\Delta_2 S_s(s_t) \\
\dot{\Delta}_{1,t} &= \Delta_{2,t} + l_1|\Delta_{1,t}|^{1/2}sign(\Delta_{1,t}) \\
\dot{\Delta}_{2,t} &= l_2 sign(\Delta_{1,t}) - \ddot{\varepsilon}_t
\end{aligned} \tag{6.9}$$

6.4 Output feedback with the estimation of the velocity

6.4.1 The problem statement in descriptive form

The control problem considered in this section is the design of an output feedback controller $\mathbf{u_x} \in U_{adm}$ such that the trajectory tracking error between the current position (x,y,z) and the reference trajectories (x^*,y^*,z^*) can be driven to the origin considering that such position error is measurable while the vector $\dot{\varphi}$ is determined implementing a robust exact differentiator. The references trajectories $\sigma^* \in \mathbb{R}^3$ are continuous time-dependent functions ($\sigma^* = \begin{bmatrix} x^*, & y^*, & z^* \end{bmatrix}^\top$.) satisfying that their second full-time derivatives satisfy the following inequality:

$$\|\ddot{\varphi}_t^*\| \leq \Phi^+ \tag{6.10}$$

with Φ^+ a positive scalar.

6.4.2 Trajectory tracking analysis

Dynamic of the tracking error

Taking the position tracking error $\mathbf{x}_a$ as in Chapter 3 for the case of the tracking error in the 3D space. According to the UV model, this vector can be expressed as:

$$\mathbf{x}_{a,t} = A\rho_t - \sigma_t^* = [x-x^*, y-y^*, z-z^*]^\top, \tag{6.11}$$

where A is the projection matrix, for this case defined as $A = \begin{bmatrix} \mathbb{I}_{3x3} & 0_{3x3} \end{bmatrix}$

The velocity of the tracking error is defined as

$$\mathbf{x}_{b,t} := A\dot{\rho}_t - \dot{\sigma}_t^* \tag{6.12}$$

Considering the UV dynamics in the equation (2.14), the complete tracking error dynamics can be expressed as follows:

$$\begin{aligned} \dot{\mathbf{x}}_{a,t} &= \mathbf{x}_{b,t}, \\ \dot{\mathbf{x}}_{b,t} &= F_{\mathbf{x},t} + G_{\mathbf{x},t}\mathbf{u}_{\mathbf{x},t}, \end{aligned} \tag{6.13}$$

For this case, the expression of $F_{\mathbf{x}}$ is the same as in the expression (4.7), and for $G_{\mathbf{x}}$ the following expression has been used:

$$\begin{aligned} G_{\mathbf{x},t} :=& A\mathbf{J}(\rho_t)\mathbb{M}^{-1}B \\ =& m^{-1}\mathbf{R}(\rho_{\mathbf{t}}) \begin{bmatrix} 1 & 0 & 0 \\ 0 & Y_{u\alpha_v} & 0 \\ 0 & 0 & -Z_{u\alpha_h} \end{bmatrix}. \end{aligned} \tag{6.14}$$

Notice that the matrix $G_{\mathbf{x}}$ satisfies the following property: $\det(G_{\mathbf{x}}) \neq 0$, hence $G_{\mathbf{x}}$ is invertible. Both matrices $F_{\mathbf{x}}$ and $G_{\mathbf{x}}$ satisfy the inequalities (4.8)

Given that the position vector ρ_t with respect to the inertial frame can be measured online, while the velocity in the frame $[a]$ cannot, the vector $\dot{\rho}$ is estimated. The estimation of vector $\dot{\mathbf{x}}_{a,}$ is using a numerical differentiator (super-twisting). The estimation of $\mathbf{x}_{a,t}$ given by the variable $\hat{\mathbf{x}}_{a,t}$ use the estimation error defined as $e_{\mathbf{x}} := \hat{\mathbf{x}}_a - \mathbf{x}_a$, considering the following general form of the super-twisting algorithm (presented for each of components of $\mathbf{x}_a$, i.e. $\mathbf{x}_{a,i}$) and remembering that $\dot{\mathbf{x}}_{a,t} = \mathbf{x}_{b,t}$:

$$\begin{aligned} \hat{\mathbf{x}}_{b,i,t} &= z_{1,t}^{(i)} - \alpha_{0,i} \left| e_{\mathbf{x},i,t} \right|^{1/2} \operatorname{sign}(e_{\mathbf{x},i,t}) \\ \tfrac{d}{dt} z_{1,t}^{(i)} &= -\alpha_{1,i} \operatorname{sign}(e_{\mathbf{x},i,t}) \end{aligned}$$

The following [32] the super-twisting algorithm must satisfy the expression

$$\alpha_{1,i} > L_{1,i}, \alpha_{0,i}^2 > 4L_{1,i}\frac{\alpha_{1,i}+L_{1,i}}{\alpha_{1,i}-L_{1,i}}, L_{1,i} \geq \left|\hat{\mathbf{x}}_{b,i,t}\right| \tag{6.15}$$

To get the finite-time recovering of the derivative of the variable under analysis.

Given the vector $\hat{\mathbf{x}}_a := \begin{bmatrix} \hat{\mathbf{x}}_{a,1} & \hat{\mathbf{x}}_{a,2} & \hat{\mathbf{x}}_{a,3} \end{bmatrix}^\top$, that satisfy the following dynamic [36]:

$$\hat{\mathbf{x}}_{b,i,t} = \tfrac{d}{dt} z_{1,t}^{(i)} - \frac{1}{2}\alpha_{0,i} sign\left(e_{\mathbf{x},i,t}\right) \left|e_{\mathbf{x},i,t}\right|^{-1/2} \times \left(\frac{d}{dt} e_{\mathbf{x},i,t}\right) sign\left(e_{\mathbf{x},i,t}\right) \tag{6.16}$$

where $\hat{\mathbf{x}}_{b,i}$ is each component of $\hat{\mathbf{x}}_b$. According to the continuity arguments in [36], the differential equation is true almost everywhere

6.4.3 Desired sliding regimen

Using the integral sliding variable s for the integral sliding mode [54] used in the Chapter 3 in the expression (4.12), subject to the expression

$$\left.\begin{aligned} s_t &= \mathbf{x}_{b,t} + \frac{\mathbf{x}_{a,t} + \eta}{t + \mu_0} + \Psi_t, \\ \Psi_t &= \frac{1}{t + \mu_0} \int_{\tau=0}^{t} \partial H(\mathbf{x}_{a,\tau}) d\tau, \end{aligned}\right\} \tag{6.17}$$

where μ_0 is a positive constant scalar.

In this chapter, the convex function $H(\mathbf{x}_a)$, non-strictly convex and not obligatory differentiable, is the same as the state feedback formulation and, for this case, is given by:

$$H(\mathbf{x}_{a,t}) = |x_t - x_t^*| + |y_t - y_t^*| + |z_t - z_t^*|, \tag{6.18}$$

The function $H(\mathbf{x}_a)$ satisfies the following inequality

$$H(\mathbf{x}_a) \geq \min_{\mathbf{x}_{a,t}} H(\mathbf{x}_{a,t}) = H^* = 0$$

(assuming that $\mathbf{x}_a$ is in a given closed set) and

$$\mathbf{x}_{a,t}^{\top} \partial H(\mathbf{x}_{a,t}) \geq H(\mathbf{x}_{a,t}) - H^* = H(\mathbf{x}_{a,t}), \quad \mathbf{x}_a \in \mathbb{R}^3 \tag{6.19}$$

(valid for any convex function).

Given the assumption for this chapter that $\mathbf{x}_b$ cannot be measured online, the use of their corresponding estimation represented by $\hat{\mathbf{x}}_b$ implies that the integral sliding surface s must be adjusted to the auxiliary integral sliding surface $\hat{s}$:

$$\left.\begin{aligned} \hat{s}_t &= \hat{\mathbf{x}}_{b,t} + \frac{\mathbf{x}_{a,t} + \eta}{t + \mu_0} + \Psi_t, \\ \Psi_t &= \frac{1}{t + \mu_0} \int_{\tau=0}^{t} \partial H(\mathbf{x}_{a,\tau}) d\tau, \end{aligned}\right\} \tag{6.20}$$

Now, the corresponding time variation of the modified sliding variable is:

$$\frac{d}{dt}\hat{s}_t = \frac{d}{dt}\hat{\mathbf{x}}_{b,t} + \frac{\mathbf{x}_{b,t} + \partial H(\mathbf{x}_{a,t}) - \Psi_t}{t + \mu_0} - \frac{\mathbf{x}_{a,t} + \eta}{(t + \mu_0)^2} \tag{6.21}$$

Considering the case that the sliding variable is in the sliding regimen beginning at the time t_0, the next equation is considered valid.

$$\|\hat{s}_t\| \leq \varepsilon_s, \ \forall t \geq t_0. \tag{6.22}$$

The instant in which the sliding variable is in the desired regimen implies a modification in the behaviour of the cost function in such a way that the value of the sliding variable decreases with respect to time. Yielding to change ε_s by a time-varying equivalent $\varepsilon_{s,t}$. The following lemma describes how to get the solution of the corresponding implication.

Lemma 4. *In the sliding regime described in equation* (6.22) *with any scalar* $\mu_0 > 0$ *and defining the time dependent function* ε_t *as*

$$\varepsilon_t = \frac{\varepsilon_0}{(t+\mu)^{1+\gamma}} \tag{6.23}$$

where $\varepsilon_0 > 0$, $\gamma > 0$ *and for any* $t \geq t_0 \geq 0$ *we can guarantee that*

$$\begin{aligned} H(\mathbf{x}_{a,t}) &\leq \frac{\Omega_{t_0}}{t+\mu_0} - \frac{\kappa\varepsilon_0}{(1-\gamma)(t+\mu_0)^{1+\gamma}}, \\ \Omega_{t_0} &= \mu_{t_0}^{-1} H(\mathbf{x}_{a,t_0}) + \frac{1}{2}\|\eta\|^2. \end{aligned} \tag{6.24}$$

where $\kappa > 0$ *and* $\mu_{t_0}^{-1} = t_0 + \mu_0$.

The proof of this lemma is provided in the Appendix part in section 10.3.

6.4.4 Control problem

In the same way as in the state feedback formulation, given the definition of $H(\mathbf{x}_a)$ in expression(6.18), reformulate the trajectory tracking problem as an optimisation of the cost functional $H(\mathbf{x}_a)$ based on the ASG approach in the following form:

Problem 1. *The optimization control problem is to design* $\mathbf{u}_\mathbf{x}$ *for the UV subject to the dynamic expression* (2.14) *such that it solves the UV tracking error* $\mathbf{x}_a$ *(difference between* $A\rho$ *and* σ^**). Forcing* $\mathbf{x}_a$ *to the optimal solution* $\mathbf{x}_a^*$*, according to an optimal trajectory. Hence, for the optimal* $\mathbf{x}_a^*$ *the functional of the tracking error* $H(\mathbf{x}_a)$ *satisfies*

$$H(\mathbf{x}_a^*) := \min_{\mathbf{x}_{a,t} \in \mathbb{R}^3} H(\mathbf{x}_a) \tag{6.25}$$

Then

$$H(\mathbf{x}_a(\mathbf{u}_\mathbf{x})) \to H^*. \tag{6.26}$$

6.4.5 Control formulation

The proposed controller for the auxiliary dynamic (6.13) satisfies the following structure:

$$\left.\begin{array}{c} \mathbf{u}_{\mathbf{x},t} = G_\mathbf{x}^{-1}\left(\mathbf{u}_{1,t} + \mathbf{u}_{2,t}\right) \\ \\ \mathbf{u}_{1,t} = -\dfrac{\hat{\mathbf{x}}_{b,t} + \partial H(\mathbf{x}_{a,t}) - \Psi_t}{t+\mu_0} + \dfrac{\mathbf{x}_{a,t} + \eta}{(t+\mu_0)^2} \\ \mathbf{u}_{2,t} = -k_t \dfrac{\hat{s}_t + e_{s,t}}{\|\hat{s}_t + e_{s,t}\| + \varepsilon_t} - \dfrac{d}{dt}\hat{\mathbf{x}}_{b,t} \\ e_{s,t} = s_t - \hat{s}_t. \end{array}\right\} \tag{6.27}$$

where $G_\mathbf{x}$ is an invertible matrix defined in expression (6.14) and $\dfrac{d}{dt}\hat{\mathbf{x}}_b$ defined in equation (6.16).

Regarding the control expression, there are two remarks:

- Taking into account the definition of s and $\hat{s}$ in equations (6.17) and (6.20) respectively, the term e_s can be expressed as:

$$e_{s,t} = \frac{d}{dt}\mathbf{x}_{b,t} - \frac{d}{dt}\hat{\mathbf{x}}_{b,t} \tag{6.28}$$

  Considering the restriction over $\dfrac{d}{dt}\mathbf{x}_b$ for the implementation of the super-twisting algorithm and the expression for $\dfrac{d}{dt}\hat{\mathbf{x}}_b$ in equation (6.4.2) the term e_s satisfies

$$\begin{array}{c} \|e_s\| \leq e_s^+ \\ e_s^+ := max\{L_{1,i}(1+\alpha_{1,i}h) + \alpha_{0,i}L_{i,t}^{1/2}h\}, \\ i = 1,2,3 \end{array} \tag{6.29}$$

  where h corresponds to the integration step size [17, 32].

- Considering the following inequalities

$$\|\hat{s}_t\| - \|e_{s,t}\| \leq \|\hat{s}_t + e_{s,t}\| \leq \|\hat{s}_t\| + \|e_{s,t}\| \tag{6.30}$$

the term $\mathbf{u}_2$ is subject to the following inequality

$$\|\mathbf{u}_{2,t}\| \leq -k_t \frac{\|\hat{s}_t\|}{\|\hat{s}_t\| + \|e_{s,t}\| + \varepsilon_t} + k_t \frac{\|e_{s,t}\|}{\|\hat{s}_t\| + \|e_{s,t}\| + \varepsilon_t}, \tag{6.31}$$

also, given the expression

$$\|\hat{s}_t\| + e_s^+ \geq \|\hat{s}_t\| + \|e_{s,t}\| \geq \|\hat{s}_t\| \tag{6.32}$$

where $e_s^+ > 0$, implies the following condition

$$-\frac{1}{\|\hat{s}_t\| + \|e_{s,t}\| + \varepsilon_t} \leq -\frac{1}{\|\hat{s}_t\| + e_s^+ + \varepsilon_t}$$

Therefore, the inequality 6.31 can be expressed as

$$\|\mathbf{u}_{2,t}\| \leq -k_t \frac{\|\hat{s}_t\|}{\|\hat{s}_t\| + e_s^+ + \varepsilon_t} + k_t \frac{\|e_{s,t}\|}{\|\hat{s}_t\| + \|e_{s,t}\| + \varepsilon_t} \tag{6.33}$$

Defining the new term $\varepsilon_1 := e_s^+ + \varepsilon_t$, finally, the expression (6.33) becomes

$$\|\mathbf{u}_{2,t}\| \leq -k_t \frac{\|\hat{s}_t\|}{\|\hat{s}_t\| + \varepsilon_1} + k_t \frac{\|e_{s,t}\|}{\|\hat{s}_t\| + \varepsilon_1} \tag{6.34}$$

Given the property of boundedness for $F_{\mathbf{x}}$ given in the expression (2.9), a kind of separation principle can be used here such that the dynamic of the ISM controller without an observer can be recovered using the STA with gains selected according to the strategy given in [3].

The next theorem describes the explicit form of the function k_t in the controller $\mathbf{u}_2$, which completes with the optimisation solution.

Theorem 5. *If the time-dependent gain k_t is chosen as*

$$k_t = 2\left(F_{\mathbf{x}}^+ + \left|\frac{d}{dt}\varepsilon_t\right| + k_0\right) \tag{6.35}$$

with

$$\frac{d}{dt}\varepsilon_t = \frac{\varepsilon_0}{(t+\mu_0)^{1+\gamma}}, \quad k_0 > 0 \tag{6.36}$$

then, the desired sliding regime (6.22) *is obtained in a finite time which is bounded by:*

$$t_0 = \sqrt{2}k_0^{-1}\|s_{t_0}\|. \tag{6.37}$$

Corollary 3. *Using the specification of the starting time t_0 in* (6.37) *implies that the following expressions are satisfied*

$$H(\mathbf{x}_{a,t}) \leq \frac{\Omega_{t_0}}{t+\mu_0} - \frac{\kappa\varepsilon_0}{(1-\gamma)(t+\mu_0)^{1+\gamma}}, \qquad (6.38)$$

$$\Omega_0 = \mu_{t_0}^{-1} H(\mathbf{x}_{a,t_0}) + \frac{1}{2}\|\eta\|^2,$$

or equivalently

$$\hat{s}_{t_0} = \hat{\mathbf{x}}_{b,t_0} + \frac{\mathbf{x}_{a,t_0}+\eta}{t_0+\mu_0} + \Psi_{t_0} = \frac{k_0}{2}t_0$$

with $\eta := -(t_0+\mu_0)(\hat{\mathbf{x}}_{b,t_0} + \Psi_{t_0} - \frac{k_0}{2}t_0) - \mathbf{x}_{b,t_0}$.

The controller realization corresponding to expression (4.13) agrees with the technical diagram presented in Figure 6.1.

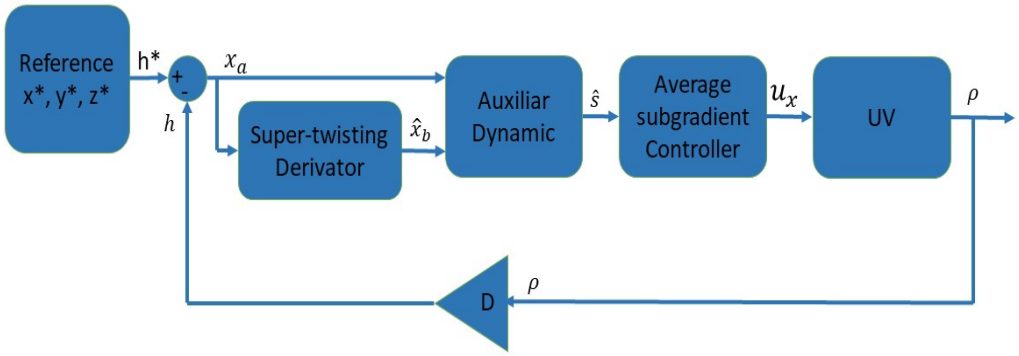

Figure 6.1: Technical diagram of the controller realisation using the ISM proposal.

Remark: The practical implementation of the suggested ISM control requires the application of modifications for the controller, including variants of the ideas proposed in studies [29,49,51]. In particular, the study introduced in [6] served to develop a well-defined practical variant for the ISM control while simplifying the fractional derivative implementation.

6.5 Numerical Evaluation

The evaluation of the output feedback controller was on manipulating an underwater UV. The algorithm employed in the numerical evaluations is the Runge-Kutta integration using a step of integration of 0.001s. The UV parameters employed are in the table (6.2) and are obtained from [10]:

Parameter	Value	Parameter	Value	Parameter	Value	Parameter	Value
m	18kg	W	176N	B	176N	z_g	0.01m
$Y_{u\delta_r}$	19.2	$Z_{u\delta_s}$	-19.2	$N_{u\delta_r}$	-7.7	$M_{u\delta_s}$	-7.7
X_u	2.4	Y_v	23	Z_w	23	K_p	0.3
M_q	9.7	N_r	9.7	Y_r	-11.5	Z_q	11.5
M_w	-3.1	N_v	3.1	$X_{u\|u\|}$	2.4	$Y_{v\|v\|}$	80
$Z_{w\|w\|}$	80	$K_{p\|p\|}$	6.10^{-4}	$M_{q\|q\|}$	9.1	$N_{r\|r\|}$	9.1
$Y_{r\|r\|}$	-0.3	$Z_{q\|q\|}$	0.3	$M_{w\|w\|}$	-1.5	$N_{v\|v\|}$	1.5

Table 6.2: Underwater Unmanned vehicle Parameters

The control task is the manipulation of the UV dynamic to track a desired trajectory in the 3-dimensional space. The trajectory is inspired in a close circuit with immersion to simulate a supervision task of a region.

Hence, this study presents the comparison implementing the three described controllers in position, orientation, and their corresponding velocities are present, as well as the magnitude of τ, the tracking error functional $H(\mathbf{x}_{a,t})$ and the energy of the tracking error $\mathbf{x}_{a,t}$. Also, implementing a state feedback controller of the form Proportional Integral Derivative and sliding mode control is a benchmark for the proposed solution. The performances of the underwater UV with the controllers in the three degrees of freedom are in Figures (6.2a), (6.2b), and (6.2c). Furthermore, the development of the tracking error, integral of the tracking error, the norm of the control signal and the sliding surface are presented for comparison between the implemented

controllers. In the first 40s. of simulation time, the three controllers force the UV dynamic to the desired trajectory reducing the tracking error in the three-dimensional displacement.

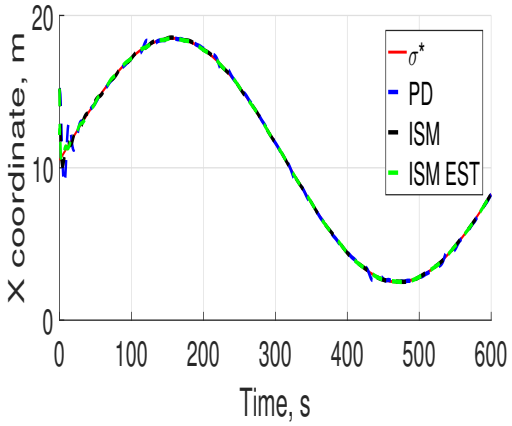

(a) Trajectory tracking on surge: reference, PD, state feedback and output feedback ISM.

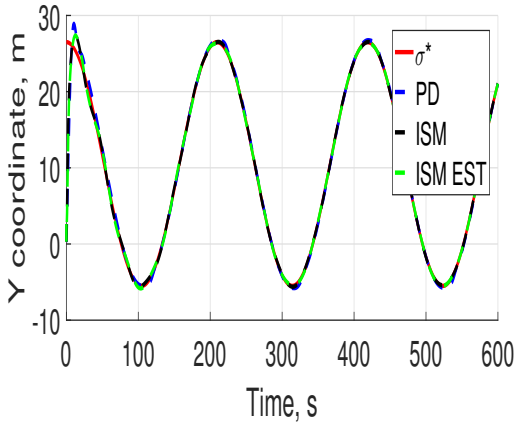

(b) Trajectory tracking on sway: reference PD, state feedback and output feedback ISM.

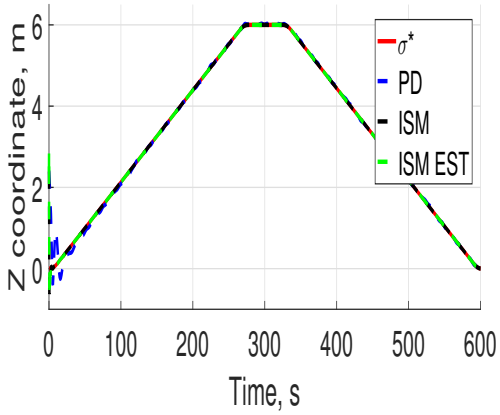

(c) Trajectory tracking on heave: reference PD, state feedback and output feedback ISM.

Figure 6.2: Trajectory tracking on the three-dimensional space: reference, PD and ISM(state and output feedback).

Perturbations are presented in the simulated dynamic in the expression (6.13) that are compensated by the controllers compensate. The control gains employed in this numerical evaluation are in the Table (8.2).

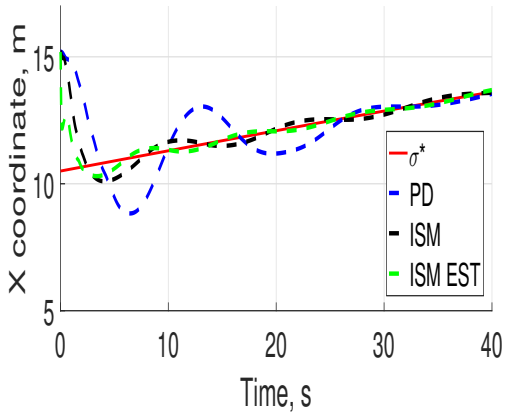

(a) First five seconds of the simulation for the trajectory tracking in surge: reference PD and ISM (state and output feedback).

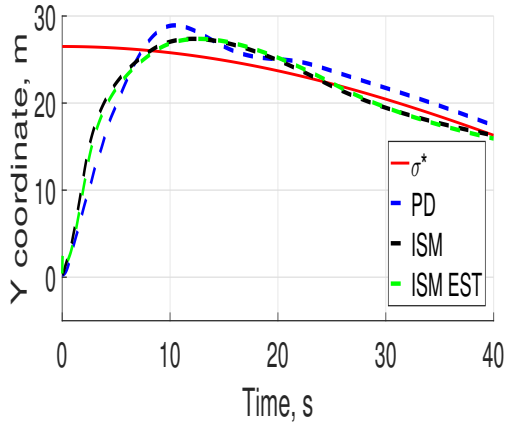

(b) First five seconds of the simulation for the tracking trajectory on sway: reference, PD and ISM (state and output feedback).

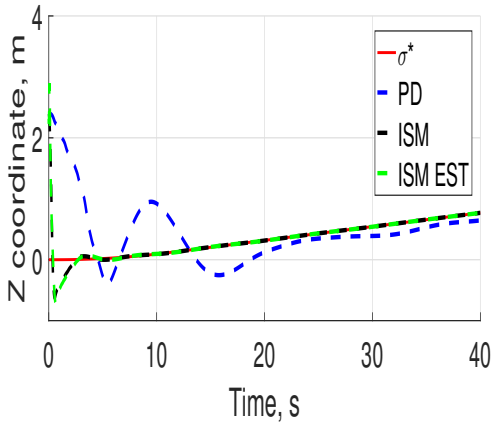

(c) First five seconds of the simulation for the tracking trajectory in Heave: reference, PD and ISM (state and output feedback).

Figure 6.3: First five seconds of the trajectory tracking on the three-dimensional space: reference, PD and ISM (state and output feedback).

The obtained trajectories present deviations in the crests of the x and y displacement. The PID tracking deviates in a more significant way than the obtained by the proposed controllers. By minimising the functional, UV motion keeps near the desired trajectory by implementing

Table 6.3: PD, ISM and ISM EST control gains for quadrotor UV

Variable	K_p	K_d	Variable	K_s	K_d	Variable	$K_{\hat{s}}$	K_d
x	2	1	x	2	1	x	2	1
y	2	1	y	2	1	y	2	1
z	350	25	z	55	35	z	55	35
θ	2	1	θ	275	0	θ	275	0
ψ	1645	5	ψ	6245	0	ψ	6245	0
ϕ	50	5	ϕ	50	5	ϕ	50	5

the ASG formulations. The development of the cost functional H is in Figure 6.4a. Figure(6.5)

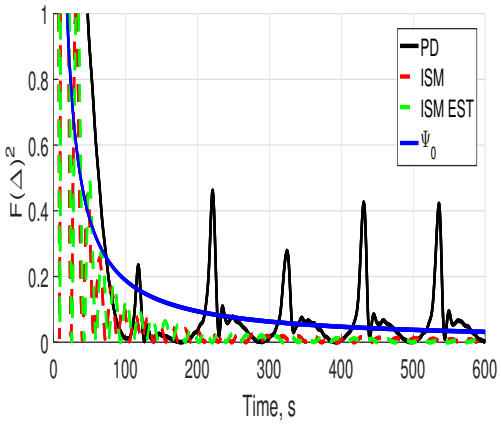

(a) Square norm of Δ: PD and ISM (state and output feedback).

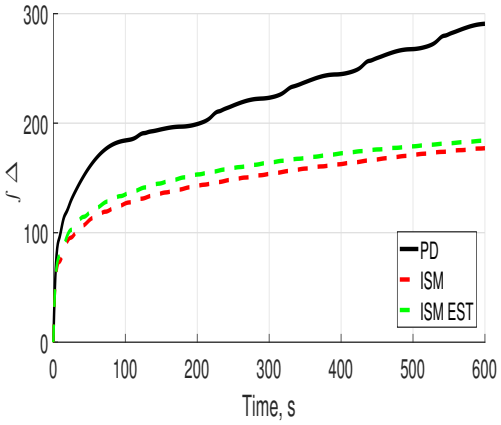

(b) Power of Δ: PD and ISM (state and output feedback).

Figure 6.4: Development of norm and power of Δ: PD and ISM (state and output feedback).

presents the development of the three controllers. For the proposed controller, the maximum value is $6.936 * 10^4$; in the case of the ISM and the PD, the maximum values are 658 and 81, respectively. For the rest of the simulation, the maximum values by the controllers are 2.5, 2.5 and 2.0, respectively. The ISM controllers' high value at the simulation's beginning is due to the velocity estimation transient period and to turn of the sliding surface.

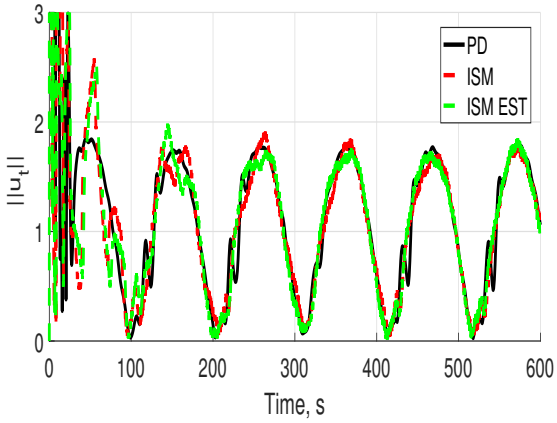

Figure 6.5: Square norm of $\mathbf{u_t}$ for PD and ISM (state and output feedback).

The cost functional development by the three controllers are depicted in Figure (6.4a). The bound for the cost functional by the PID is less than 0.6; for the case of the two controllers, the bound of the cost functional is less than 0.2 and keeps decreasing throughout the simulation time.

Also, the tracking error's integral is presented in Figure (6.4b) to give another point of view for comparison. The difference between the ISM and the output feedback version is 2%, demonstrating that the estimation technique does not affect the tracking quality. A similar conclusion can be obtained from the evolution of the torque applied over the UV (Figure (6.5)).

Figure (6.6) shows the three controllers' UV development in the three-dimensional space. The more significant deviations around the trajectory are by the PID controller in different moments of the tracking. The ISM controller ISM using the proposed observer presents a better tracking of the reference even with the presence of the estimation error and perturbations, with only partial knowledge of the UV model.

For the proposed solutions, Figure (6.7) shows the sliding surface for comparison.

6.6 Pseudo-code algorithm

The algorithm steps are:

1. Define the reference trajectory ρ^*.

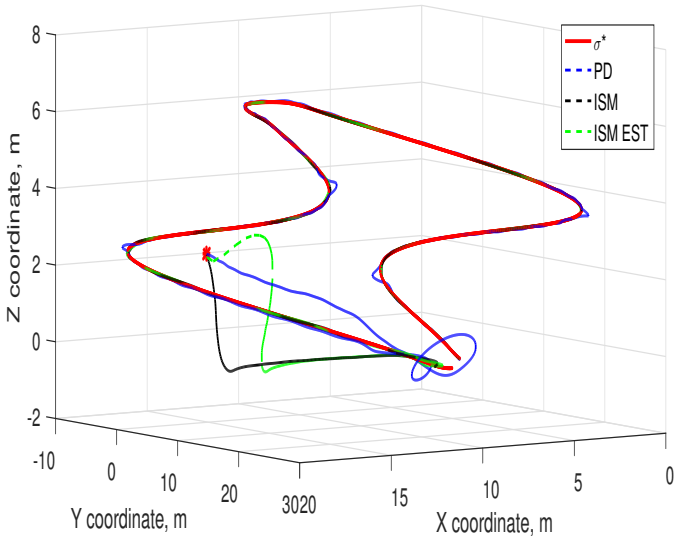

Figure 6.6: Tracking trajectory in the coordinate system xyz: reference, PD and ISM (state and output feedback).

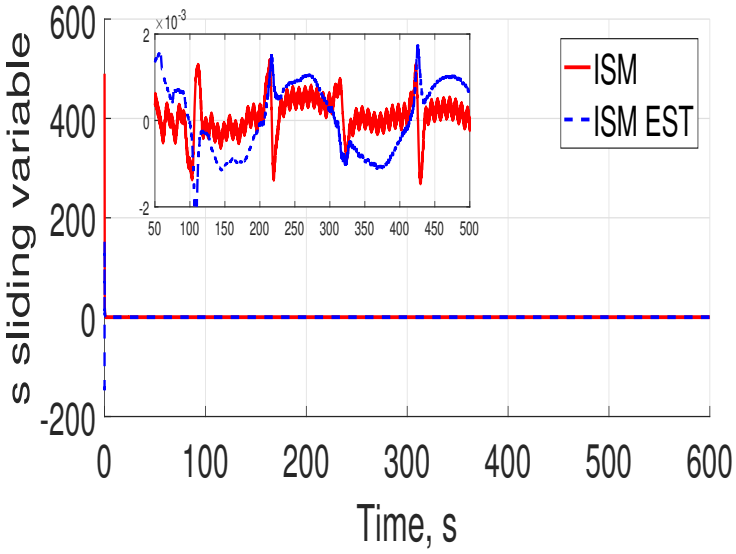

Figure 6.7: Sliding variable for the state feedback controller and the output feedback controller.

2. Calculate the tracking trajectory error x_a.

3. Estimate the first and second derivatives of the tracking error applying the robust exact differentiator over x_a.

4. Calculate the estimate sliding variable $\hat{s}$ according to the definition presented in expression (6.20) using the estimates of the tracking error and its first and second derivatives.

5. Implement the tracking error in the dynamic control law $u_{\mathbf{x}}$ presented in expression (6.27).

6.7 Chapter Conclusions

In this chapter, two solutions were developed based on the ASG algorithm and the estimation by the technique of super twisting. The boundedness of the tracking error was obtained even with the employment of estimation of variables. This chapter demonstrates that the output feedback tracking performance is comparable to the one with state feedback with similar energy consumption. Consequently, it implies reducing the instrumentation complexity and cost without more energy investment and good reference tracking. The numerical results confirm that the designed controller presents a better tracking over the trajectory even with the estimation error and the same steady-state behaviour.

Chapter 7

Backstepping Realization of Averaged Subgradient Integral Sliding Mode using Integral of the tracking error

7.1 Chapter Introduction

As mentioned before, different formulations exist that estimate the dynamic of variables with the task of getting better control over the UV. However, employment of the derivative often introduces noises to the signals concerning the sampling period and the numeric algorithm to employ. This chapter is presented the position tracking problem of a UV device as an optimisation problem of a cost functional of the integral of the tracking error by the algorithm of average subgradient with the technique of ISM. A numerical evaluation is presented to support the proposed solution. Comments on the results and conclusions are at the end of the chapter.

7.2 Variables

A list of the variables used in this chapter is included in Table 7.1

ρ	Position vector
ρ^*	Position vector
Δ_1	Translation position tracking error
Δ_2	Integral of the translation position tracking error
φ_1	Translational velocity vector
φ_1^*	Desired translational velocity vector
Δ_3	Translation Velocity tracking error
Δ_4	Integral of translation velocity tracking error
Δ_5	Velocity tracking error
Δ_6	Integral of velocity tracking error
H_1	Cost functional of integral of the translation position tracking error
H_2	Cost functional of integral of translation velocity tracking error
H_3	Cost functional of integral of velocity tracking error
s_1	Integral sliding variable
s_2	Integral sliding variable
s_3	Integral sliding variable

Table 7.1: Backstepping formulation using integral of the tracking error Variables

7.3 Guidance laws by control

Given the simplified structure of the underwater UV, to solve the tracking error in position, the control design problem, following the suggested backstepping-ASG version of ISM, is tackled in three stages, described below. A diagram is Figure (7.1) illustrates the proposed formulation.

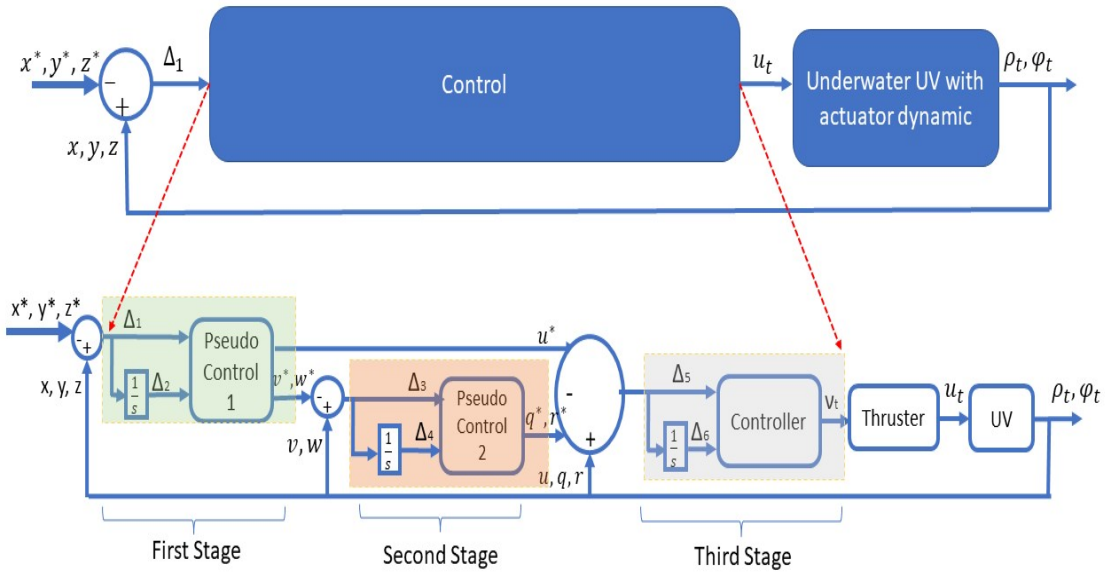

Figure 7.1: System stage diagram

7.3.1 First back-stage: Translation position tracking

First define the position tracking error as $\Delta_{1,t} := \rho_t - \rho_t^*$. Considering the translation kinematics (2.20), the time derivative of $\dot{\Delta}_{1,t}$ satisfies

$$\dot{\Delta}_{1,t} = R_a^b(0,\theta_t,\psi_t)\,\varphi_{1,t} + \xi_{1,t} - \dot{\rho}_t^* \tag{7.1}$$

The stabilization of $\Delta_{1,t}$ uses the cascade formulation [28] considering the "*translation velocity*" $\varphi_{1,t}$ as a new auxiliary *pseudo-controller* (this strategy is similar to the back-stepping formulation presented by [15]). To realize the auxiliary pseudo-controller $\varphi_{1,t}$ that can stabilize $\Delta_{1,t}$ let consider that such control must minimize a cost function depending on integral of $\Delta_{1,t}$ defined as

$$\Delta_{2,t} := \int_0^t \Delta_{1,\tau} d\tau \tag{7.2}$$

Based on the application of the ASG descendent method. This technique has been successfully applied for controlling systems modelled by the Euler-Lagrange equations with uncertain

models [41]. The proposed cost function is

$$H_1(\Delta_2) = \sum_{i=1}^{3} \left|\Delta_{2,i}\right|, \tag{7.3}$$

where the variable $\Delta_{2,i}$ corresponds to the i-the component of Δ_2. H_1 is a smooth convex functional. The problem formulation for this first stage consists of designing a reference vector $\varphi_{1,t}^* = \begin{bmatrix} u_t^* & v_t^* & w_t^* \end{bmatrix}^\top$ such that:

$$\begin{aligned} H_1(\Delta_2) &\to \min_{\varphi_{1,t}\in\mathbb{R}^3}, \\ \varphi_{1,t}^* &= \arg\min_{\varphi_{1,t}\in\mathbb{R}^3} H_1(\Delta_2). \end{aligned} \tag{7.4}$$

According to the ASG method, the optimisation problem can be solved with the suitable definition of a integral sliding surface $s_{1,t}$ and the application of the integral SM. The*integral sliding variable* $s_{1,t}$ satisfies [54],

$$\left.\begin{aligned} s_{1,t} &= \Delta_{1,t} + \mu_t\left[\Delta_{2,t} + \eta_1\right] + \Psi_{1,t}, \\ \Psi_{1,t} &= \mu_t \int_{\tau=0}^{t} \partial H_1(\Delta_{2,\tau}) d\tau, \\ \mu_t &= (t+\mu)^{-1}, \;\; \sigma > 0 \end{aligned}\right\} \tag{7.5}$$

with $\Psi_\mathbf{1}$ the temporal average of the gradient for the cost function H_1.

Theorem 6 (on the first back-step controller)**.** *The proposed ISM controller, which solves the optimisation problem (7.4), has the following structure*

$$\left.\begin{aligned} \varphi_{1,t}^* &= \left(R_a^b\right)^{-1}(0,\theta_t,\psi_t)\,\varsigma_{comp,t} - k_1\left(R_a^b\right)^{-1}(0,\theta_t,\psi_t)\,\frac{\mathbf{s}_{1,t}}{\left\|\mathbf{s}_{1,t}\right\| + \varepsilon_{1,t}}, \\ \varsigma_{comp,t} &= \dot{\rho}_t^* - h_{0,1,t} + \frac{\mathbf{s}_{1,t}}{\left\|\mathbf{s}_{1,t}\right\| + \varepsilon_{1,t}}\dot{\varepsilon}_{1,t}, \end{aligned}\right\} \tag{7.6}$$

where

$$\begin{aligned} k_{1,t} &= 2\left(\lambda_1 + h_{1,1,t}\right) \\ h_{1,1} &:= \xi_1^+ + \frac{\left|\dot{\varepsilon}_{1,t=0}\right|}{2}, \\ h_{0,1,t} &:= \mu_t\left[\Delta_{1,t} + \partial H_1(\Delta_{2,t}) - \Psi_{1,t}\right] - \mu_t^2\left[\Delta_{2,t} + \eta_1\right] \\ k_0 &> 0, \quad \eta_1 = \mu_0^{-1}\Delta_{1,0}, \;\; \left\|\xi_{1,t}\right\| \le \xi_1^+, \end{aligned} \tag{7.7}$$

providing for all $t \ge 0$ *the property*

$$\left\|s_{1,t}\right\| \le \varepsilon_{1,t}. \tag{7.8}$$

Lemma 5 (on ASG-algorithm)**.** *The property (7.8), valid form the beginning of the process, guarantees that*

$$\begin{gathered} H_1(\Delta_{2,t}) \leq \mu_t \Omega_{1,t} + \sqrt{3}\mu_t \int_{\tau=t_0}^{t} (\tau+\mu)\,\varepsilon_{1,\tau} d\tau, \\ \Omega_{1,t} := \mu_{t_0}\left[H_1(\Delta_{2,t_0}) - H_1(\Delta_2^*)\right] + \frac{1}{2}\left\|\Phi_{1,t} - (\Delta_2^* - \eta_1)\right\|^2 \\ -\frac{1}{2}\left\|\Delta_2^* - \eta_1\right\|^2 - \frac{1}{2}\left\|\Phi_{1,t_0}\right\|^2 + \Phi_{1,t_0}^{\top}\Delta_2^* \end{gathered} \tag{7.9}$$

where

$$\Phi = \int_0^t \partial H(\Delta_{2,\tau}) d\tau$$

Corollary 4. *If*

$$\varepsilon_{1,t} = \mu_t^{-(1+\beta)}\sqrt{3}\varepsilon_{1,0}, \;\; \beta \in (0,1)\,, \; \varepsilon_{1,0} > 0, \tag{7.10}$$

finally, (7.9) becomes

$$H_1(\Delta_{2,t}) \leq \mu_t \Omega_{1,t} + \mu_t^{-\beta}\sqrt{3}\varepsilon_{1,0}. \tag{7.11}$$

7.3.2 Second back-stage-Translational Velocity tracking

Now let's solve the second part of the control formulation, consisting of using $\rho_\psi = \begin{bmatrix} q_t & r_t \end{bmatrix}^\top$ as a second pseudo-controller that must solve the stabilisation of the sway and heave velocity tracking errors, defined as:

$$\Delta_3 := \begin{bmatrix} v - v^* & w - w^* \end{bmatrix}^\top. \tag{7.12}$$

Inspired by the approach presented in the first stage, let's define the integral of the tracking error Δ_3 as

$$\Delta_{4,t} := \int_0^t \Delta_{3,\tau} d\tau \tag{7.13}$$

and propose that exists an optimal solution ρ_ψ^* for a given convex (even not-strict) functional

$$H_2(\Delta_4) = \sum_{i=1}^{2} \left|\Delta_{4,i}\right|,$$

such that

$$\rho_{\psi,t}^* = \underset{\rho_{\psi,t}\in\mathbb{R}^2}{\arg\min} H_2(\Delta_4) \tag{7.14}$$

subjected to the dynamics of the auxiliary variable $\Delta_{3,t}$ given by

$$\left.\begin{aligned} \dot{\Delta}_{3,t} = \begin{bmatrix} -\dfrac{d_{22}v_t}{m_{22}} \\ -\dfrac{d_{33}w_t}{m_{33}} \end{bmatrix} - \begin{bmatrix} \dot{v}_t^* \\ \dot{w}_t^* \end{bmatrix} + u_t M \begin{bmatrix} q_t \\ r_t \end{bmatrix} + \begin{bmatrix} \dot{\xi}_{v,t} \\ \dot{\xi}_{w,t} \end{bmatrix}, \\ M := \begin{bmatrix} 0 & -\dfrac{m_{11}}{m_{22}} \\ \dfrac{m_{11}}{m_{33}} & 0 \end{bmatrix}, \end{aligned}\right\} \tag{7.15}$$

where $\dot{v}_t^*$ and $\dot{w}_t^*$ are time derivatives of the controller calculated in expressionn (7.6). Based on the Cauchy-Schwarz inequality, the following relation is valid (with $\alpha^{(0)}$ a positive scalar)

$$\left\| \begin{bmatrix} \dfrac{d_{22}v_t}{m_{22}} \\ \dfrac{d_{33}w_t}{m_{33}} \end{bmatrix} \right\| = \left\| \begin{bmatrix} \dfrac{d_{22}}{m_{22}} & 0 \\ 0 & \dfrac{d_{33}}{m_{33}} \end{bmatrix} \begin{bmatrix} v_t \\ w_t \end{bmatrix} \right\| \leq \alpha^{(0)} \left\| \begin{bmatrix} v_t \\ w_t \end{bmatrix} \right\|$$

The second optimization problem (7.14) can be solved (according to the ASG method), using a suitable integral sliding surface $s_{2,t}$ and a second application of the ISM. The integral sliding variable $s_{2,t}$ corresponds is defined as follows:

$$\left.\begin{aligned} s_{2,t} = \Delta_{3,t} + \mu_t \left[\Delta_{4,t} + \eta_2\right] + \Psi_{2,t}, \\ \Psi_{2,t} = \mu_t \int_{\tau=0}^{t} \partial H_2(\Delta_{4,\tau}) d\tau, \\ \eta_2 = \mu_0^{-1} \Delta_{3,0} \end{aligned}\right\} \tag{7.16}$$

In this case, $\Psi_{\mathbf{2},t}$ the temporal average of the gradient for the cost function H_2.

Theorem 7 (on the second back-step controller)**.** *The proposed ISM controller, which solves the optimisation problem (7.14), has the following structure*

$$\begin{bmatrix} q^* \\ r^* \end{bmatrix} := \begin{bmatrix} -\mathring{k}_{2,t} s_{22,t} u_t - k_{2,t} \dfrac{s_{22,t}}{\left\|\mathbf{s}_{2,t}\right\| + \varepsilon_{2,t}} u_t \\ \mathring{k}_{2,t} s_{21,t} u_t + k_{2,t} \dfrac{s_{21,t}}{\left\|\mathbf{s}_{2,t}\right\| + \varepsilon_{2,t}} u_t \end{bmatrix}, \text{ for } u \neq 0,\ \mathring{k}_{2,t}, k_{2,t} > 0, \tag{7.17}$$

where

$$\begin{gathered}
\mathring{k}_{2,t} = \frac{\left\|\mathbf{h}_{02,t}\right\| + d^{+}\varphi_t + \left|\dot{\varepsilon}_{2,t=0}\right|}{d^{-}u_t^2\varepsilon_{2,t}} \\
k_{2,t} = \left(2/u_t^2 d^{-}\right)\left(\lambda_2 + F_2^{+}\right) \\
h_{0,2,t} := -\begin{bmatrix} \dot{v}_t^* \\ \dot{w}_t^* \end{bmatrix} + \mu_t\left[\Delta_{3,t} + \partial H_2(\Delta_{4,t}) - \Psi_{2,t}\right] - \mu_t^2\left[\Delta_{4,t} + \eta_2\right] \\
F_2^{+} \geq \left\|\begin{bmatrix} \xi_{v,t} \\ \xi_{w,t} \end{bmatrix}\right\|, \quad \sqrt{\left(\frac{d_{22}}{m_{22}}\right)^2 + \frac{d_{33}}{m_{33}}} \leq d^{+}, \quad \phi_t := \sqrt{\|v_t\|^2 + \|w_t\|^2}
\end{gathered} \tag{7.18}$$

providing for all $t \geq 0$ *the property*

$$\left\|s_{2,t}\right\| \leq \varepsilon_{2,t}. \tag{7.19}$$

Lemma 6 (on ASG-algorithm)**.** *The property (7.19), valid from the beginning of the process, guarantees that*

$$\begin{gathered}
H_2\left(\Delta_{3,t}\right) \leq \mu_t\Omega_{2,t} + \sqrt{3}\mu_t \int_{\tau=t_0}^{t} \left(\tau + \mu_0\right)\varepsilon_{2,\tau}d\tau, \\
\Omega_{2,t} := \mu_{t_0}\left[H_2\left(\Delta_{4,t_0}\right) - H_2\left(\Delta_4^*\right)\right] + \frac{1}{2}\left\|\phi_{2,t} - \left(\Delta_4^* - \eta_2\right)\right\| \\
-\frac{1}{2}\left\|\Delta_4^* - \eta_2\right\|^2 - \frac{1}{2}\left\|\phi_{2,t_0}\right\|^2 + \phi_{2,t}^{\top}\Delta_4^*.
\end{gathered} \tag{7.20}$$

Corollary 5. *If*

$$\varepsilon_{2,t} = \frac{\varepsilon_{2,0}}{\left(t + \mu_0\right)^{1+\beta}}, \ \beta \in (0,1), \ \varepsilon_{2,0} > 0, \tag{7.21}$$

finally, (7.20) becomes

$$H_2\left(\Delta_{4,t}\right) \leq \mu_t\Omega_{2,0} + \mu_t^{-\beta}\sqrt{2}\varepsilon_{2,0} \to 0. \tag{7.22}$$

7.3.3 Third back-stage-Velocity Tracking by average SG robust algorithm

The third part of the control formulation corresponds to selecting the voltages that drive actuators $\nu_d = \begin{bmatrix} \nu_{u,t} & \nu_{q,t} & \nu_{r,t} \end{bmatrix}^{\top}$ as the controller that must solve the stabilization of the tracking error in the surge, pitch angular and yaw angular velocity tracking errors, which are defined as:

$$\Delta_5 := \begin{bmatrix} u - u^* & q - q^* & r - r^* \end{bmatrix}^{\top} \tag{7.23}$$

where u^* is given in expression (7.6) while (q^*, r^*) are defined in equality (7.17). Considering the translation and angular dynamics in equations (2.21) and (2.22), the time variation of the tracking error $\dot{\Delta}_{5,t}$ satisfies:

$$\dot{\Delta}_{5,t} = \mathbb{M}^{-1}\left[F\left(\rho_t, \varphi_t\right) + \tau_t\right] + C\xi_t - C\dot{\varphi}_t^* \tag{7.24}$$

where

$$C = \begin{bmatrix} 1 & 0 & 0 & 0 & 0 & 0 \\ 0 & 0 & 0 & 0 & 1 & 0 \\ 0 & 0 & 0 & 0 & 0 & 1 \end{bmatrix}^\top, \quad \mathbb{M}^{-1} = \begin{bmatrix} \frac{1}{m_{11}} & 0 & 0 \\ 0 & \frac{1}{m_{55}} & 0 \\ 0 & 0 & \frac{1}{m_{66}} \end{bmatrix}$$

$$\mathbb{M}^{-1} \leq \lambda_{\mathbb{M}}^- I_{3x3}, \quad \mathbb{M} \leq \lambda_{\mathbb{M}}^+ I_{3x3}, \quad \lambda_{\mathbb{M}}^+ = \frac{1}{\lambda_{\mathbb{M}}^-}$$

$$F\left(\rho_t, \varphi_t\right) = \begin{bmatrix} -d_{11} & 0 & 0 \\ 0 & -d_{55} & 0 \\ 0 & 0 & -d_{66} \end{bmatrix} C\varphi_t + \begin{bmatrix} 0 & -m_{33}w & m_{22}v \\ (m_{33}-m_{11})w & 0 & 0 \\ (m_{11}-m_{22})v & 0 & 0 \end{bmatrix} C\varphi + \begin{bmatrix} 0 \\ -mghs_\theta \\ 0 \end{bmatrix}$$

$$F_3^+ \geq d_1^- \|\varphi\| + d_2 \|\varphi\|^2 + mgh$$

$$d_1^- = \max(d_{11}, d_{55}, d_{66})$$

$$C\xi = \begin{bmatrix} \xi_{u,t} & \xi_{q,t} & \xi_{r,t} \end{bmatrix}^\top.$$

Considering the actuators dynamic given in equation (2.14) the dynamic of the auxiliary variable Δ_5 can be expressed as

$$\begin{gathered} \dot{\Delta}_{5,t} = \mathbb{M}^{-1}\left[F\left(\rho_t, \varphi_t\right) + E_f\left(\mathbf{I}_{t_0} + \int_{\tau=t_0}^{t} Z_L^{-1}\left[F_I\left(\rho_\tau, \varphi_t\right) + \nu_{d,\tau}\right] d\tau\right)\right] + C\xi_t - C\dot{\varphi}_t^* \\ \mathbf{I}_{t_0} = \begin{bmatrix} I_{u,0} & I_{q,0} & I_{r,0} \end{bmatrix}^\top, \quad F_I\left(\rho_\tau, \varphi_t\right) = \begin{bmatrix} f_{u,t} & f_{q,t} & f_{r,t} \end{bmatrix}^\top \end{gathered} \tag{7.25}$$

Let's use the control action $\upsilon_{d,t}$ satisfying the following integral equation

$$\nu_{d,t} = -F_I\left(\rho_t, \varphi_t\right) + \nu_{c,t} \tag{7.26}$$

with $\nu_{c,t}$ defined below.

The substitution of the controller $\nu_{d,t}$ in (7.25) leads to

$$\begin{gathered}\dot{\Delta}_{5,t}=\mathbb{M}^{-1}\left(f_{0,t}\right)+B\mathbf{u}_{\nu,t}+C\xi_t \\ f_{0,t}=F\left(\rho_t,\varphi_t\right)+E_f\mathbf{I}_{t_0} \\ \left\|f_{0,t}\right\|\leq F_3^+ +\lambda^{(0)}-\lambda_{\mathbb{M}}^+\|\dot{\varphi}_t^*\|=F^+ \\ B:=\mathbb{M}^{-1}E_f Z_L^{-1},\ \ B\in\mathbb{R}^{3\times 3},\ det(B)\neq 0 \\ \|B\|\leq B^+,\quad \left\|B^{-1}\right\|\leq B^-,\quad B^-=\left(B^+\right)^{-1}\end{gathered} \tag{7.27}$$

with $\mathbf{u}_{\nu,t}=\int\limits_{\tau=t_0}^{t}\nu_\tau d\tau$.

Once more, taking into account the approach presented in the previous cases, first defining the integral of the tracking error $\Delta_{5,t}$ as

$$\Delta_{6,t}:=\int\limits_{0}^{t}\Delta_{5,\tau}d\tau. \tag{7.28}$$

Lets propose that exists an optimal solution $\mathbf{u}_{\nu,t}^*$ for a given convex (even not-strict) functional $H_3(\Delta_{6,t})$such that

$$\begin{gathered}\mathbf{u}_{\nu,t}^*=\underset{\mathbf{u}_{\nu,t}\in\mathbb{R}^3}{\arg\min}H_3(\Delta_{6,t}) \\ H_3(\Delta_6)=\sum_{i=1}^{3}\left|\Delta_{6,i}\right|,\ \ \Delta_{6,i}\text{ the i-th component of }\Delta_6\end{gathered} \tag{7.29}$$

subjected to the dynamics of the auxiliary variable $\Delta_{5,t}$, described before in equation (7.27). Using the method proposed in the article [41], a feasible solution for $\mathbf{u}_{\nu,t}^*$ that optimises the cost function of the average tracking error (based on the integral SM theory) can be obtained with the introduction of a third sliding surface defined as follows:

$$\left.\begin{gathered}s_{3,t}=\Delta_{5,t}+\mu_t\left[\Delta_{6,t}+\eta_3\right]+\Psi_{3,t},\ \ \eta_3=const \\ \Psi_{3,t}=\mu_t\int\limits_{\tau=t_0}^{t}\partial H_3(\Delta_{6,\tau})d\tau, \\ \partial H_3(\Delta_{6,t})=\left[\text{sign}\left(\Delta_{6,1}\right),\text{sign}\left(\Delta_{6,2}\right),\text{sign}\left(\Delta_{6,3}\right)\right]^\top\end{gathered}\right\} \tag{7.30}$$

In this case, the temporal average of the gradient for the cost function H_3 is $\Psi_{\mathbf{3},t}$.

Theorem 8 (on the second back-step controller)**.** *The proposed ISM controller, which solves the optimisation problem (7.14), has the following structure*

$$\nu_{c,\tau} := \frac{d}{d\tau}\left(-\mathring{k}_{3,\tau} - k_{3,\tau}\frac{s_{3,\tau}}{\left\|\mathbf{s}_{3,\tau}\right\| + \varepsilon_\tau}\right) \tag{7.31}$$

According to the definition of $\mathbf{u}_{\nu,t}$*, the control is given by*

$$\begin{gathered}
\mathbf{u}_{\nu,t} = \left(-\mathring{k}_{3,t} + \mathring{k}_{3,t_0} - k_{3,t}\frac{s_{3,t}}{\left\|\mathbf{s}_{3,t}\right\| + \varepsilon_t} - k_{3,t_0}\frac{s_{3,t_0}}{\left\|s_{3,t_0}\right\| + \varepsilon_{t_0}}\right), \\
k_{3,t} = 2\left(k_4 + h_{1,3,t}\right) \\
\mathring{k}_{3,t} = \mathring{k}_{3,t_0} + h_{0,3,t} + B^-\lambda_{\mathbb{M}}^-\left\|f_{0,t}\right\| + k_{3,t_0}\frac{s_{3,t_0}}{\left\|s_{3,t_0}\right\| + \varepsilon_{t_0}} \\
\mathring{k}_{3,t_0} = h_{0,3,t_0} + B^-\lambda_{\mathbb{M}}^-\left\|f_{0,t_0}\right\| + k_{3,t_0}\frac{s_{3,t_0}}{\left\|s_{3,t_0}\right\| + \varepsilon_{t_0}} \\
k_{3,t_0} = 2\left(\lambda_3 + h_{1,3,t_0}\right)
\end{gathered} \tag{7.32}$$

where

$$\begin{gathered}
h_{0,3,t} = B^-\left[\mu_t\left[\Delta_{5,t} + \partial H_3(\Delta_{6,t}) - \Psi_{3,t}\right] - \mu_t^2\left[\Delta_{6,t} + \eta_3\right]\right]. \\
h_{0,3,t_0} = B^-\left[\mu_t\left[\Delta_{5,t_0} + \partial H_3(\Delta_{6,t_0}) - \Psi_{3,t_0}\right] - \mu_t^2\left[\Delta_{6,t_0} + \eta_3\right]\right]. \\
h_{1,3,t} = B^-\left\|\xi\right\| - B^-\left|\dot{\mu}_{3,t}\right| \\
\varepsilon_{3,t} = \varepsilon_t = \frac{\sqrt{2}}{\beta}\mu^{-\beta}\varepsilon_0, \quad \alpha \geq 0 \\
k_4 > 0, \;\; \mu_{3,0} = \varepsilon_0, \;\; \dot{\varepsilon}_{3,t} = -\sqrt{2}\mu_t^{1+\beta}\varepsilon_{3,0}
\end{gathered}$$

Notice that $\left|-k_{3,t_0}\dfrac{s_{3,t_0}}{\left\|s_{3,t_0}\right\| + \varepsilon_{t_0}}\right| \leq \Omega_0$, $\Omega_0 \in \mathbb{R}$*. Providing for all* $t \geq 0$ *the property*

$$\left\|s_{3,t}\right\| \leq \varepsilon_{3,t}. \tag{7.33}$$

Lemma 7 (on ASG-algorithm)**.** *The property (7.33), valid from the beginning of the process, guarantees that*

$$\begin{gathered}
H_3\left(\Delta_{6,t}\right) \leq \mu_t\Omega_{3,t} + \sqrt{3}\mu_t\int\limits_{\tau=t_0}^{t}\left(\tau+\sigma\right)\varepsilon_{3,\tau}d\tau, \\
\Omega_{3,t} := \mu_{t_0}\left[H_3\left(\Delta_6\right) - H_3\left(\Delta_6^*\right)\right] + \frac{1}{2}\left\|\phi_{3,t} - \left(\Delta_6^* - \eta_3\right)\right\| \\
-\frac{1}{2}\left\|\Delta_6^* - \eta_3\right\|^2 - \frac{1}{2}\left\|\phi_3\right\|^2 + \phi_{3,t}^\top\Delta_6^*.
\end{gathered} \tag{7.34}$$

Corollary 6. *If*

$$\varepsilon_{3,t} = \mu_t^{1+\beta}\varepsilon_{3,0},\ \ \beta \in (0,1)\,,\ \varepsilon_{3,0} > 0, \tag{7.35}$$

then

$$\mu_t \int_{\tau=t_0}^{t} \mu^{-1}\varepsilon_{3,\tau}d\tau \leq \mu^{\beta}\frac{\varepsilon_{3,0}}{1-\beta} \leq \mu^{\beta}\varepsilon_{3,0},$$

finally, (7.34) becomes

$$H_3\left(\Delta_{6,t}\right) \leq \mu_t\Omega_{3,0} + \mu^{\beta}\sqrt{3}\varepsilon_{3,0} \to 0. \tag{7.36}$$

The mathematical proof of the Theorem, Lemma, and Corollary are shown in Appendix section 10.4.

7.4 Numerical Simulations

The numerical simulations were realised in Matlab/Simulink with an integration step of $1.0 * 10^{-5}s$. All the simulations were evaluated using an integration method known as ODE-3 with the fixed integration step already mentioned. For the technical evaluation of the sliding mode controllers, the implementation of first-order filters was considered with a constant filtering time of $0.1s$. This value was selected according to the suggestions provided by [54]. The gains selected for the ISM controllers are detailed in Table 7.2. These gains were chosen according to the method described at each stage.

The desired translation reference for the Underwater UV is given by the composition of a circle trajectory on the plane (x, y) and a smooth change on the deep level. This result is obtained with the development of individual trajectories for the three coordinates with a simultaneous motion formed by a sequence of Bezier curves (Figures (7.2), (7.3) and (7.4)). The desired trajectory is described by:

$$x^* = 15sin(0.02t)$$
$$y^* = 15cos(0.02t)$$
$$z^* = -5\left[\frac{1}{1+|0.01t-2|^8}\right]$$

For comparison purposes, a state feedback control corresponding to a Proportional-Integral-Derivative (PID) form is implemented in each stage. The such comparison includes the analysis

of the tracking for each coordinate and the evaluation of the three-dimensional movement. The selection of PID as the comparative controller is made considering the significant distribution of this type of controller in industrial, technical and research applications.

The tracking error in the surge, sway and heave is reduced towards the origin within the first 5s of numerical simulation, even though disturbances are affecting the kinematics of the Underwater UV (Figures (7.2), (7.3) and (7.4)). The proposed composite ISM can compensate for perturbations (shown in figures as the lack of oscillations forced by the PID control form) and, consequently, provides a smaller convergence region. PID controllers induce high-frequency oscillations, affecting the control effectiveness in the controlled motion around the reference trajectories.

Both controllers, proposed in this study and used for comparison purposes, may force the Underwater UV to the desired trajectory in the three-dimensional space (Figure 7.5). The mentioned figure presents a comparison between the desired trajectories and those corresponding to the controlled trajectories by both the ISM and the PID. This fact confirms the simultaneous convergence of three reference trajectories, which shows the ASG form's advantages. There are deviations between the reference and the states controlled with the PID at all times. On the contrary, the ISM controller forces the Underwater UV coordinates to reach the desired reference trajectories without deviations. This three-dimensional representation emphasises the variations of the Underwater UV trajectory from the references in opposition to the precise tracking induced by the ISM form. Notice also that the ASG controller may introduce an initial *jump* at the initial time, which is a consequence of the ISM design characteristics.

The three-dimensional trajectory enforced by the PID controller shows that there is no effective convergence to the reference at all times. This condition is satisfied with the application of the ISM controller.

The quality of the proposed controller is reflected in the tracking error and the magnitude of the cost function $H_{\mathbf{1}}$, which is a consequence of the individual tracking errors for all the coordinates. This fact can be noticed in Figure 7.6, which shows the comparison of the absolute

Table 7.2: Table of gains used for evaluating ISM and PID controllers.

Stage	ASG-**ISM**	**PID**
First	ρ_1 0 α_1 $= diag([\ -40 \quad 50 \quad -60\ ])$	K_p $diag([\ -40 \quad 50 \quad -60\ ])$ K_d 0 Ki 0
Second	ρ_2 $2.5\mathbb{I}_2$ $\alpha^{(1)}$ $2.5\mathbb{I}_2$	K_p $10\mathbb{I}_2$ K_d $1.5\mathbb{I}_2$ Ki $5\mathbb{I}_2$
Third	ρ_3 $diag([\ 0.2 \quad 2 \quad 2\ ])$ $c_{1,t}$ 7	K_p $20\mathbb{I}_3$ K_d $\mathbb{I}_3$ Ki $12\mathbb{I}_3$

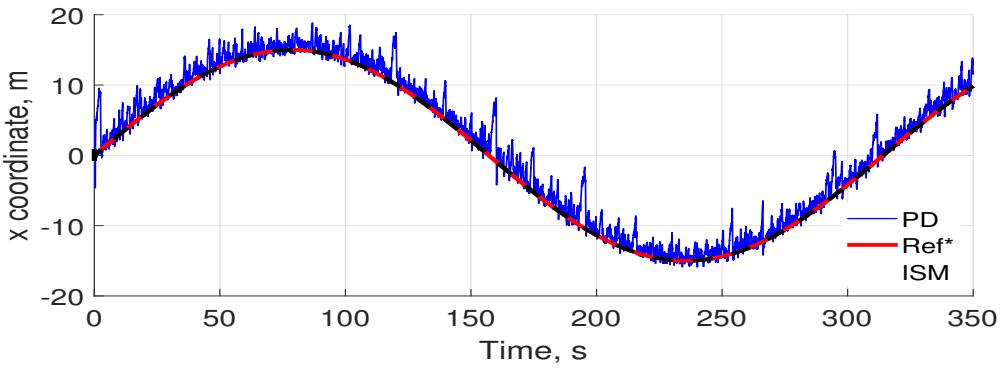

Figure 7.2: Displacement in surge axis (x) for the Underwater UV.

values of the tracking errors for the set of three coordinates that define the motion of the Underwater UV using both controllers. This comparative analysis confirms the norms of tracking error forced by the ASG controller are at least ten times smaller than the ones produced by the PID form. Also, all the tracking errors made with the ASG are not oscillating near the origin, which is also a desirable condition for the motion of the class of actuators for the Underwater UV device, taking into consideration that such oscillations introduce mechanical and electrical hazards.

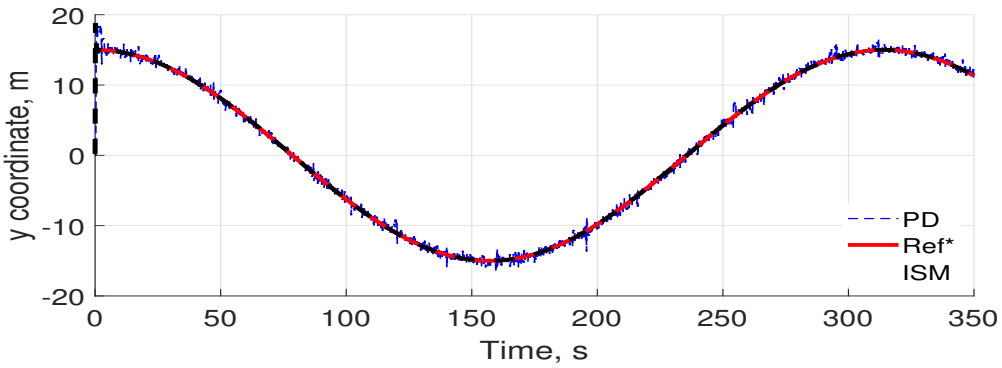

Figure 7.3: Displacement in sway axis (y) for the Underwater UV.

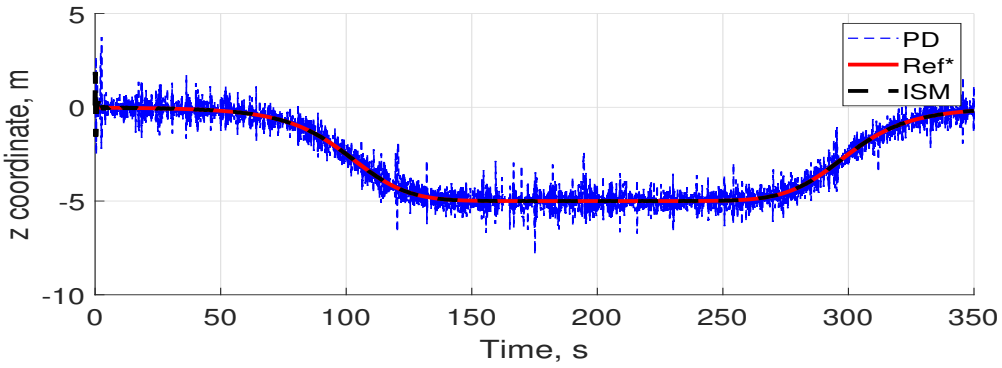

Figure 7.4: Displacement in heave axis (z) for the Underwater UV.

Due to the magnitude of displacement in the heave axis, the deviation from the reference is more minor compared to the surge and sway evolution (Figure (7.4)). In the deviation analysis for the three axes, the integral of the tracking error is growing continuously for the PID controller. For the proposed controller, the norm of the integral for the tracking error is bounded, which represents a significant contribution to the proposed controller. The cost functional calculated with the trajectories forced by the PID controller is 100 times bigger than the proposed ISM controller's. This condition motivates the application of the ASG controller over the state feedback form performed as a PID.

The desired and controlled trajectories of the sway and heaved states with respect to the body frame are determined according to the expression proposed in (7.6). For both controllers (ISM and PID), the tracking error in sway and heave velocities are reduced close to the origin after the

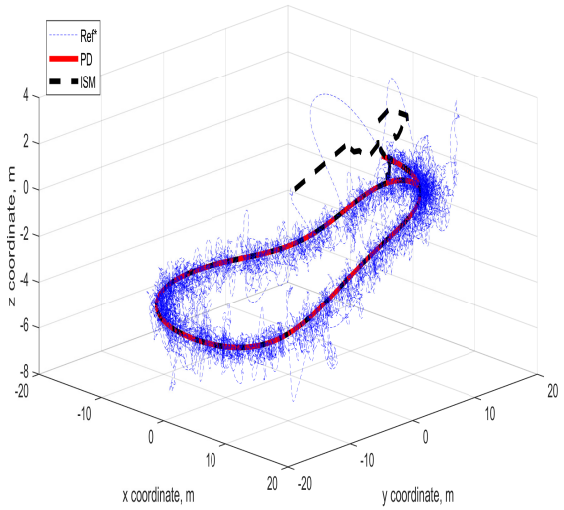

Figure 7.5: Three-dimensional tracking trajectory for the UV using the proposed controller as well as the ones used for comparison.

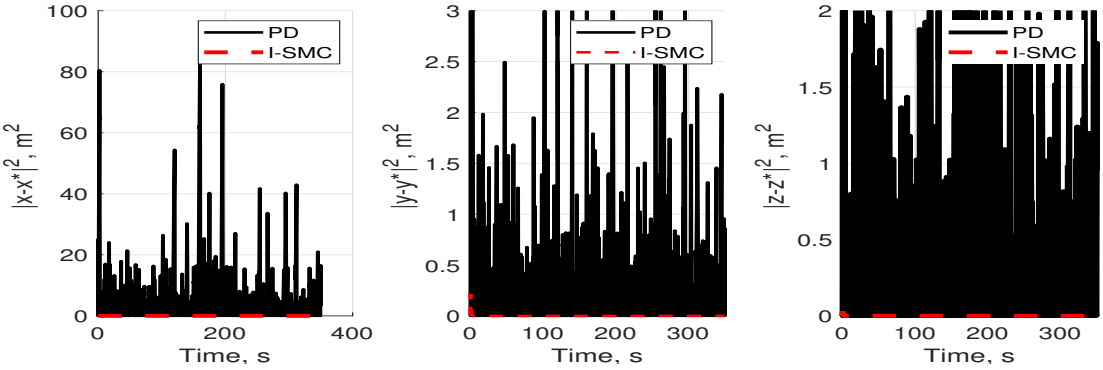

Figure 7.6: Square norm of x, y and z of the Underwater UV.

first 5 seconds (Figures (7.7) and (7.8)). Both controllers endorse translation velocities to the desired references, but with continuous deviations in the case of the PID controller (+/- 40 m/s), and keep the velocity in a zone near the desired trajectory if the ISM is considered (+/- 3 m/s). The relative convergence zone to the reference justifies the convergence of the tracking error, as the back-stepping form predicts. This step-by-step form simplifies the design of the controller form but increases control power as the number of steps grows.

The superiority of the proposed ISM controller for the second stage is reflected in the tempo-

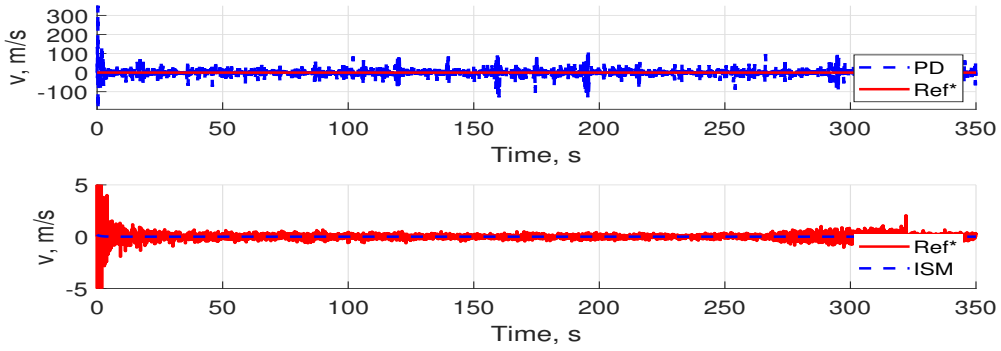

Figure 7.7: Translation velocity v by the state feedback and the ISM controllers.

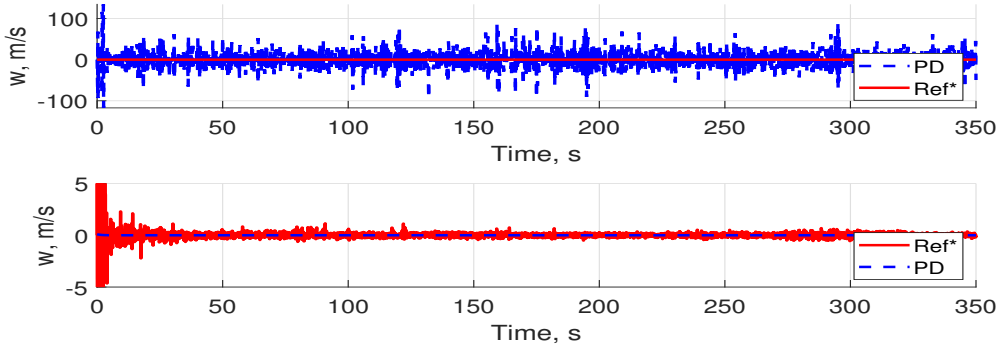

Figure 7.8: Translation velocity w by the state feedback and the ISM controllers.

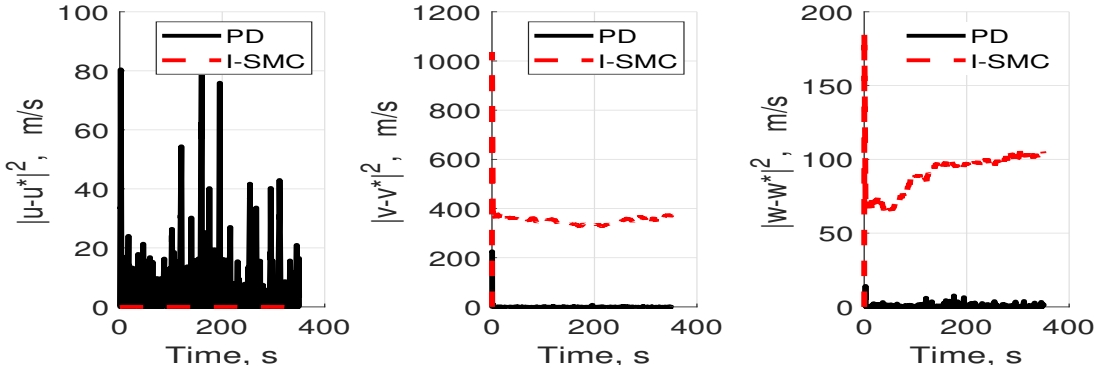

Figure 7.9: Tracking error u, v and w by the state feedback and the ISM controllers.

ral evolution of the norm of the tracking error and the magnitude of the cost function H_2 (Figure (7.9)). For the tracking error in the sway velocity, the magnitude of the norm of the tracking error produced by the PID controller is smaller than the magnitude by the proposed ISM controller.

For the case of the heave velocity, the tracking error norm enforced by the proposed controller is larger than the PID outcomes. Nevertheless, these results demonstrate the tracking of the velocities, which are comparable for the variable u; therefore, the comparison for variables v and w shows PID may track velocities as well as the ISM, but the proposed controller successfully follows the three-dimensional coordinates despite the differences in v and w.

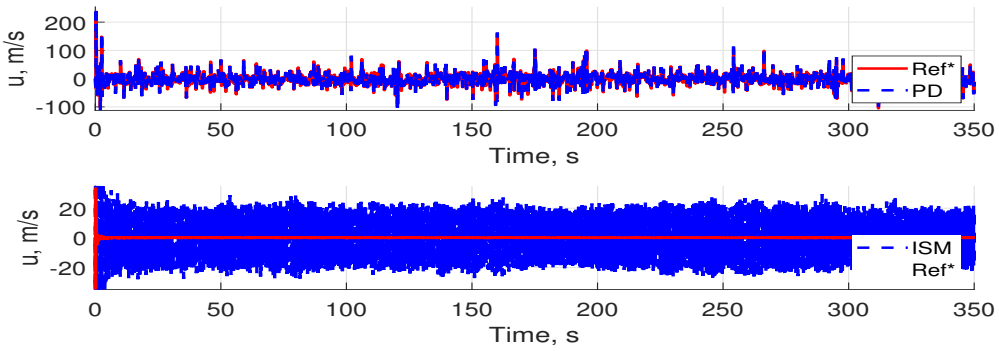

Figure 7.10: Translation velocity u by the state feedback and the ISM controllers.

Due to the magnitude of displacement in the heave axis, the deviation at the tracking in the heave velocity is even more minor (Figure (7.8)). The tracking error integral of these two velocities for the case of the PID controller is constantly growing, and for the other case, is bounded. The performance of the cost functional for the integral of the sway and heave velocities errors are presented in Figure 7.9. The cost function associated with the velocities differences produced by the PID controller is 9 and 5100 times bigger than the proposed ISM controller's.

For the third stage, the references for the surge, pitch and yaw angular velocities are given by equation (7.17). As mentioned above, the reference for the PID controller is given by state feedback control in PID form. The norm of the tracking errors for the surge, pitch angular and yaw angular velocities are reduced within the first 4 s (Figures (7.10), (7.11) and (7.12)).

The control actions over the actuators of the UV are depicted in Figures (7.13), (7.14) and (7.15). These figures show that the magnitude of the PID controller is bigger than the ISM controller. In the case of the voltage for the corresponding actuators that control the temporal evolution of either q and r, the PID controller forces the presence of overshoots for the controlled trajectories at different moments. This fact is another remarkable advantage of the developed

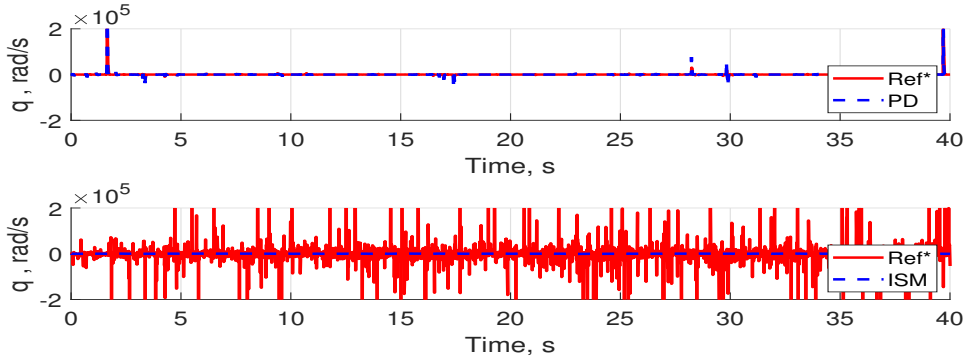

Figure 7.11: Angular velocity q by the state feedback and the ISM controllers.

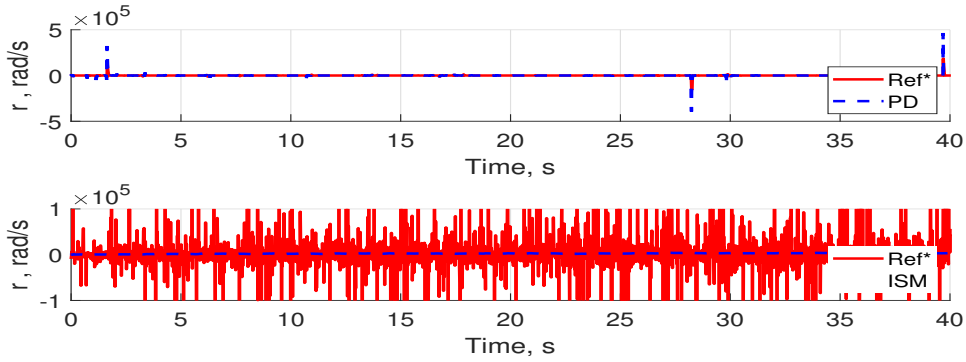

Figure 7.12: Angular velocity r by the state feedback and the ISM controllers.

sliding mode controller.

The proposed controller exhibits a better performance considering only partial knowledge of the Underwater UV and the actuator models even in the presence of different kinds of perturbations (nonlinear phenomena, external hydrodynamic, the poor knowledge of the $\mathbb{M}$ and Z_L and non-modelled dynamics). Both controllers keep the velocities in zones near to the desired trajectory, which is reflected in the norm of the tracking errors and the magnitude of the cost function H_3 (Figure 7.16). This last result also confirms that the proposed back-stepping formulation yields the satisfactory tracking of the reference trajectories in a three-dimensional space without increasing the amplitude of control forms in the sequence of steps needed in the proposed formulation.

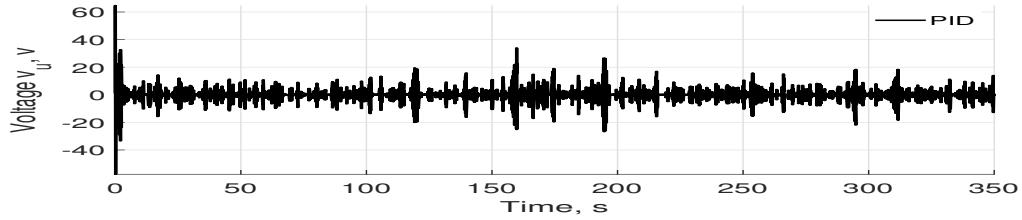

(a) Voltage v_u in the Underwater UV by state feedback control

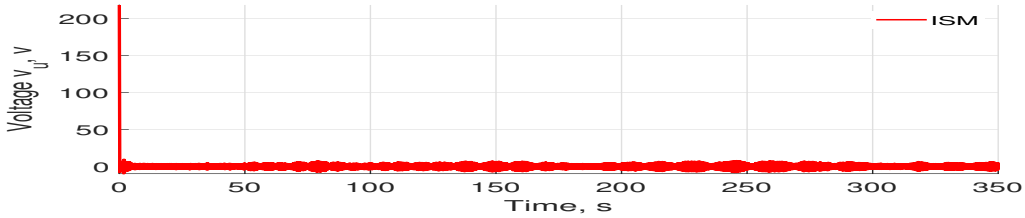

(b) Voltage v_u in the Underwater UV by ISM control

Figure 7.13: Voltage v_u in the Underwater UV.

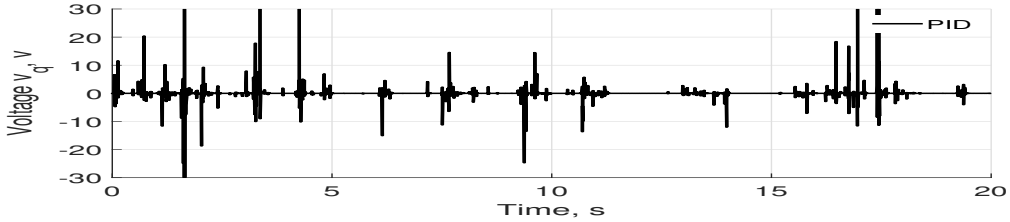

(a) Voltage v_q in the Underwater UV by state feedback control

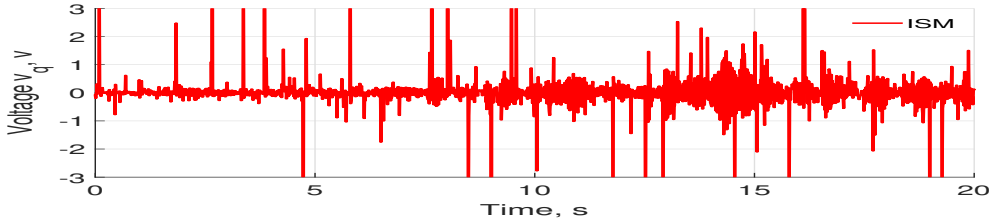

(b) Voltage v_q in the Underwater UV by ISM control

Figure 7.14: Voltage v_q in the Underwater UV.

7.5 Pseudo-code algorithm

The algorithm steps for each stage are:

1. Define the reference trajectory ρ^*.

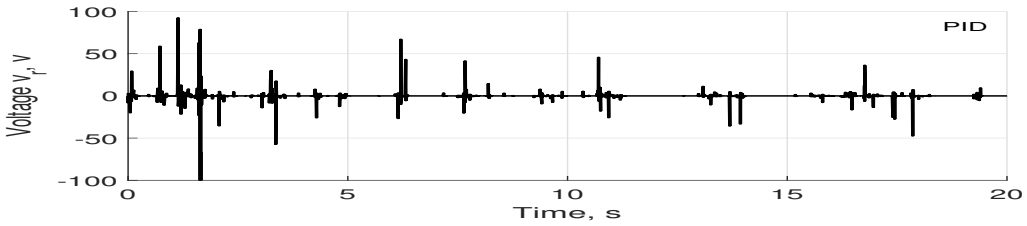

(a) Voltage v_r in the Underwater UV by state feedback control

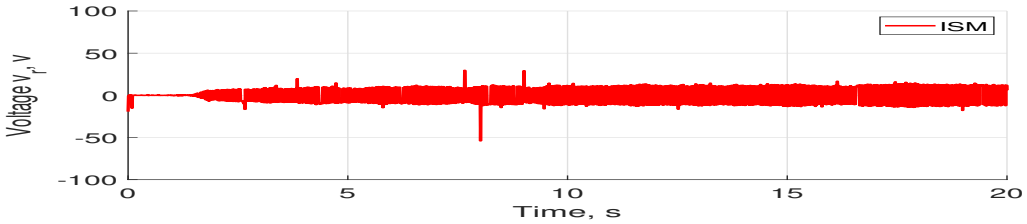

(b) Voltage v_r in the Underwater UV by ISM control

Figure 7.15: Voltage v_r in the Underwater UV.

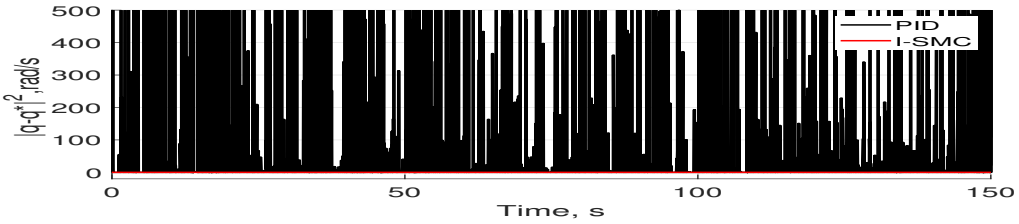

(a) Tracking error of "q" by the state feedback and the ISM controllers.

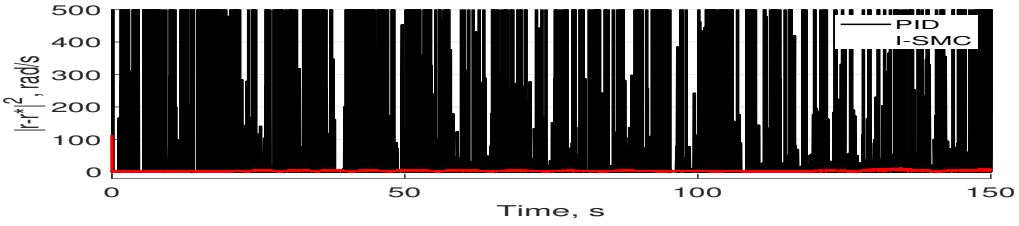

(b) Tracking of "r" by the state feedback and the ISM controllers.

Figure 7.16: Tracking error for q and r by the state feedback and the ISM controllers.

2. Calculate the tracking trajectory error Δ_1.

3. Calculate the integral of the tracking trajectory error Δ_2.

4. Estimate the first derivative of the tracking error applying the robust exact differentiator

over Δ_1.

5. Calculate the first integral sliding surface s_1 according to the definition presented in expression (7.5) using the tracking error and its integral.

6. Implement the tracking error in the dynamic control law u_1 presented in (7.6).

7. Fix the desired velocity φ^* to the result gotten for the first back-stepping stage: $\varphi^* = u_1$

8. Calculate the first and second-time derivatives of φ^* using a robust exact differentiator such as a super-twisting algorithm for each component of φ^*

9. Calculate the second integral sliding surface s_2 according to the definition presented in (7.16) using the estimates of the error between φ and φ^* and its first and second derivatives.

10. Implement the tracking error in the dynamic control law u_2 presented in expression (7.17).

11. Fix the desired current I^* to the result for the second back-stepping stage depending on the estimation of u_2.

12. Calculate the first and second-time derivatives of I^* using a robust exact differentiator such as a super-twisting algorithm.

13. Calculate the third integral sliding surface s_3 according to the definition presented in (7.30) using the estimates of the error between I and I^* and its first and second derivatives.

14. Implement the tracking error in the dynamic control law u_3 presented in (7.31)

7.6 Chapter Conclusions

In this chapter, a back-stepping solution was developed based on the ASG algorithm for optimising a cost functional of the integral of the tracking error. The boundedness of the cost functional of the integral tracking error was obtained. This chapter demonstrates that the tracking error can

be minimised even with optimising the corresponding integral given a solution with less introduction of noises by the time derivative estimation. Consequently, it reduces the instrumentation complexity and cost without more energy investment and good reference tracking. The numerical results confirm that the designed controller presents a better tracking over the trajectory even with disturbances.

Chapter 8

Experimental verification

8.1 Chapter Introduction

Theory and numerical evaluations have demonstrated the controllers' effectiveness in the last chapters, aiming to demonstrate the proposed controller's effect and consequences. Implementation for the tracking trajectory in a terrestrial UV was developed in the UPIBI Robotics Laboratory and the Laboratory of Advanced Cyber-Physical Systems in the Instituto Tecnologico de Estudios Superiores de Monterrey, Campus Guadalajara. A complete description of all the elements in the platform is included. In the following chapter, the control problem of tracking a reference in the horizontal plane for a terrestrial UV is boarding. By a state feedback linearisation, the dynamic of the terrestrial vehicle is simplified. The formulation of the problem statement is presented over the displacement in the right and left of the vehicle. The tracking problem is boarded as an optimisation problem of a cost functional of a non-convex functional depending on the tracking error. Numerical evaluations are presented to support the theory. Some comments and conclusions are in the part of the chapter.

8.2 Variables

A list of the variables used in this chapter is included in Table 8.1

ρ	Position vector
ρ^*	Desired position vector
ξ	Perturbation vector
δ_1	Position tracking error
δ_2	Velocity tracking error
δ_3	Acceleration tracking error
H	Cost functional of the position tracking error
H_2	Cost functional of integral of translation velocity tracking error
H_3	Cost functional of integral of velocity tracking error
s_1	Integral sliding variable
s_2	Integral sliding variable
s_3	Integral sliding variable

Table 8.1: Backstepping formulation using integral of the tracking error Variables

8.3 Mathematical model of the terrestrial UV

Taking into count the linearisation of the auxiliary vector z defined in the introduction by the equation (2.35), the left and right velocity of a terrestrial UV is described by the vector $z_1 = \begin{bmatrix} z_{1,1} & z_{1,2} \end{bmatrix}^\top$. The dynamic model of a terrestrial UV is given in the differential equation (2.36).

8.4 Assumptions

- The position vector $\rho = \begin{bmatrix} X & Y & \theta \end{bmatrix}$ is measured for all $t > 0$.
- The perturbations over the terrestrial dynamic given by the vector ξ are unknown but fulfil the following inequality

$$|\xi| \leq \xi^+, \qquad |\dot{\xi}| \leq \dot{\xi}^+ \tag{8.1}$$

where $\dot{\xi}$ corresponds to the time derivative of the perturbation vector.

8.5 General Problem statement

Given a terrestrial vehicle with a dynamic subject to the differential equation (2.36). Also, given the desired reference z_1^* on the function of the reference ρ^*, defining a tracking error given by:

$$\delta_{1,t} := z_{1,t} - z_{1,t}^*. \tag{8.2}$$

Using the cost functional H as a function of the tracking error expressed as:

$$H = \sum_{i=1}^{2} |\delta_{1,i}| \tag{8.3}$$

The main problem is to design a control u as function of the state that forces the development of z_1 to the desired reference z_1^*. Looking to reduce the difference between them and, in consequence, minimise the tracking error and get optimisation of the cost functional H expressed in the following form:

$$H(\delta_1) \rightarrow \min_{u^* \in U} H^* = 0 \tag{8.4}$$

where U is the set of all the feasible controllers. Given the dimension of the state, the control problem can be formulated by a back-stepping formulation divided into three stages that are:

- Translation stage
- Velocity stage
- Acceleration stage

The problem statement of each stage is described below.

8.6 Translation stage

8.6.1 Problem statement

Given a desired trajectory z_1^* on the function of ρ^* by the following expression

$$z_1^* = \begin{bmatrix} X^* + d_0^* \cos\theta^* \\ Y^* + d_0^* \sin\theta^* \end{bmatrix}$$

The dynamic of the tracking error δ_1 is described by:

$$\begin{aligned}\dot{\delta}_1 &= \dot{z}^*_{1,t} - \dot{z}_{1,t} \\ &= z^*_{1,t} - \dot{z}_{2,t}\end{aligned} \tag{8.5}$$

Taking in the dynamic expression (8.5) to z_2 as a pseudo controller for the position tracking error. The control problem for the first stage is to define the desired value z^*_2 that force the dynamic of z_1, such that z_1 goes to the desired reference z^*_1 and makes the difference between z_1 and z^*_1 as small as possible and in consequence the integral of the tracking error too.

8.6.2 Pseudo Control formulation

The proposed value of z^*_2 for the position tracking error δ_1 is:

$$z^*_{2,t} = -k_1 \delta^{1+\varepsilon}_{1,t} \tag{8.6}$$

Where k_1 corresponds to a constant positive gain and ε is a positive constant integer.

8.7 Velocity stage

8.7.1 Problem statement

Given the desired reference z^*_2 in expression (8.6), that force the dynamic of z_1 to the desired reference. Subsequently, defining the velocity tracking error δ_2, given by:

$$\delta_{2,t} = z^*_{2,t} - z_{2,t} \tag{8.7}$$

where the dynamic of the tracking error is subject to the following differential equation

$$\begin{aligned}\dot{\delta}_{2,t} &= \dot{z}^*_{2,t} - \dot{z}_{2,t} \\ &= \dot{z}^*_{2,t} - z_{3,t}\end{aligned} \tag{8.8}$$

In the dynamic equation, the vector z_3 can be taken as pseudo control for the velocity tracking error. For the velocity stage, the control problem is to define the desired value for z^*_3, that force the dynamic of z_2 to make the velocity tracking error tend to zero and get that z_2 equal to z^*_2.

8.7.2 Pseudo Control formulation

Taking into count the proposed pseudo control z_2^* in the equation (8.6), defining the velocity tracking error as

$$\delta_{2,t} = z_{2,t} - z_{2,t}^* \tag{8.9}$$

subject to a dynamic expression given by:

$$\dot{\delta}_{2,t} = -k_1(1+\varepsilon)\delta_{1,t}^{\varepsilon}\dot{\delta}_{1,t} - z_{3,t} \tag{8.10}$$

Where in this stage, the variable z_3 can be considered as a pseudo control in the second stage. Where force the dynamic of z_2 to stabilise the state δ_2. The proposed z_3^* is:

$$z_{3,t}^* = -k_1(1+\varepsilon)\delta_{1,t}^{\varepsilon}\dot{\delta}_{1,t} + k_2\delta_{2,t}^{1+\varepsilon} \tag{8.11}$$

Where the constant gain k_2 is a positive constant value, and k_1 and $epsilon$ are defined in the desired pseudo control z_2^*.

8.8 Acceleration stage

8.8.1 Problem statement

For the third stage considering the proposed z_3^* in the expression (8.11) is possible to define the acceleration tracking error given by

$$\delta_3 = z_3^* - z_3 \tag{8.12}$$

where the integral of the tracking error as

$$\delta_4 = \int_{\tau=0}^{t} \delta_{3,\tau} d\tau \tag{8.13}$$

Considering the time derivative of the expression (8.11) and the dynamic of the auxiliary variable given in the equation (2.36), the dynamic of the acceleration tracking error is subject to the following expression:

$$\begin{aligned} \dot{\delta}_{3,t} &= \dot{z}_{3,t}^* - \dot{z}_{3,t} \\ &= \dot{z}_{3,t}^* - A\eta_t - Bv_t - P(\eta_t)\xi_t - G\dot{\xi}_t \end{aligned} \tag{8.14}$$

where v corresponds to the real control. This stage is taking the cost functional H on the function of the tracking error integral of z_3^* given by

$$H(\delta_{4,t}) = \sum_{i=1}^{2} \left\| \delta_{4,i,t} \right\| \tag{8.15}$$

In this form, the tracking problem can be formulated as an optimisation problem where the main objective is to minimise the value of the cost functional H that can be defined as

$$H(\delta_4) \rightarrow \min_{v^* \in U} H^* = 0 \tag{8.16}$$

8.8.2 Control formulation

It is proposed that the following integral sliding variable

$$\begin{aligned} s_t &= \delta_{3,t} + \frac{\delta_{4,t} + \gamma}{t + \mu_0} + \Psi(\delta_{4,t}) \\ \Psi(\delta_{4,t}) &= \frac{1}{t + \mu_0} \int_{\tau=0}^{t} \partial H(\delta_{4,\tau}) d\tau \end{aligned} \tag{8.17}$$

The corresponding time variation of the sliding variable is given by:

$$\dot{s}_t = \dot{\delta}_{3,t} + \frac{\delta_{3,t}}{t + \mu_0} - \frac{\delta_{4,t} + \gamma}{(t + \mu_0)^2} + \frac{1}{t + \mu_0} \partial H(\delta_{4,t}) - \frac{1}{(t + \mu_0)^2} \Psi(\delta_{4,t}) \tag{8.18}$$

the time derivative of the sliding variable in the equation (8.18) becomes

$$\begin{aligned} \dot{s}_t &= \dot{z}_{3,t}^* - A\eta_t - Bu_t - P(\eta_t)\xi_t - G\dot{\xi}_t \\ &+ \frac{\delta_{3,t}}{t + \mu_0} - \frac{\delta_{4,t} + \gamma}{(t + \mu_0)^2} + \frac{1}{t + \mu_0} \partial H(\delta_{4,t}) - \frac{1}{(t + \mu_0)^2} H(\delta_{4,t}) \end{aligned} \tag{8.19}$$

Defining the variable κ

$$\kappa_t = \frac{\delta_{3,t}}{t + \mu_0} - \frac{\delta_{4,t} + \gamma}{(t + \mu_0)^2} + \frac{1}{t + \mu_0} \partial H(\delta_{4,t}) - \frac{1}{(t + \mu_0)^2} H(\delta_{4,t}) \tag{8.20}$$

the sliding dynamic in the equation 8.19 can be expressed:

$$\dot{s}_t = \dot{z}_{3,t}^* - A\eta_t - Bu_t - P(\eta_t)\xi_t - G\dot{\xi}_t + \kappa_t \tag{8.21}$$

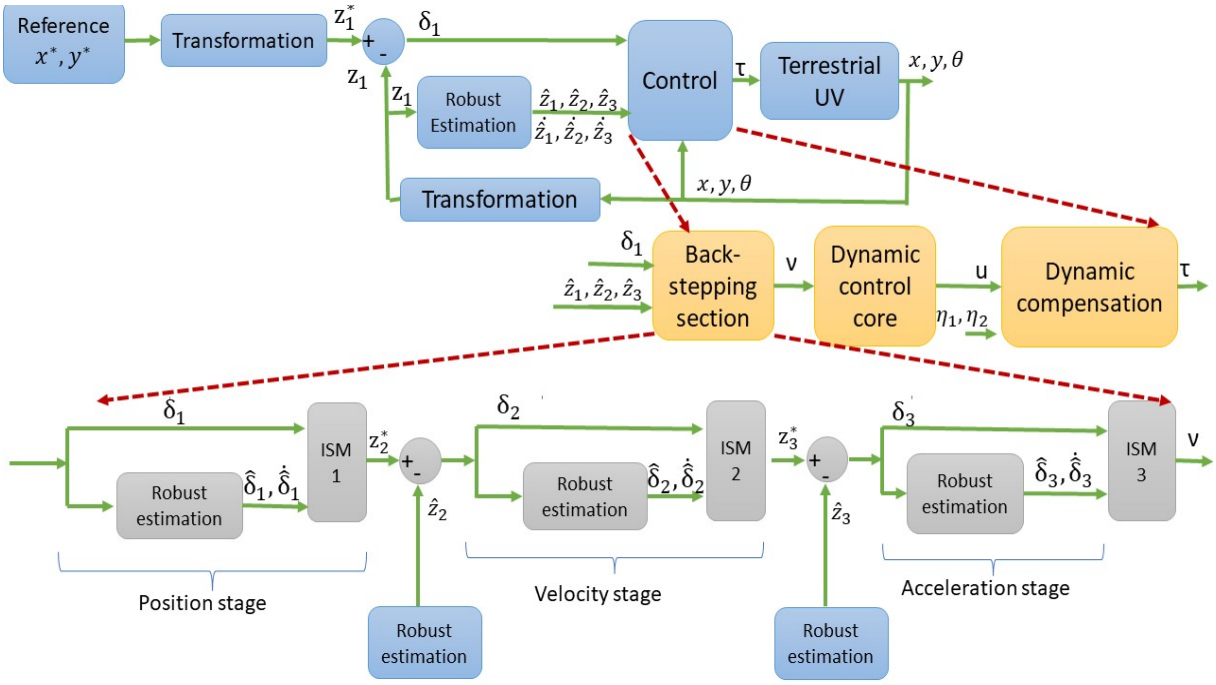

Figure 8.1: System diagram

Looking to satisfy the following expression

$$-\alpha_3 sign(s_t) = \dot{z}^*_{3,t} - A\eta_t - Bu_t + \kappa_t$$

the dynamic controller is proposed as:

$$\begin{aligned} B\dot{u}_t &= \alpha_3 sign(s_t) + \dot{z}^*_{3,t} - A\eta_t - Bu_t + \kappa_t \\ \dot{u}_t &= B^{-1}\left[\alpha_3 sign(s_t) + \dot{z}^*_{3,t} - A\eta_t - Bu_t + \kappa_t\right] \end{aligned} \tag{8.22}$$

The system diagram and outlining of the back-stepping formulation are schematised in the diagram in Figure (8.1)

8.9 Numerical evaluation

The model of the car was simulated in Simulink/Matlab, using as solver Ode4 Runge-Kutta with a fixed step-size of $1 * 10^{-4}$s. For use as a benchmark, a state feedback controller in the form of proportional derivative (PD) was implemented for comparison with the proposed formulation.

Table 8.2: PD, ISM and ISM EST control gains for quadrotor UV

Variable	K_p	K_d	K_i
z_3	100	1	.01

Variable	γ_0	γ_1	γ_2
z_3	.1	100	.1

The desired reference for the car is given by

$$\begin{aligned} X^* &= 8 * sin(0.1t) \\ Y^* &= 8 * cos(0.1t) \\ \theta^* &= atan\left(\frac{Y^*}{X^*}\right) - \frac{\pi}{2} \end{aligned} \tag{8.23}$$

The set of control gains used in the numerical evaluations is in Table (8.2).

In Figures, (8.2a) and (8.2b) can be observed the desired reference for z_1^* and how the state feedback controller and the average sub gradient formulation force the dynamic of the terrestrial vehicle to the desired reference since the first instant. Both controllers reduce the tracking error of z_1; these can be observed in Figure (8.3a) where are the square norm of the tracking error and both controllers keep the same values. The integral of the square of the tracking error is in Figure (8.3b), where both controllers are similar. The difference between the ISM controller and the PID is that the controller's energy forces the sliding surface from the first instance. The development of the controllers is in Figure (8.4). The square norm of the controller is in Figure (8.4a), where it can be observed that at the first instant, the magnitude of the ISM controller is more significant than the PID controller; this is because the formulation requires much energy for force the sliding surface at the first instant. For the rest of the time, the controllers are less than 1. The power employed by the proposed solution is also considered and is shown in Figure (8.4b). The power employed by the ISM controller is more significant than the PID controller, but even with that, it keeps almost constant for the rest of the time.

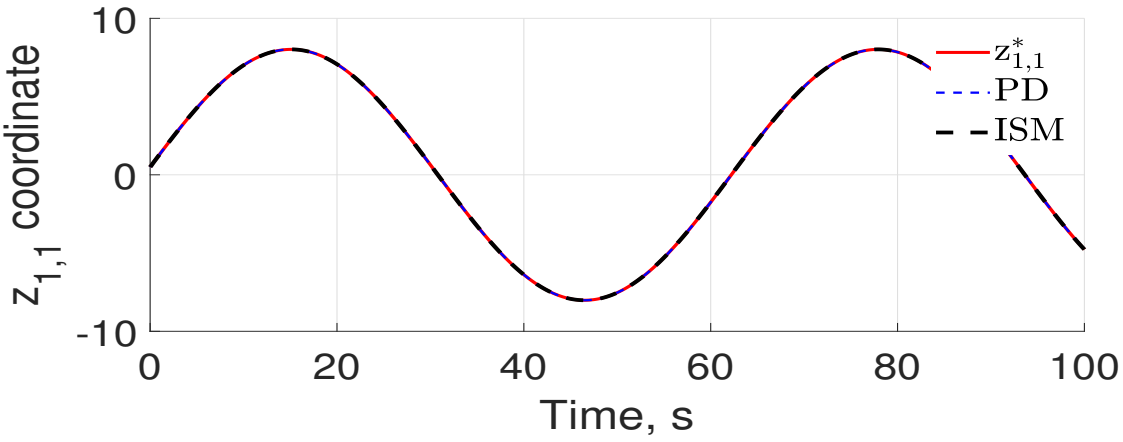

(a) Tracking of $z_{1,1}$ by state feedback controller and ISM controller

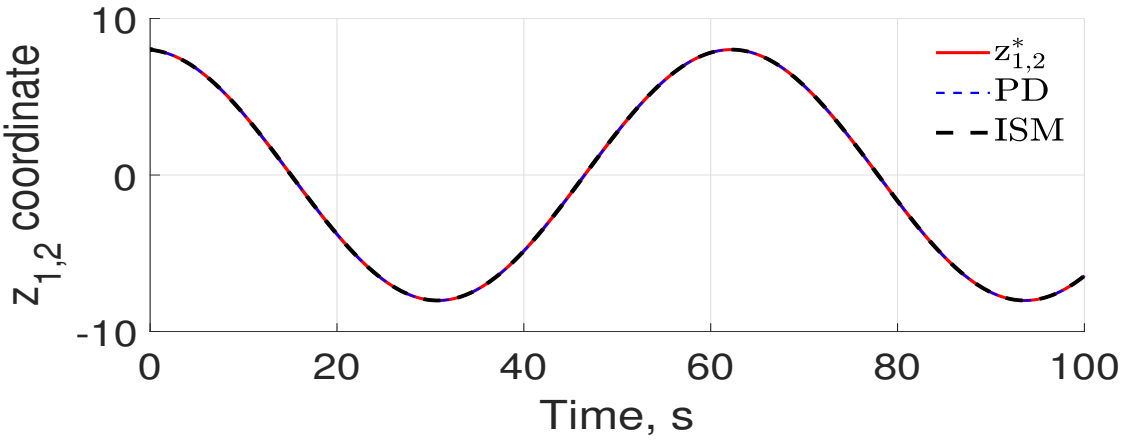

(b) Tracking of $z_{1,2}$ by state feedback controller and ISM controller

Figure 8.2: Tracking of the desired trajectory of z_1^*

8.10 Experimental Validation

A terrestrial prototype was developed to validate the theoretical results of the chapter. The UV was constructed in the Robotic Lab of Interdisciplinary Professional Unit of Biotechnology IPN (Unidad Profesional Interdisciplinaria de Biotecnología IPN -UPIBI) under the supervision of the Dr. Isaac Chairez Oria. The validation was realised in the Mechatronic department of At the School of Engineering and Sciences of the Western Region of the Tecnológico de Monterrey at the Guadalajara Campus under the supervision of Dr Isaac Chairez Oria.

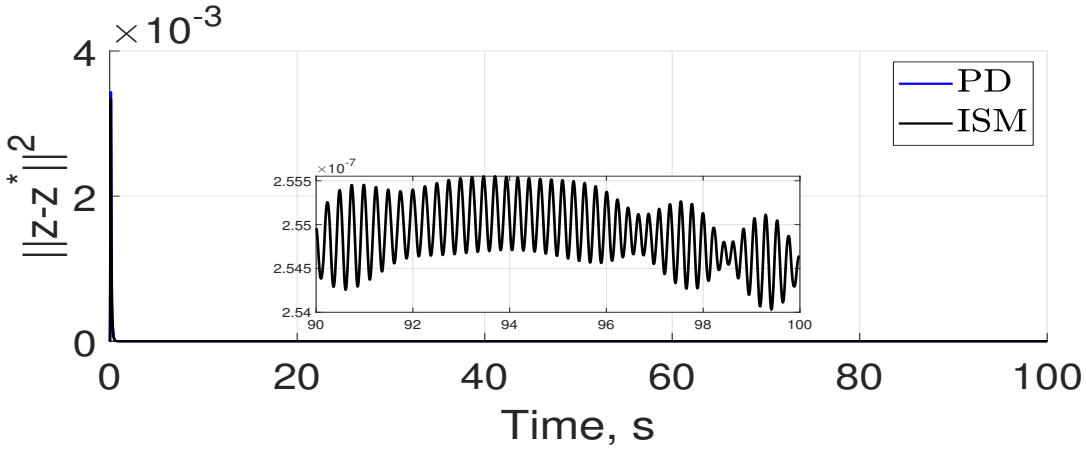

(a) Square norm of the tracking error of $z_{1,1}$ by state feedback controller and ISM controller

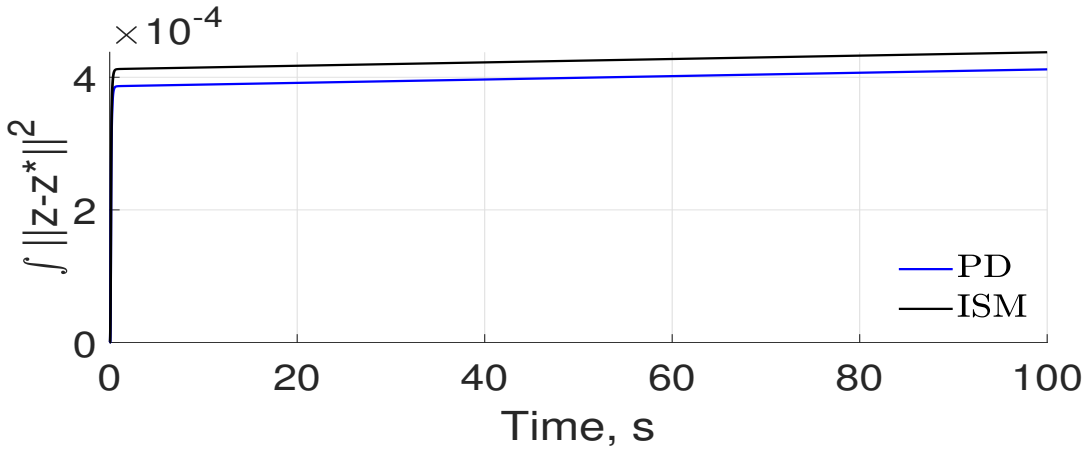

(b) Integral of the tracking error of $z_{1,2}$ by state feedback controller and ISM controller

Figure 8.3: Tracking error δ_1

8.10.1 Prototype Mechanics

The mechanical part of the terrestrial vehicle is shown in Figure (8.17)

The dimension of the car are described in the table 8.3

8.10.2 Prototype Diagrams

The complete electronic diagram is in Figure (8.6) Power supply diagram The diagram connection of the power supply is shown in Figure(8.7)

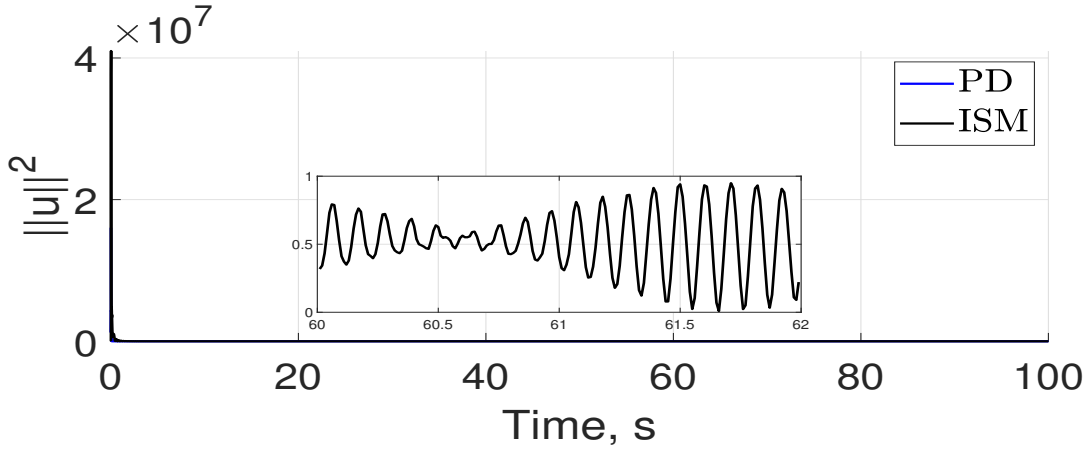

(a) Square norm of the state feedback control and the ISM control

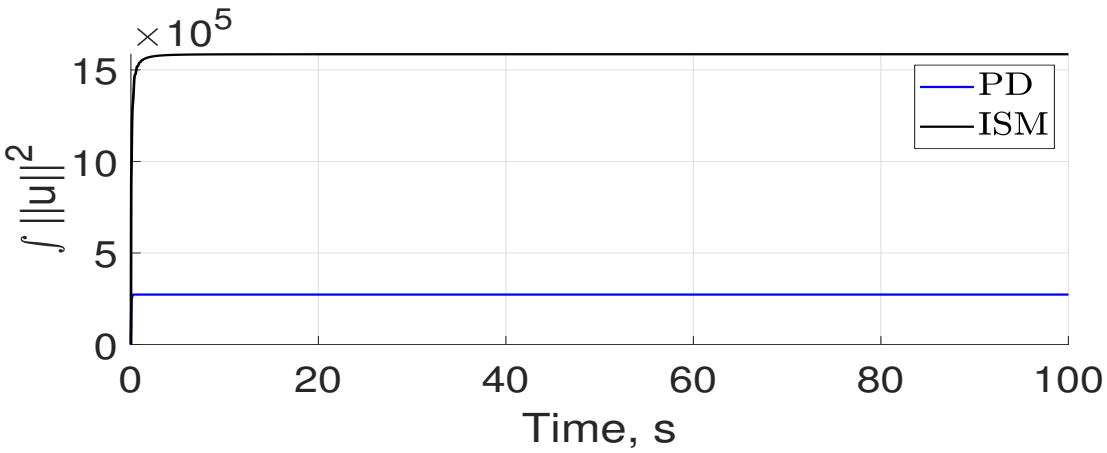

(b) Tracking of $z_{1,1}$ by state feedback controller and ISM controller

Figure 8.4: Integral of the PID control and the ISM controller

The encoder signals **A** and **B** correspond to the sensors to get the wheel's position. The encoder is connected as is shown in Figure(8.8).

The communication was realised by Bluetooth using the modul HC 05 and HC 06. The diagram connection of the Arduino cards is shown in Figure(8.9).

. The terrestrial vehicle's position was realised by vision using a camera.

Parameter	Variable	Value	Unity
Radius of wheels	r	4.82	cm
Large	a	15	cm
Width	a	21.66	cm

Table 8.3: Terrestrial UV parameters

8.10.3 Prototype Software

The Wheels velocity control was realised with the proposed solution and implemented by a micro-controller board of Arduino Mega 2560. The pseudo-code for the micro-controller board was the following:

Algorithm **Left and Right velocity control**

- Including library SoftwareSerial.h, Separador.h

- Define pins
- Define strings
- Define left and right object
- Define int variables
- Define float variables

function setup

- Beginning serial communication
- Beginning Bluetooth communication
- Define the pin mode of the pins
- Attach interruption in pins 0 and 1 for call I_updateEncoder algorithm

- Attach interruption in pins 4 and 5 for call D_updateEncoder algorithm

end setup

function loop

- Write High in pins for the enable of the H-bridge
- Reading of the Bluetooth communication and separation of a character string
- Definition of time variables
- Calculus of the velocity by the super-twisting algorithm
- Filtering of the derivative
- Calculus of the velocity tracking error
- Filtering of the tracking error
- Calculus of the time derivative of the velocity tracking error
- Filtering of the derivative
- Calculus of the Integral of the velocity tracking error
- Calculus of the ASG control
- Calculus of sliding variables and the sign of the sliding variable
- Control stop
- Limit the control signal
- Generation of PWM signal
- Initialising of for loop with *i* as the counter

    if(i<U_DM)

        if sign(U_DM)>0 $->$ ADELANTE(DERECHO)

if sign(U_DM)$< 0 ->$ ATRAS(DERECHO)

if sign(U_DM)$= 0 ->$ DETENER(DERECHO)

if(i>U_DM) $->$DETENER(DERECHO)

if(i<U_IM)

if sign(U_IM)$> 0 ->$ ADELANTE(IZQUIERDO)

if sign(U_IM)$< 0 ->$ ATRAS(IZQUIERDO)

if sign(U_IM)$= 0 ->$ DETENER(IZQUIERDO)

if(i>U_IM) $->$ DETENER(IZQUIERDO)

i$<-$i+1

end loop

function **I_updateEncoder()**

Read the signal A and B of the encoder

D_encoded = (D_MSB $<<$ 1) — D_LSB

D_sum=D_lastEncoded $<<$ 2) — D_encoded

if(D_sum $==$ 0b1101|| D_sum $==$ 0b0100|| D_sum $==$ 0b0010|| D_sum $==$ 0b1011)

D_MED=D_MED +1

if (D_sum $==$ 0b1110|| D_sum $==$ 0b0111|| D_sum $==$ 0b0001|| D_sum $==$ 0b1000)

D_MED=D_MED -1

D_lastEncoded = D_encoded

end

Algorithm **ADELANTE(int LADO[6])**

LADO[2]=1, LADO[4]=1

LADO[3]=0, LADO[5]=0

end

Algorithm **ATRAS(int LADO[6])**

Start

LADO[2]=0, LADO[4]=0

LADO[3]=1, LADO[5]=1

end

Algorithm **DETENER(int LADO[6])**

Start

LADO[2]=0, LADO[3]=0, LADO[4]=0, LADO[5]=0

end

The localisation of the terrestrial vehicle and the implementation of the control by the ASG formulation was by Matlab code. The Matlab pseudo-code employed was the following:

- Cleaning of workspace and communications
- Loading of camera parameters R and trans
- Initialising of Variables
- Serial communication initialisation
- Setting of camera conditions
- While ($i < 10000$)

  Setting of the desired point

  Calculus of auxiliary variable $z-1$,

  Processing of camera vision to get the terrestrial position by RGB values

Calculus of the position of the vehicle and estimation of the auxiliary variable z_1

Estimation of variables z_2 and z_3

Calculus of the tracking error of z_1^*

Estimation of the time derivative of the tracking error of z_1^*

Calculus of desired reference z_2^* and z_3^*

Calculus of derivative of the desired z_3^*

Calculus of tracking error, their corresponding derivative, the integral of the tracking error and the derivative of z_3^*

Calculus of the ASG control formulation

Control restrictions

Sending of the desired velocity by the serial port communication

Actualisation of time, time variable and i

- Closing of the serial communication

8.10.4 Validation

Three scenarios were carried out with the implementation of a state feedback controller to serve as a reference for the proposed solution with the ASG algorithm formulation. For evaluation, the displacement in the plane $x-y$ is also presented as the control signal obtained by the state feedback formulation and the proposed ASG algorithm and the tracking error of the auxiliary variable z_1.

Scenario 1

The first scenario consists of putting the terrestrial UV to the left of the desired position in the $X-Y$ plane, forcing a turn to the right by the terrestrial vehicle. The displacement of the UV in the plane $x-y$ is in Figure (8.18), where the state feedback controller's development force arrives nearer to the desired position than the one obtained by the ISM controller. Both controllers'

success in the minimisation of the tracking error of z_1 can be observed in Figure(8.19), where the absolute value of each component of the tracking error is shown. The tracking error is minimised at the first 0.02 seconds by the PID controller, and the ISM proposed. It can be observed that the development of tracking error by the PID controller is faster than the ISM. The control signal obtained by both formulations is shown in Figure (8.20), where the magnitude of the ISM controller is 1000 bigger than the PID solution. Figures (8.13a), (8.13b) and (8.13c) show the development of the terrestrial UV by the PID controller. In Figures (8.13d), (8.13e) and (8.13f) show the development of the terrestrial UV by the ISM controller.

Scenario 2

The second starting point for the terrestrial UV is on the right of the desired position to get a turn to the left by the UV. In this scenario, the ISM controller force the UV nearest to the desired position, and the horizontal displacement by the two controllers is shown in Figure (8.14). Both controllers minimise the tracking error of z_1 in the first 0.05 seconds. The magnitude of the ISM controller's tracking error for $z_{1,1}$ is .5 times smaller than the PID controller. For the case of $z_{1,2}$, the tracking error by the PID controller is 300 times more significant than the one obtained by the ISM controller, and this can be observed in Figure (8.15). Figure (8.16) shows the control signals by both controllers, where it can be observed that the magnitude of the ISM controller is 100 and 10 times smaller than that obtained by the PID controller. Images 8.17a, 8.17b, and 8.17c show the UV development at different instants of the experiment.

Scenario 3

The third starting point is at the left of the desired point. Both controllers force the UV to the desired point; the performance of both controllers in the $x-y$ plane is in Figure (8.18). The tracking error of z_1 is minimised by both controllers in the first 0.04 seconds, as can be observed in Figure (8.19). The control signals employed by the implemented propositions are in Figure (8.20) that ISM control is ten times smaller than the PID control signal.

8.11 Chapter Conclusions

The theoretical implementation of the ISM controller forces the dynamic of the terrestrial vehicle to the desired trajectory. In the real-world implementation, the ISM controller also manipulates the UV to the desired position. The ISM control minimises the auxiliary variable's tracking error, and the control signal is competitive with the PID controller. However, the implementation in the real world also implies aspects to consider for improving the controller's efficiency as restrictions in the trajectory and the control magnitude. Also another important aspect is to consider the delays in communication. These aspects can be considered to improve the development of the ISM formulation.

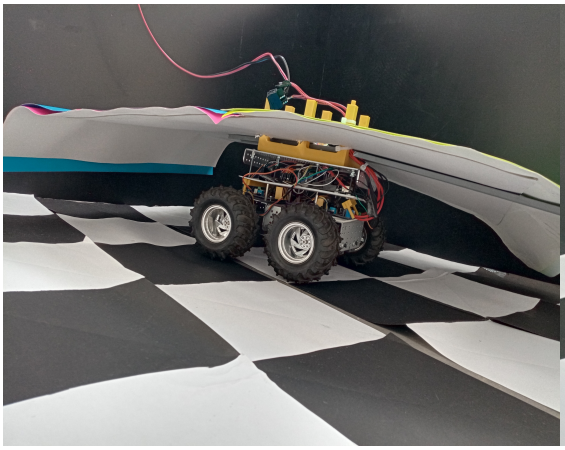

(a) Terrestrial Unmanned vehicle

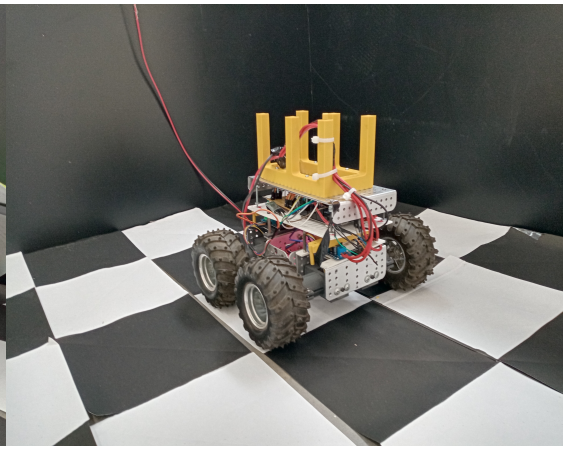

(b) Terrestrial Unmanned vehicle

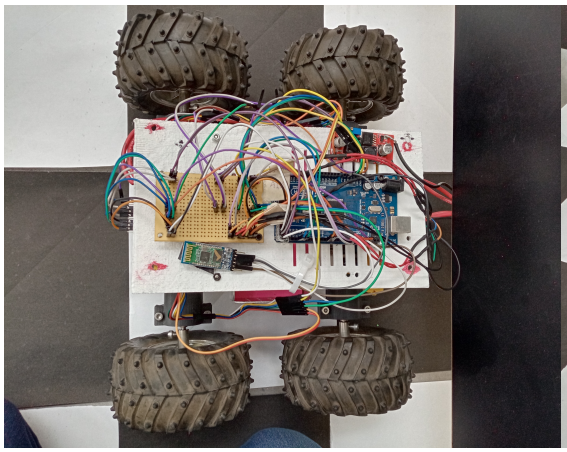

(c) Terrestrial Unmanned vehicle

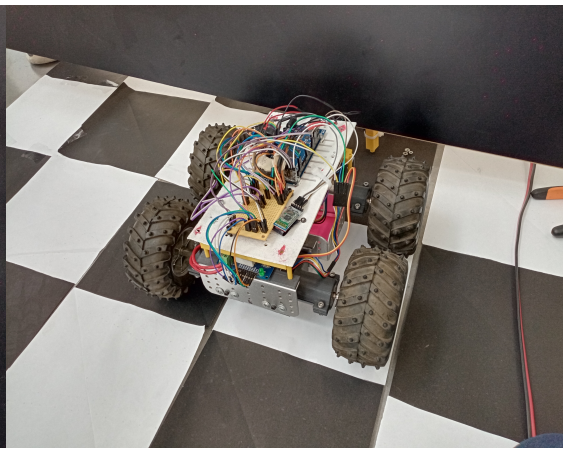

(d) Terrestrial Unmanned vehicle

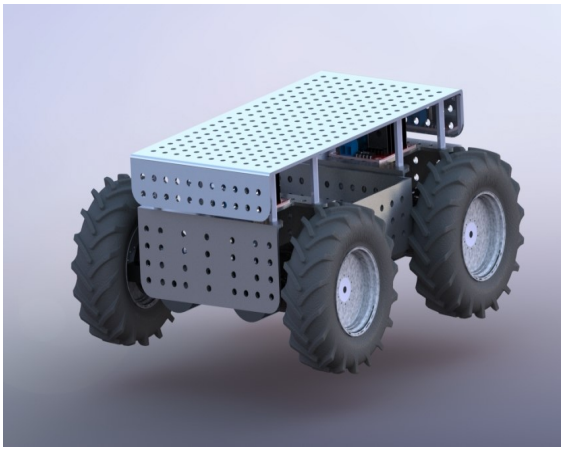

(e) Terrestrial Unmanned vehicle

Figure 8.5: Terrestrial Unmanned vehicle.

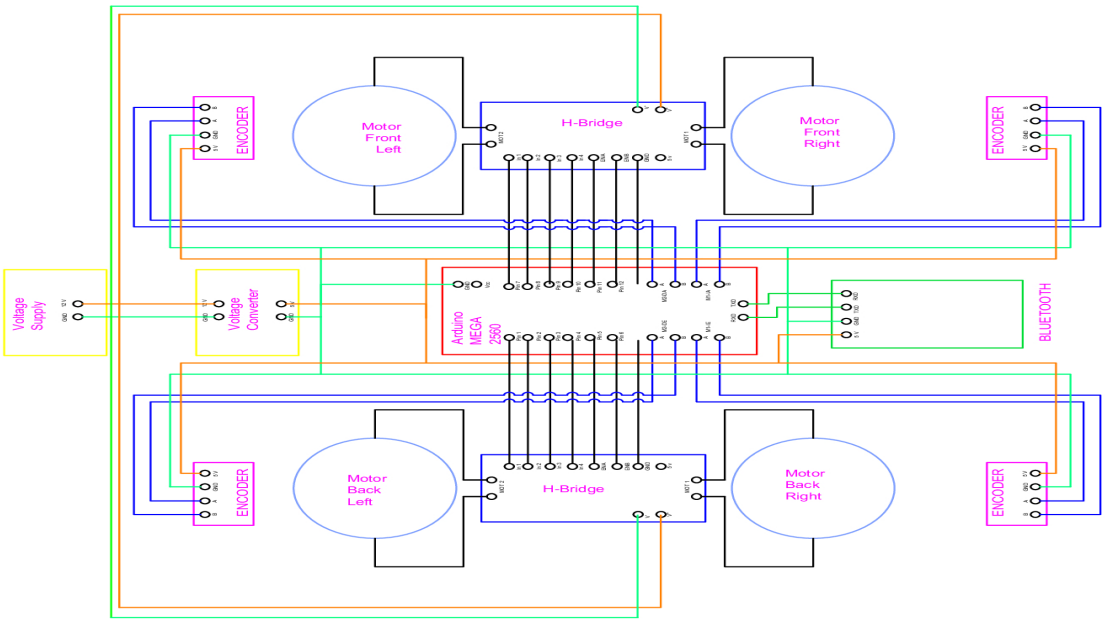

Figure 8.6: Electronic diagram

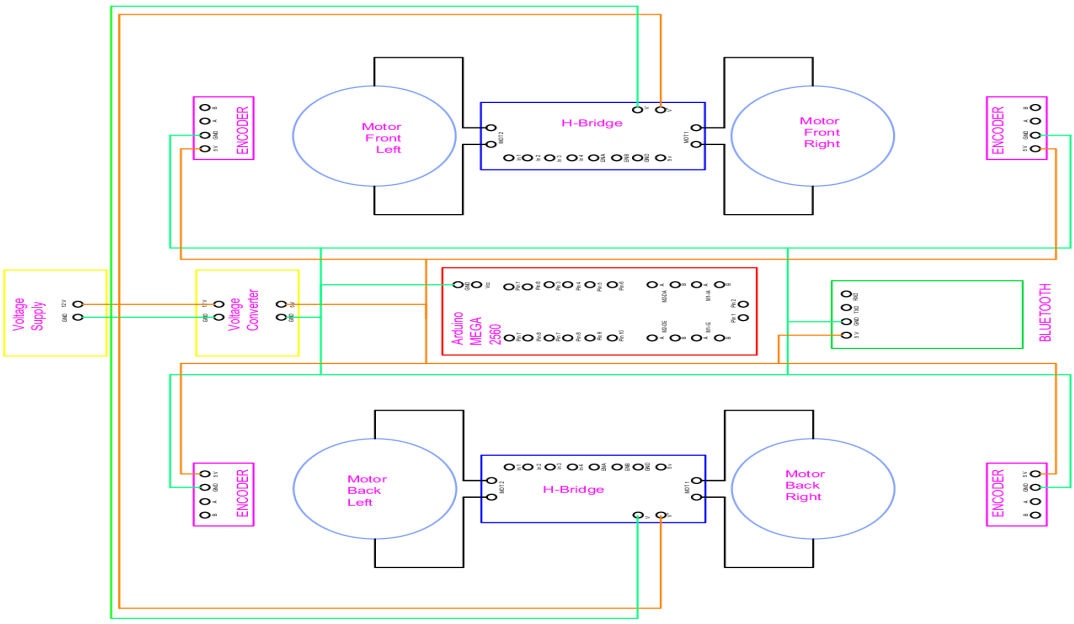

Figure 8.7: Power supply diagram

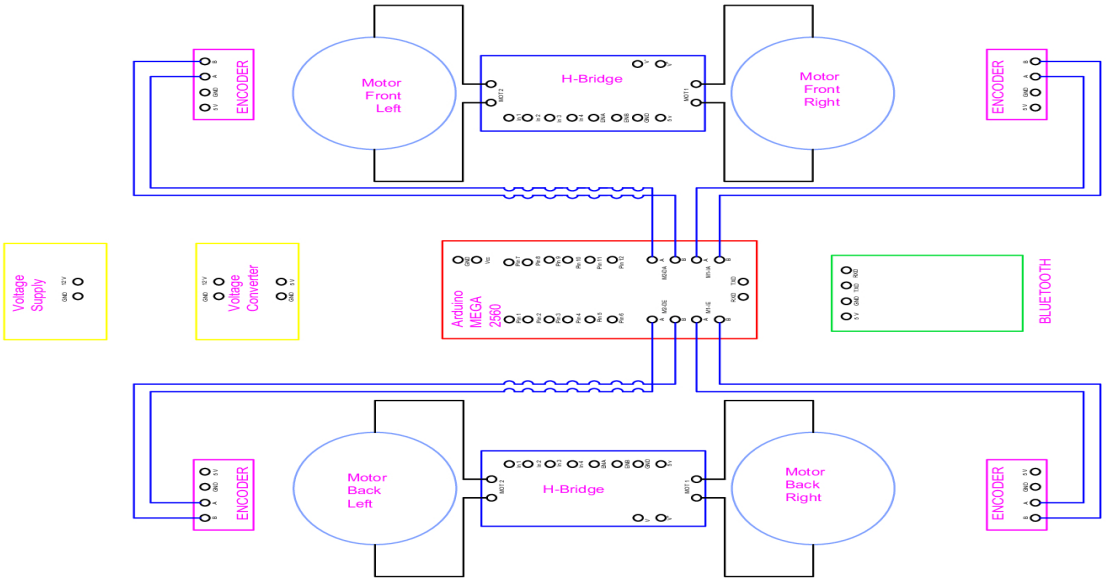

Figure 8.8: Sensors connection diagram

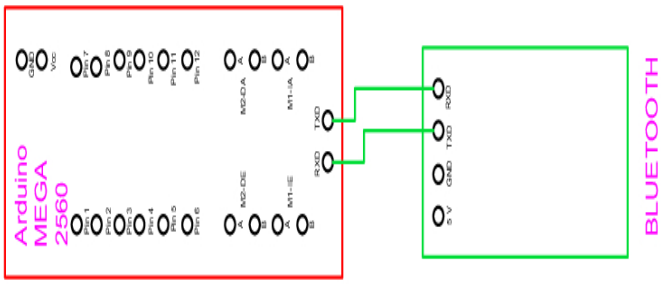

Figure 8.9: Communication diagram

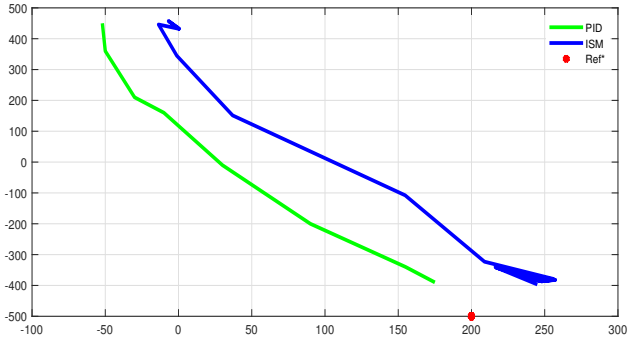

Figure 8.10: Scenery 1 $x-y$ plane terrestrial displacement by the state feedback controller and the ISM controller

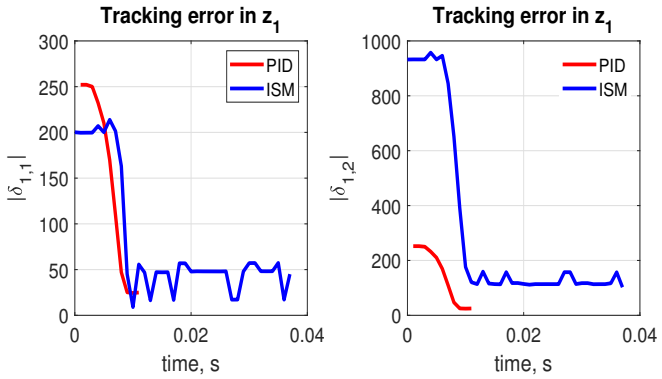

Figure 8.11: Scenery 1 tracking error of the auxiliary variable z_1 by the state feedback controller and the ISM controller

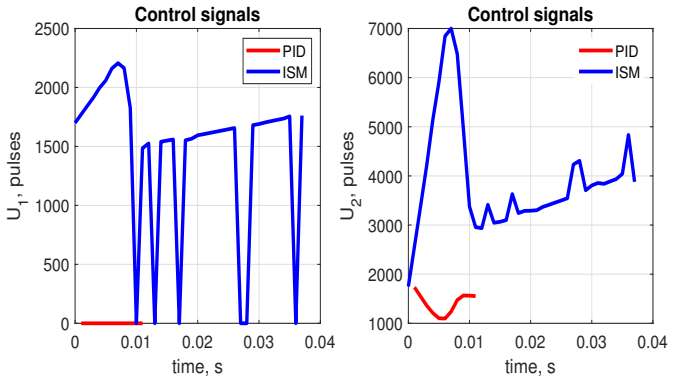

Figure 8.12: Scenery 1 control u by the state feedback controller and the ISM controller

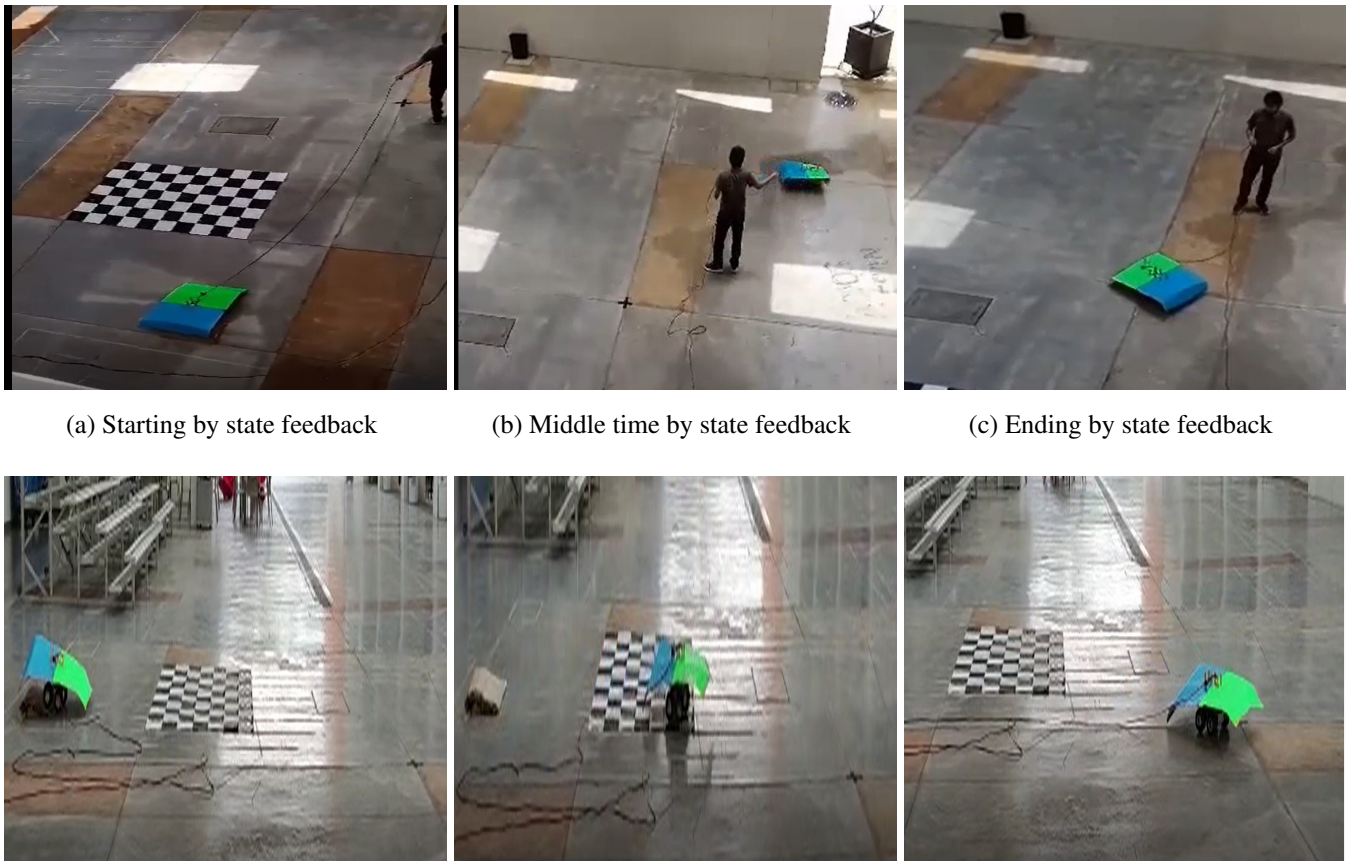

(a) Starting by state feedback (b) Middle time by state feedback (c) Ending by state feedback

(d) Starting by ASG (e) Middle time by ASG (f) Ending by ASG

Figure 8.13: Terrestrial Unmanned vehicle Scenery 1.

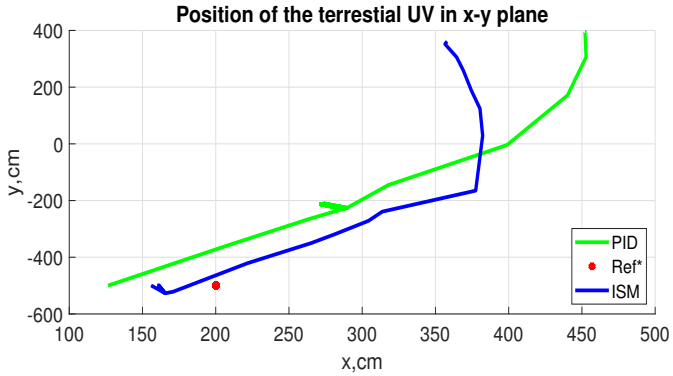

Figure 8.14: Scenery 2 $x-y$ plane terrestrial displacement by the state feedback controller and the ISM controller

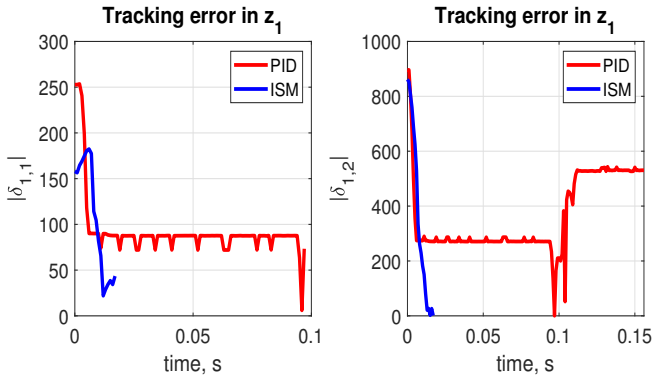

Figure 8.15: Scenery 2 tracking error of the auxiliary variable z_1 by the state feedback controller and the ISM controller

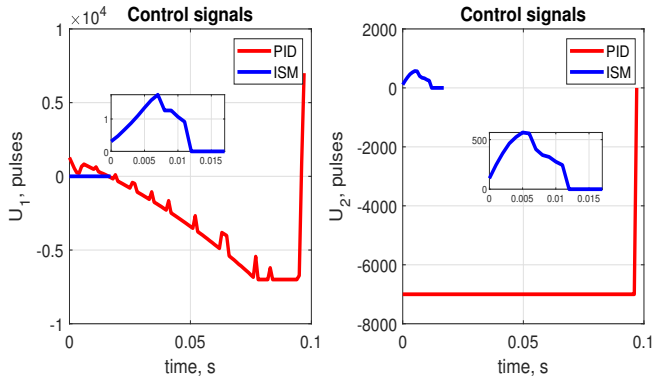

Figure 8.16: Scenery 2 control u by the state feedback controller and the ISM controller

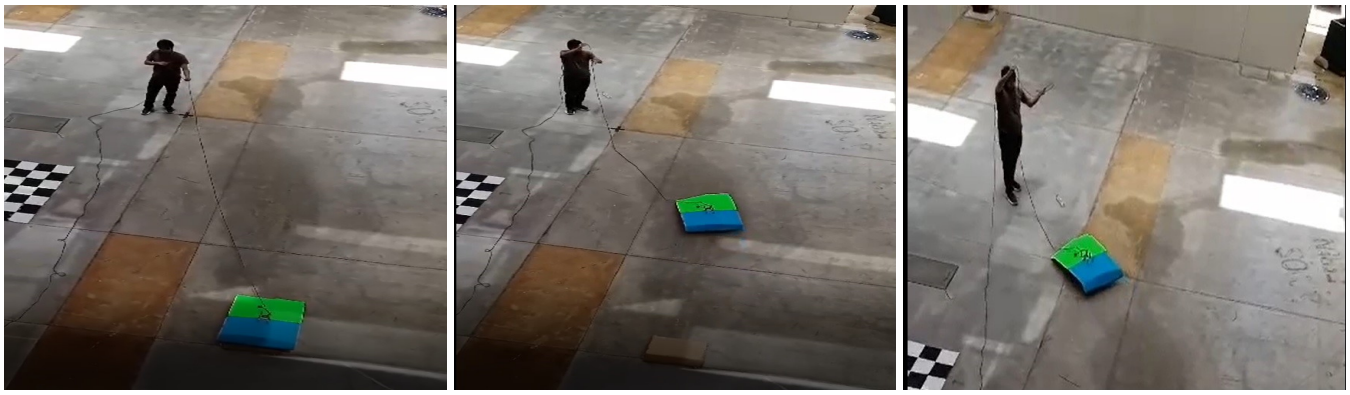

(a) Starting by ASG (b) Middle time by ASG (c) Ending by ASG

Figure 8.17: Terrestrial Unmanned vehicle Scenario 2.

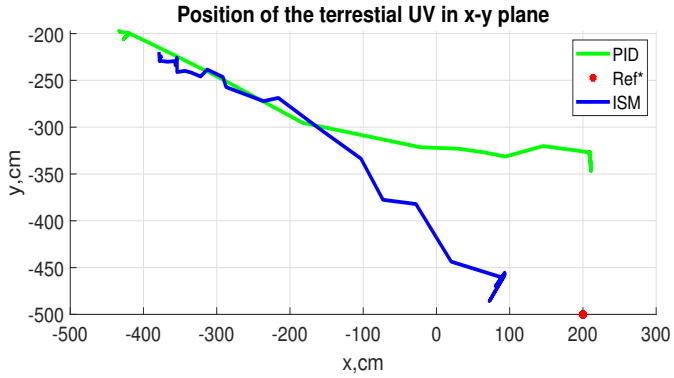

Figure 8.18: Scenery 3 $x-y$ plane terrestrial displacement by the state feedback controller and the ISM controller

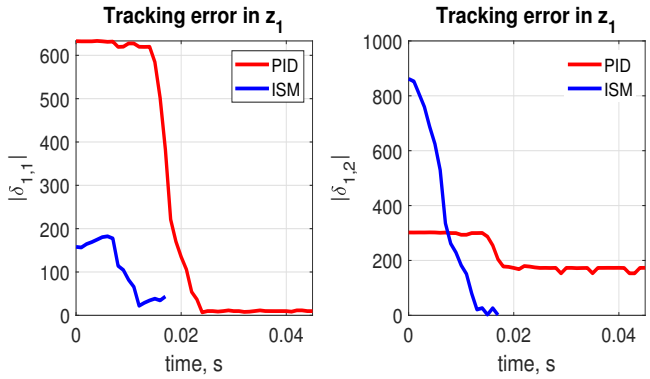

Figure 8.19: Scenery 3 tracking error of the auxiliary variable z_1 by the state feedback controller and the ISM controller

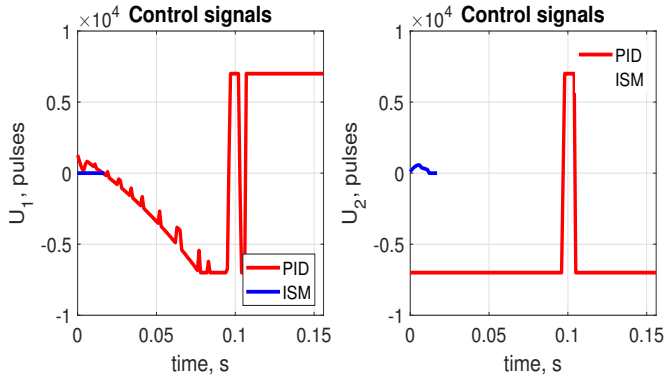

Figure 8.20: Scenery 3 control u by the state feedback controller and the ISM controller

Publications

Conference

- Hernandez-Sanchez, A., Chairez, I., & Poznyak, A. (2020, June). **Extended integral sliding mode robust sub-gradient extremum seeking control for tracking trajectory of autonomous underwater vehicle.** In 2020 7th International Conference on Control, Decision and Information Technologies (CoDIT) (Vol. 1, pp. 433-438). IEEE. DOI: 10.1109/CoDIT49905.2020.9263845

Journal

- Hernández-Sánchez, A., Poznyak, A., Chairez, I., & Andrianova, O. (2021). **Robust 3-D autonomous navigation of submersible ship using averaged sub-gradient version of integral sliding mode.** Mechanical Systems and Signal Processing, 149, 107169. https://doi.org/10.1016/j.ymssp.2020.107169

- Hernandez-Sanchez, A., Andrianova, O., Poznyak, A., & Chairez, I. (2021). **Tridimensional autonomous motion robust control of submersible ship based on averaged sub-gradient integral sliding mode approach.** International Journal of Systems Science, 52(3), 541-554. https://doi.org/10.1080/00207721.2020.1832285

- Hernandez-Sanchez, A., Chairez, I., & Poznyak, A. (2020, June). **Extended integral sliding mode robust sub-gradient extremum seeking control for tracking trajectory of autonomous underwater vehicle.** In 2020 7th International Conference on Control, Decision and Information Technologies (CoDIT) (Vol. 1, pp. 433-438). IEEE. DOI: 10.1109/CoDIT49905.2020.9263845

- Hernandez-Sanchez, A., Chairez, I., Poznyak, A., & Andrianova, O. (2021). **Dynamic Motion Backstepping Control of Underwater Autonomous Vehicle Based on Averaged Sub-gradient Integral Sliding Mode Method.** Journal of Intelligent & Robotic Systems, 103(3), 1-17.DOI https://doi.org/10.1007/s10846-021-01466-3

- Hernández-Sánchez, A., Poznyak, A., Andrianova, O., & Chairez, I. (2021). **Output feedback averaged sub-gradient integral sliding mode control to regulate the tridimensional autonomous motion of autonomous submersible vehicles.** Proceedings of the Institution of Mechanical Engineers, Part I: Journal of Systems and Control Engineering, 09596518211056415. https://doi.org/10.1177/09596518211056415

- Chertopolokhov, V., Andrianova, O., Hernandez-Sanchez, A., Mireles, C., Poznyak, A., & Chairez, I. (2022). **Averaged sub-gradient integral sliding mode control design for cueing end-effector acceleration of a two-link robotic arm.** ISA Transactions. https://doi.org/10.1016/j.isatra.2022.07.024

- Alejandra Hernandez-Sanchez,Olga Andrianova, Alexander Poznyak and Isaac Chairez. (2022).**Robust Dynamic Backstepping Averaged SubGradient Integral Sliding Mode Control for Navigation of Mobile Robots.** Proceedings of the Institution of Mechanical Engineers. Part I: Journal of Systems and Control Engineering. https://doi.org/10.1177/09596518221082801

In review

- Alejandra Hernandez-Sanchez,Olga Andrianova, Alexander Poznyak and Isaac Chairez.**Robust Motion Control of SARV With Dynamic Actuator by Backstepping-ASG Version of Integral Sliding Mode Method**

In process

- Alejandra Hernandez-Sanchez, Alexander Poznyak and Isaac Chairez.**"Diferential neural network feedback controller for UAV devices based on ASG version of Integral Sliding Mode concept"**

- A. Hernandez-Sanchez, A. Poznyak and I. Chairez, **"Adaptive neural network output feedback controller for mobile robotic autonomous devices using the integral sliding mode averaged sub-gradient theory"**

Internship

- Internship at the Moscow State University 'M. V. Lomonosov'MSU. Under the supervision of Dr. D.V. Georgievskii was developed an interconnection between RoboDK and MATLAB/Simulink for the control of a robotic arm of 6 degrees of freedom. Between the 18 of February 2022 and the 29 of April 2022.

- Internship at Instituto Tecnológico de Estudios Superiores de Monterrey, Campus Guadalajara. Under the supervision of Dr. Isaac Chairez Oria, a terrestrial platform was developed for the experimental validation of the ASG formulation. In the period 30 of May 2022 to 18 of July 2022.

Chapter 9

General conclusions

Se logró el control del desplazamiento de vehículos no tripulados de diferente naturaleza, con conocimiento parcial de la dinámica, en diferentes dimensiones, a través de diversas formulaciones. La optimización de los errores de seguimiento se logró mediante el algoritmo de subgradiente promedio implementado con la técnica de modo deslizante Integral. Además, la implementación del control propuesto se llevó a cabo en un vehículo terrestre no tripulado.

Se desarrolló una formulación de control utilizando la técnica de ISM para obtener la optimización de una función convexa o no estrictamente convexa del error de seguimiento de posición UV con formulación de retroalimentación de estado, retroceso y retroalimentación de salida.

La estabilidad asintótica de las superficies deslizantes de los controladores se demuestra a travez de la función de Lyapunov.

Se demuestra la eficiencia del controlador ISM que optimiza la función de costo de la integral del error de seguimiento considerando la dinámica de los actuadores a través de simulaciones numéricas.

Se demuestra mediante simulaciones numéricas que el controlador ISM tiene una mayor eficiencia en el seguimiento de trayectorias con una magnitud de control menor que el controlador PID.

Se obtuvo controladores que se pueden implementar en todo tipo de modelos mecánicos con

representaciones de modelos Newton-Euler, Lagrangian y Hamiltonian.

9.1 Future Work

- Development of an output feedback controller for optimisation of a neural network-based tracking error function for UV model estimation. Design the learning laws of the neural networks for the identification of the UV model and take the estimation of the missing states by neural networks for the implementation of the ISM robust controller by subgradient average for the optimisation of trajectory tracking in the backstepping formulation.

- Development of a robust controller for constrained optimisation, considering constraint on the UV, the dynamics of the actuators and the implemented control. Robust controller formulation with variable gains considering the different constraints for trajectory tracking optimisation.

- Development of robust adaptive control considering constraints on the unmanned vehicle, variable constraints on the trajectory, and controller saturation. Control formulation based on ISM with adaptive gains and through observers for identifying objects around the vehicle.

- Experimental validation of the controllers proposed in the study in different devices. Implementing the proposed controllers in a quadrotor for trajectory tracking, considering constraints on the controller output.

- Development of an observer by the estimation error optimisation for the modelling and control of a UV. Functional optimisation of the variable estimation error of an unmanned vehicle. Furthermore, the development of robust control by using the estimated states with the robust observer.

- Development of a robust controller for the synchronisation of unmanned vehicles. Development of a controller for trajectory tracking by unmanned vehicles and formulation for

the control of the synchronisation of other vehicles to optimise the distance error between the vehicles.

- Development of a controller for the manipulation of a robotic arm included in the structure of a vehicle for the manipulation of various tools such as grippers, welders, paint compressors, etc. Modelling of an unmanned vehicle with a robotic arm and formulation of a robust controller for the displacement of the unmanned vehicle and manipulation of the axes of freedom of the robotic arm considering restrictions in the actuators and the control output.

Chapter 10

Appendix

10.1 A.State feedback formulation-Position tracking error

I. Stability analysis by Lyapunov function

Given the function for $k_{\mathbf{x},t}$, and the proposed controller in the equation (4.14) and (4.13) respectively, provides the desired dynamics which is shown below. Introducing the candidate of Lyapunov function as $V_{\mathbf{x},t}(s_t) = \frac{1}{2}\left(\left[\sqrt{s_t^\top G_{\mathbf{x}}^{-1} s_t} - \varepsilon_t\right]_+\right)^2$, $\varepsilon_t > 0$. Defining $\chi_{\mathbf{x},t} := \frac{\left[\sqrt{s_t^\top G_{\mathbf{x}}^{-1} s_t} - \varepsilon_t\right]_+}{\sqrt{s_t^\top G_{\mathbf{x}}^{-1} s_t}}$ in view of, the condition of the dynamic of the tracking error in expression (4.8) for $t \geq t_0$,, defining $\mu_t = \frac{1}{t+\mu}$ and using the definition of $\dot{s}_t$ described by:

$$\dot{s}_t = \dot{\mathbf{x}}_{b,t} + \lambda_t \left[\mathbf{x}_{b,t} + \partial H(\mathbf{x}_{a,t}) - \Psi_t\right] - \lambda_t^2 \left[\mathbf{x}_{a,t} + \eta\right]. \tag{10.1}$$

we have as the time derivative of the Lyapunov function

$$\left.\begin{aligned} \dot{V}_{\mathbf{x},t}(s_t) &= \left[\sqrt{s_t^\top G_{\mathbf{x}}^{-1} s_t} - \varepsilon_t\right]_+ \left(\frac{s_t^\top G_{\mathbf{x}}^{-1} \dot{s}_t}{\sqrt{s_t^\top G_{\mathbf{x}}^{-1} s_t}} - \dot{\varepsilon}_t\right) \\ &= \frac{\left[\sqrt{s_t^\top G_{\mathbf{x}}^{-1} s_t} - \varepsilon_t\right]_+}{\sqrt{s_t^\top G_{\mathbf{x}}^{-1} s_t}} \left(s_t^\top G_{\mathbf{x}}^{-1} \dot{s}_t - \sqrt{s_t^\top G_{\mathbf{x}}^{-1} s_t}\,\dot{\varepsilon}_t\right) \\ &= \chi_{\mathbf{x},t} s_t^\top G_{\mathbf{x}}^{-1} \left[F_{\mathbf{x}} + G_{\mathbf{x}} \mathbf{u}_{\mathbf{x},t} + \mathbf{z}_{\mathbf{x},t}^{(0)}\right] - \chi_{\mathbf{x},t} \dot{\varepsilon}_t \sqrt{s_t^\top G_{\mathbf{x}}^{-1} s_t} \end{aligned}\right\} \tag{10.2}$$

where

$$\mathbf{z}_{\mathbf{x},t}^{(0)} := \lambda_t \left[\mathbf{x}_{b,t} + \partial H(\mathbf{x}_{a,t}) - \Psi_t\right] - \lambda_t^2(\mathbf{x}_{a,t} + \eta). \tag{10.3}$$

Since the conditions in the expression (4.8), given by

$$\left.\begin{array}{c} \left\|F_{\mathbf{x}}\left(\mathbf{x}_{a,t}, \mathbf{x}_{b,t}, \ddot{\mathbf{h}}_t^*\right)\right\| = F_{\mathbf{x},t}^+, \\ F_{\mathbf{x},t}^+ = \gamma_0 + \gamma_1 \left\|\rho_t\right\| + \gamma_2 \left\|\varphi_t\right\| \\ \gamma_0 = \gamma + \beta_\xi \\ \gamma_j > 0,\ \beta_\xi > 0;\ \ j = 0, ..., 2 \\ \left\|G_{\mathbf{x}}\right\| \leq \gamma_G,\ \ \gamma_G > 0 \end{array}\right\}. \tag{10.4}$$

the last equation for the Lyapunov time derivative function (10.2) becomes

$$\begin{aligned} \dot{V}_{\mathbf{x},t}(s_t) &\leq \chi_{\mathbf{x},t} s_t^\top \mathbf{u}_{\mathbf{x},t} + \gamma_G^{-1} \chi_{\mathbf{x},t} \left\|s_t\right\| \left(F_{\mathbf{x},t}^+ + \left\|\mathbf{z}_{\mathbf{x},t}^{(0)}\right\| + \left|\dot{\varepsilon}_t\right|\right) \\ &= \gamma_G^{-1} \chi_{\mathbf{x},t} \left\|s_t\right\| \mathbf{z}_{\mathbf{x},t}^{(1)} + \chi_{\mathbf{x},t} s_t^\top \mathbf{u}_{\mathbf{x},t} \end{aligned} \tag{10.5}$$

Here $\mathbf{z}_{\mathbf{x},t}^{(1)} := F_{\mathbf{x},t}^+ + \left\|\mathbf{z}_{\mathbf{x},t}^{(0)}\right\| + \left|\dot{\varepsilon}_t\right|$. Taking $\mathbf{u}_{\mathbf{x}}$ as in the expression (4.13), given by

$$\mathbf{u}_{\mathbf{x},t} = -G_{\mathbf{x}}^+ \left(k_{\mathbf{x},t} \frac{s_t}{\left\|s_t\right\| + \varepsilon_t}\right), \tag{10.6}$$

leads to

$$\begin{aligned} \dot{V}_{\mathbf{x},t}(s_t) &\leq \gamma_G^{-1} \chi_{\mathbf{x},t} \left\|s_t\right\| \mathbf{z}_{\mathbf{x},t}^{(1)} - \chi_{\mathbf{x},t} s_t^\top \left(k_{\mathbf{x},t} \frac{s_t}{\left\|s_t\right\| + \varepsilon_t}\right) \\ &\leq \chi_{\mathbf{x},t} \left\|s_t\right\| \left(\gamma_G^{-1} \mathbf{z}_{\mathbf{x},t}^{(1)} - k_{\mathbf{x},t} \frac{\left\|s_t\right\|}{\left\|s_t\right\| + \varepsilon_t}\right). \end{aligned} \tag{10.7}$$

Since the inequality (10.7) is not trivial only when $\chi_{\mathbf{x},t} = 1$, or equivalently, when $\left\|s_t\right\| \geq \varepsilon_t$. This condition is fulfilled if $\left\|s_t\right\|$ satisfies $\left\|s_t\right\| > \varepsilon_t$. Therefore, within this region, we have

$$\frac{\left\|s_t\right\|}{\left\|s_t\right\| + \varepsilon_t} \geq \frac{\varepsilon_t}{\varepsilon_t + \varepsilon_t} = \frac{1}{2}$$

So, the inequality (10.7) becomes

$$\dot{V}_{\mathbf{x},t}(s_t) \leq \left\|s_t\right\| \left(\gamma_G^{-1} \mathbf{z}_{\mathbf{x},t}^{(1)} - \frac{k_{\mathbf{x},t}}{2}\right) \tag{10.8}$$

Selecting $k_{\mathbf{x},t}$ in such a way that the following inequality is fulfilled $(1/2)k_{\mathbf{x},t} - \gamma_G^{-1} \mathbf{z}_{\mathbf{x},t}^{(1)} = k_0 > 0$, we get that $k_{\mathbf{x},t} = 2\left(\gamma_G^{-1} \mathbf{z}_{\mathbf{x},t}^{(1)} + k_0\right)$ and in consequence the inequality (10.8) becomes

$$\dot{V}_{\mathbf{x},t}(s_t) \leq -k_0 \left\|s_t\right\| \leq -k_0 \sqrt{2V_{\mathbf{x},t}(s_t)} \tag{10.9}$$

From expression (10.9), a finite time convergence of $V_{\mathbf{x},t}(s_t)$ to the origin. Indeed, we have $0 \leq \sqrt{V_{\mathbf{x},t}(s_t)} \leq \sqrt{V_{\mathbf{x},t}(s_t)} - \dfrac{k_0}{2\sqrt{2}}t$ implying $V_{\mathbf{x},t}(s_t) = 0$ for any $t \geq t_{reach} = \dfrac{2\sqrt{2}}{k_0}\|s_0\| = 0$. But taking $s_0 = 0$, one may get $t_{reach} = t_0 = 0$.

II. Practical desired regimen

Proof. Define $\tilde{\mathbf{x}}_{a,t} := \mathbf{x}_{a,t} - w_t$, $\mu_t := t + \mu_0$ and the auxiliary variable $\zeta_t := \int_0^t -\partial H(\mathbf{x}_{a,\tau})\, d\tau$ and satisfies

$$\zeta_t = \gamma_t \mathbf{x}_{b,t} + \mathbf{x}_{a,t} + \eta$$

Starting with

$$\begin{aligned} \frac{d}{dt}\left[\frac{1}{2}\|\zeta_t\|^2\right] &= \dot{\zeta}_t^\top \zeta_t \\ &= -\partial^\top H(\mathbf{x}_{a,t})\left[\mu_t \mathbf{x}_{b,t} + \mathbf{x}_{a,t} + \eta\right] \\ &= -\partial^\top H(\mathbf{x}_{a,t})(\mathbf{x}_{a,t}) - \partial^\top H(\mathbf{x}_{a,t})\left(\mu_t \mathbf{x}_{b,t} + \eta\right). \end{aligned}$$

By the inequality (3.21) and using the identity

$$\begin{aligned} \partial^\top H(\mathbf{x}_{a,t})\mathbf{x}_{b,t} &= \partial H(\mathbf{x}_{a,t})\left[\dot{\mathbf{x}}_{a,t} - w_t\right] \\ &= \frac{d}{dt}\left[H(\mathbf{x}_{a,t}) - H^*\right] + \partial^\top H(\mathbf{x}_{a,t}) w_t \end{aligned}$$

the following inclusion is estimated

$$\begin{aligned} \frac{d}{dt}\left[\frac{1}{2}\|\zeta_t\|^2\right] \leq &-\left[H(\mathbf{x}_{a,t}) - H^*\right] - \partial^\top H(\mathbf{x}_{a,t})\eta \\ &-\mu_t\left[\frac{d}{dt}\left[H(\mathbf{x}_{a,t}) - H^*\right] + \partial^\top H(\mathbf{x}_{a,t}) w_t\right] \end{aligned}$$

or equivalently

$$\begin{aligned} \left[H(\mathbf{x}_{a,t}) - H^*\right] \leq &-\frac{d}{dt}\left[\frac{1}{2}\|\zeta_t\|^2\right] - \partial^\top H(\mathbf{x}_{a,t})\eta \\ &-\mu_t\left[\frac{d}{dt}\left[H(\mathbf{x}_{a,t}) - H^*\right] + \partial^\top H(\mathbf{x}_{a,t}) w_t\right]. \end{aligned}$$

By integrating both sides of the inequality on interval $[t_0, t]$, the following expression is obtained

$$\int_{\tau=t_0}^{t} [H(\mathbf{x}_{a,\tau}) - H^*]\, d\tau \leq \frac{1}{2}\left(\|\zeta_{t_0}\|^2 - \|\zeta_t\|^2\right) -$$
$$\mu_t \left[H(\mathbf{x}_{a,t}) - H^*\right]_{t_0}^{t} + \int_{\tau=t_0}^{t} [H(\mathbf{x}_{a,\tau}) - H^*]\, \dot{\mu}_\tau d\tau$$
$$+\zeta_t^\top \eta - \int_{\tau=t_0}^{t} \mu_\tau \|\partial H(\mathbf{x}_{a,\tau})\| \, \|w_\tau\| \, d\tau.$$

Considering that $\dot{\mu}_\tau = 1$ and $\|\partial H(\mathbf{x}_{a,\tau})\| \leq h_g$ and $\|w_t\| \leq \varepsilon_t$ by the last expression, the following relation holds

$$\mu_t \left[H(\mathbf{x}_{a,t}) - H^*\right] \leq \mu_{t_0} \left[H(\mathbf{x}_{a,t_0}) - H^*\right] + \zeta_t^\top \eta +$$
$$\frac{1}{2}\left(\|\zeta_{t_0}\|^2 - \|\zeta_t\|^2\right) - \int_{\tau=t_0 \delta\tau}^{t} h_g \varepsilon_\tau d\tau$$
$$= \mu_{t_0} \left[H(\mathbf{x}_{a,t_0}) - H^*\right] + \frac{1}{2}\|\zeta_{t_0}\|^2 + \frac{1}{2}\|\eta\|^2 -$$
$$\frac{1}{2}\left[\|\zeta_t\|^2 + 2\zeta_t^\top \eta + \|\eta\|^2\right] + h_g \int_{\tau=t_0}^{t} \mu_\tau \varepsilon_\tau d\tau$$
$$= \mu_{t_0} \left[H(\mathbf{x}_{a,t_0}) - H^*\right] - \frac{1}{2}\|\zeta_t + \eta\|^2 + \frac{1}{2}\|\zeta_{t_0}\|^2 +$$
$$\frac{1}{2}\|\eta\|^2 + h_g \int_{\tau=t_0}^{t} \mu_\tau \varepsilon_\tau d\tau = \Omega_{t_0} + h_g \int_{\tau=t_0}^{t} \mu_\tau \varepsilon_\tau d\tau.$$

In consequence, the expression (4.18) is obtained. Then, Lemma is proven. □

10.2 A.Back stepping formulation-Intermediate stages

10.2.1 First order

I. Lyapunov function analysis for sliding variable with the pseudo controllers (1°and 2°stages)

For the general formulation of trajectory tracking error for the cases of position and speed, with the proposed controller in expression (5.11) and (5.25). Stability is analyzed by employing the Lyapunov candidate function

$$V_{\delta,i}(s_{i,t}) = \frac{1}{2}\left(\left[\sqrt{s_{i,t}^\top \mathbb{G}_i s_{i,t}} - \varepsilon_{i,t}\right]_+\right)^2 \tag{10.10}$$

, $\varepsilon_{i,t} > 0$ where the cutting function $[\cdot]_+$ satisfies

$$[z]_+ = \begin{cases} z & if \quad z \geq 0 \\ 0 & if \quad z < 0 \end{cases} \tag{10.11}$$

Notice that the function $\left([z]_+\right)^2$ is differentiable. Defining

$$\chi_{i,t} := \frac{\left[\sqrt{s_{i,t}^\top \mathbb{G}_i s_{i,t}} - \varepsilon_{i,t}\right]_+}{\sqrt{s_{i,t}^\top \mathbb{G}_i s_{i,t}}} \tag{10.12}$$

where $\mathbb{G}_i$ corresponds for the case i=1 to $\mathbb{G}_1 = g_1^{-1}$ and for the case $i = 2$ to $\mathbb{G}_2 = G_2^+$. In view of, the corresponding bounds for the tracking error dynamic, for $t \geq t_0$, and using the dynamic of $s_{i,t}$ given by

$$\dot{\mathbf{s}}_{i,t} = \dot{\delta_{i,t}} - \frac{\delta_{i,1} + \eta_i}{t + \mu_0} + \frac{\partial H(\delta_{i,t}) - \Psi_{i,t}}{t + \mu_0} \tag{10.13}$$

we have

$$\left.\begin{aligned} \dot{V}_{\delta,i,t}(s_{i,t}) &= \left[\sqrt{s_{i,t}^\top \mathbb{G}_i s_{i,t}} - \varepsilon_{i,t}\right]_+ \left(\frac{s_{i,t}^\top \mathbb{G}_i \dot{s}_{i,t}}{\sqrt{s_{i,t}^\top \mathbb{G}_i s_{i,t}}} - \dot{\varepsilon}_{i,t}\right) \\ &= \frac{\left[\sqrt{s_{i,t}^\top \mathbb{G}_i s_{i,t}} - \varepsilon_{i,t}\right]_+}{\sqrt{s_{i,t}^\top \mathbb{G}_i s_{i,t}}} \left(s_{i,t}^\top \mathbb{G}_i \dot{s}_{i,t} - \sqrt{s_{i,t}^\top \mathbb{G}_i s_{i,t}} \dot{\varepsilon}_{i,t}\right) \\ &= \chi_{i,t} s_{i,t}^\top \mathbb{G}_i \left[F_i + G_i u_i + \mathbf{z}_{i,t}^{(0)}\right] - \chi_{i,t} \dot{\varepsilon}_{i,t} \sqrt{s_{i,t}^\top \mathbb{G}_i s_{i,t}} \end{aligned}\right\} \tag{10.14}$$

where

$$\mathbf{z}_{i,t}^{(0)} := \dot{\delta}_{i,t} + \partial H_i(\delta_{i,t}) - \Psi_{i,t}. \tag{10.15}$$

Since the conditions of bounds for each case given in the expressions (5.7) and (5.21), the expression (10.14) becomes

$$\begin{aligned} \dot{V}_{\delta,i}(s_{i,t}) &\leq \chi_{i,t} s_{i,t}^\top u_i + g_i^- \chi_{i,t} \|s_{i,t}\| \left(F_{i,t}^+ + \left\|\mathbf{z}_{i,t}^{(0)}\right\| + |\dot{\varepsilon}_{i,t}|\right) \\ &\leq g_i^- \chi_{i,t} \|s_{i,t}\| \mathbf{z}_{i,t}^{(1)} + \chi_{i,t} s_{i,t}^\top u_i \end{aligned} \tag{10.16}$$

where $\mathbf{z}_{i,t}^{(1)} := F_{i,t}^+ + \left\|\mathbf{z}_{i,t}^{(0)}\right\| + |\dot{\varepsilon}_{i,t}|$. Taking u_i as in expression (5.11) and (5.25) for the corre-

sponding $i = 1, 2$, leads to

$$\begin{aligned} \dot{V}_{\delta,i}(s_{i,t}) &\leq g_i^- \chi_{i,t} \|s_{i,t}\| \mathbf{z}_{i,t}^{(1)} + \chi_{i,t} s_{i,t}^\top u_i \\ &\leq \chi_{i,t} g_i^- \|s_{i,t}\| \mathbf{z}_{i,t}^{(1)} - \chi_{i,t} s_{i,t}^\top \left(\beta_{i,t} \frac{s_{i,t}}{\|s_{i,t}\| + \varepsilon_{i,t}} \right) \\ &\leq \chi_{i,t} \|s_{i,t}\| \left(g_i^- \mathbf{z}_{i,t}^{(1)} - \beta_{i,t} \frac{\|s_{i,t}\|}{\|s_{i,t}\| + \varepsilon_{i,t}} \right). \end{aligned} \tag{10.17}$$

Since the inequality (10.17) is not trivial only when $\chi_{i,t} = 1$, or equivalently, when $\|s_{i,t}\| \geq \varepsilon_{i,t}$. This condition is fulfilled if $\|s_{i,t}\|$ satisfies $\|s_{i,t}\| > \varepsilon_{i,t}$. Therefore, within this region, we have

$$\frac{\|s_{i,t}\|}{\|s_{i,t}\| + \varepsilon} \geq \frac{\varepsilon_{i,t}}{\varepsilon_{i,t} + \varepsilon} = \frac{1}{2}$$

So, the inequality (10.17) becomes

$$\dot{V}_{\delta,i}(s_{i,t}) \leq \chi_{i,t} \|s_{i,t}\| \left(g_i^- \mathbf{z}_{i,t}^{(1)} - \frac{\beta_{i,t}}{2} \right) \tag{10.18}$$

Selecting $\beta_{i,t}$ in such a way that the following inequality is fulfilled

$$(1/2)\beta_{i,t} - g_i^- \mathbf{z}_{i,t}^{(1)} = \rho_i > 0 \tag{10.19}$$

we get that $\beta_{i,t} = 2\left(g_i^- \mathbf{z}_{i,t}^{(1)} + \rho_i \right)$ and then inequality (10.18) can be express as

$$\dot{V}_{\delta,i}(s_{i,t}) \leq -\rho_i \chi_{i,t} \|s_{i,t}\| \leq -\rho_i \chi_{i,t} \sqrt{2 V_{\delta,i}(s_{i,t})} \tag{10.20}$$

From expression (10.20), a finite time convergence of $V_{\delta,i}(s_{i,t})$ to the origin when $\chi_{i,t} = 1$. Indeed, for $\chi_{i,t} = 1$ we have

$$0 \leq \sqrt{V_{\delta,i}(s_{i,t})} \leq \sqrt{V_{\delta,i}(s_{i,0})} - \frac{\rho_i}{2\sqrt{2}} t \tag{10.21}$$

implying $V_{\delta,i}(s_{i,t}) = 0$ for any $t \geq t_{reach} = \dfrac{2\sqrt{2}}{\rho_i} \left\| s_{i,0} \right\| = 0$. But taking $s_{i,0} = 0$, one may get $t_{reach} = t_0 = 0$. In addition, notice that $\mathbf{s}_{i,t_0}$ satisfies

$$\mathbf{s}_{i,0} = \delta_{i,0} + \eta_i.$$

Defining the constant η_i as

$$\eta_i := \delta_{i,0} \tag{10.22}$$

II. Stability analysis of the sliding surface for the $s_{3,t}$ with real control

Proof. By proposing the following Lyapunov candidate function as

$$V_{\delta,3}(s_{3,t}) = \frac{1}{2} s_{3,t} G_3^{-1} s_{3,t} \tag{10.23}$$

Its full-time derivative (evaluated over the sliding surface $\mathbf{s}_{3,t}$) is

$$\dot{V}_{\delta,3}(s_{3,t}) = s_{3,t}^{\top} G_3^{-1} \dot{s}_{3,t} \tag{10.24}$$

Employing the dynamic of $\mathbf{s}_{3,t}$ given by

$$\dot{\mathbf{s}}_{3,t} = \dot{\delta}_{3,t} + \mu_t \left[+\partial H(\delta_{3,t}) - \delta_{3,t} - \eta_3 - \Psi_{3,t} \right] \tag{10.25}$$

Taking the variable μ_t as in the stability analysis for the sliding surface $s_{1,t}$ and $s_{2,t}$ with the virtual controls. Then the expression (10.24) can be presented as:

$$\dot{V}_{\delta,3}(s_{3,t}) = s_{3,t}^{\top} G_3^{-1} \left[\dot{\delta}_{3,t} + \mu_t \left[+\partial H(\delta_{3,t}) - \delta_{3,t} - \eta_3 - \Psi_{3,t} \right] \right] \tag{10.26}$$

Considering the expression for $F_{3,t}$ and G_3, the time variation $V_{\delta,3}(s_{3,t})$ given in equation (10.26) leads to

$$\dot{V}_{\delta,3}(s_{3,t}) = s_{3,t}^{\top} G_3^{-1} \left[F_{3,t} + G_3 u_{3,t} + \mathbf{z}_{3,t}^{(0)} \right] \tag{10.27}$$

where

$$\mathbf{z}_{3,t}^{(0)} := \mu_t \left[+\partial H(\delta_{3,t}) - \delta_{3,t} - \eta_3 - \Psi_{3,t} \right]. \tag{10.28}$$

The expression (10.27), by considering the bounds conditions given in expression (5.34), is reduced to

$$\dot{V}_{\delta,3}(s_{3,t}) \leq s_{3,t}^{\top} u_{3,t} + g_3^{-} \left\| s_{3,t} \right\| \left(F_{3,t}^{+} + \left\| \mathbf{z}_{3,t}^{(0)} \right\| \right) \tag{10.29}$$

where it was considered the (5.34) for $t \geq t_0$. Given (5.38) as the applied controller, the following differential equation can be estimated for the time derivative of the Lyapunov function $V_{\delta,3}$ as

$$\dot{V}_{\delta,3}(s_{3,t}) \leq \left\| s_{3,t} \right\| \left(g_3^{-} (F_{3,t}^{+} + \left\| \mathbf{z}_{3,t}^{(0)} \right\|) - \beta_{3,t} \right). \tag{10.30}$$

Selecting $\beta_{3,t} = g_3^{-1}(F_{3,t}^{+} + \left\| \mathbf{z}_{3,t}^{(0)} \right\|) + \rho_3$, the expression (10.30) results in

$$\dot{V}_{\delta,3}(s_{3,t}) \leq -\rho_3 \left\| s_{3,t} \right\| \leq -\rho_3 \sqrt{(2/g_3^{-}) V_3(s_{3,t})}. \tag{10.31}$$

From (10.31), the finite time convergence of $V_{\delta,3}(s_{3,t})$ can be obtained yielding

$$0 \leq \sqrt{V_{\delta,3}(s_{3,t})} \leq \sqrt{V_{\delta,3}(s_{3,0})} - \frac{\rho_3 g_3^-}{\sqrt{2}} t. \tag{10.32}$$

This result implies $V_{\delta,3}(s_{3,t}) = 0$ for any $t \geq t_0$. In addition, notice that $\mathbf{s}_{3,t_0}$ satisfies

$$\mathbf{s}_{3,0} = \delta_{3,t} + \eta_3.$$

Defining the constant η_3 as

$$\eta_3 := -(I_{t_0} - I_{t_0}^*) \tag{10.33}$$

for any $t_0 \geq 0$, we get $\mathbf{s}_{3,t_0} = 0$, and hence $t_0 = (\sqrt{2}\rho_3 g_3^-) \left\| \mathbf{s}_{3,t_0} \right\| = 0$, with $t_0 = 0$. In consequence, the desired regimen $\mathbf{s}_{3,0} = 0$ starts from the beginning of the control process. □

III. Desired trajectory-Proof of Lemma 2 and 3

Proof. Given that $s_{i,t}$ satisfies the condition of the inequality (5.14) and (5.28), for $i = 1,2$ corresponding to the position and velocity tracking problems, exist $\omega_{i,t}$ such that $s_{i,t} \leq \omega_{i,t}$ and $\| - \omega_{i,t} \| \leq \varepsilon_{i,t}$. Then defining $\mu_t := \dfrac{1}{t + \mu_0}$, $\dot{\zeta}_{i,t} = -\partial H(\delta_{i,t})$ and in view of the sliding variable defined in expression (5.10) and (5.24), we have

$$\omega_{i,t} = \delta_{i,t} + \eta_i - \mu_t \zeta_{i,t}, \tag{10.34}$$

in consequence, ζ is given by

$$\zeta_{i,t} = \mu_t^{-1} (\delta_{i,t} + \eta_i - \omega_{i,t}) \tag{10.35}$$

where $\zeta_{i,t_0} = 0$ by design of $\eta_{\delta,i}$, we have:

$$\begin{aligned} \frac{d}{dt}\left[\frac{1}{2}\|\zeta_{i,t}\|^2\right] &= \dot{\zeta}_{i,t}^\top \zeta_{i,t} \\ &= -\partial H(\delta_{i,t})^\top \left[\mu_t^{-1}(\delta_{i,t} + \eta_i - \omega_{i,t})\right] \\ &= -\mu_t^{-1}\partial H^\top(\delta_{i,t})\delta_{i,t} - \mu_t^{-1}\partial H^\top(\delta_{i,t})\eta_i - \mu_t^{-1}\partial H^\top(\delta_{i,t})\omega_{i,t} \end{aligned} \tag{10.36}$$

by the consideration of Jensen's inequality expressed in equation (3.21), the equality (10.36) satisfies

$$\frac{d}{dt}\left[\frac{1}{2}\|\zeta_{i,t}\|^2\right] \leq -\mu_t^{-1} H(\delta_{i,t}) - \mu_t^{-1}\partial H^\top(\delta_{i,t})\eta_i - \mu_t^{-1}\partial H^\top(\delta_{i,t})\omega_{i,t} \tag{10.37}$$

Taking the first term in the right side to the left side and the term of the left side to the right side in the inequality (10.37) gives

$$\begin{aligned}
\mu_t^{-1}H(\delta_{i,t}) &\leq \frac{d}{dt}\left[\frac{1}{2}\|\zeta_{i,t}\|^2\right] - \mu_t^{-1}\partial H^\top(\delta_{i,t})\eta_i - \mu_t^{-1}\partial H^\top(\delta_{i,t})\omega_{i,t} \\
H(\delta_{i,t}) &\leq \mu_t\left[\frac{d}{dt}\left[\frac{1}{2}\|\zeta_{i,t}\|^2\right] - \mu_t^{-1}\partial H^\top(\delta_{i,t})\eta_i - \mu_t^{-1}\partial H^\top(\delta_{i,t})\omega_{i,t}\right] \\
\|H(\delta_{i,t})\| &\leq \mu_t\|\left[\frac{d}{dt}\left[\frac{1}{2}\|\zeta_{i,t}\|^2\right] - \mu_t^{-1}\left(\partial H^\top(\delta_{i,t})\eta_i + \kappa_t\partial H^\top(\delta_{i,t})\omega_{i,t}\right)\right]\| \\
\|H(\delta_{i,t})\| &\leq \mu_t\left[\|\frac{d}{dt}\left[\frac{1}{2}\|\zeta_{i,t}\|^2\right]\| + \mu_t^{-1}\|\left(\partial H^\top(\delta_{i,t})\eta_i + \partial H^\top(\delta_{i,t})\omega_{i,t}\right)\|\right] \\
\|H(\delta_{i,t})\| &\leq \mu_t\|\frac{d}{dt}\left[\frac{1}{2}\|\zeta_{i,t}\|^2\right]\| + \|\partial H^\top(\delta_{i,t})\|\|\left(\eta_i + \omega_{i,t}\right)\|
\end{aligned} \tag{10.38}$$

Since $\|\partial H(\delta_{i,t})\| \leq d_i$

$$\begin{aligned}
\|H(\delta_{i,t})\| &\leq \mu_t\|\frac{d}{dt}\left[\frac{1}{2}\|\zeta_{i,t}\|^2\right]\| + d_i\|\left(\eta_i + \omega_{i,t}\right)\| \\
&\leq \mu_t\|\zeta_{i,t}^\top\dot{\zeta}_{i,t}\| + d_i\|\eta_i + \omega_{i,t}\| \\
&\leq \mu_t\|\partial H(\delta_{i,t})\|\|\left[\delta_{i,t} + \eta_i - \omega_{i,t}\right]\| + d_i\|\eta_i + \omega_{i,t}\| \\
&\leq \mu_t\|\partial H(\delta_{i,t})\|\left[\|\delta_{i,t}\| + \|\eta_i\| + \|\omega_{i,t}\|\right]\| + d_i\|\eta_i + \omega_{i,t}\| \\
&\leq \mu_t d_i\left[\|\delta_{i,t}\| + \|\eta_i\| + \|\omega_{i,t}\|\right]\| + d_i\|\eta_i + \omega_{i,t}\| \\
&\leq \mu_t\|\partial H(\delta_{i,t})\|\|\delta_{i,t}\| + \mu_t\|\eta_i\| + \mu_t\|\omega_{i,t}\|\| + d_i\|\eta_i + \omega_{i,t}\| \\
&\leq \mu_t d_i\|\delta_{i,t}\| + \mu_t d_i\|\eta_i\| + \mu_t d_i\|\omega_{i,t}\|\| + d_i\|\eta_i\| + d_i\|\omega_{i,t}\| \\
&\leq \mu_t d_i\|\delta_{i,t}\| + (\mu_t+1)d_i\|\eta_i\| + (\mu_t+1)d_i\|\omega_{i,t}\|
\end{aligned} \tag{10.39}$$

Given $(\mu_t + 1) = \dfrac{1+t+\mu}{t+\mu}$

$$\begin{aligned}
\|H(\delta_{i,t})\| &\leq \mu_t d_i\|\delta_{i,t}\| + \frac{1+t+\mu}{t+\mu}d_i\|\eta_i\| + \frac{1+t+\mu}{t+\mu}d_i\|\omega_{i,t}\| \\
&\leq \mu_t d_i\|\delta_{i,t}\| + \frac{1+t+\mu}{t+\mu}d_i\|\eta_i\| + \frac{1+t+\mu}{t+\mu}d_i\|\omega_{i,t}\| \\
&\leq \mu_t d_i\|\delta_{i,t}\| + \frac{1+t+\mu}{t+\mu}d_i\|\eta_i\| + \frac{1+t+\mu}{t+\mu}d_i\frac{\varepsilon_{i,0}}{(t+\mu)^\alpha} \\
&\leq \mu_t d_i\|\delta_{i,t}\| + \frac{1+t+\mu}{t+\mu}d_i\|\eta_i\| + \frac{(1+t+\mu)d_i\varepsilon_{i,0}}{(t+\mu)^{1+\alpha}}
\end{aligned} \tag{10.40}$$

□

10.3 Desired regimen variable on time for the output feedback solution

Using $\mu_t := \frac{1}{t+\mu}$, $\quad \dot{\varsigma}_t = -\partial H(\mathbf{x}_{a,t})$ with $\varsigma_{t_0} = 0$ and in view of (6.17), we have:

$$\begin{aligned} \varsigma_t &= \mu_t^{-1}\mathbf{x}_{b,t} + \mathbf{x}_{a,t} + \eta - \mu_t^{-1}\varepsilon_t, \\ 0 &= \mu_0\mathbf{x}_{b,t_0} + \mathbf{x}_{a,t_0} + \eta - \mu_t^{-1}\varepsilon_0 \end{aligned}$$

and in then

$$\begin{aligned} \frac{d}{dt}\left[\frac{1}{2}\|\varsigma_t\|^2\right] &= \varsigma_t^\top \frac{d}{dt}\varsigma_t \\ = -\partial H^\top(\mathbf{x}_{a,t})\left[\mu_t^{-1}\mathbf{x}_{b,t} + \mathbf{x}_{a,t} + \eta - \mu_t^{-1}\varepsilon_t\right]. \end{aligned} \tag{10.41}$$

The substitution of $\frac{d}{dt}\varsigma_t$ yields to the following equation

$$\frac{d}{dt}\left[\frac{1}{2}\|\varsigma_t\|^2\right] = -\partial H^\top(\mathbf{x}_{a,t})\mathbf{x}_{a,t} - \partial H^\top\left[\mathbf{x}_{a,t})(\mu_t^{-1}\mathbf{x}_{b,t} + \eta - \mu_t^{-1}\varepsilon_t\right] \tag{10.42}$$

Applying the inequality (6.19) to the first term on the right-hand side of (10.42) and using the identity

$$\partial^\top H(\mathbf{x}_{a,t})\mathbf{x}_{b,t} = \frac{d}{dt}\left[H(\mathbf{x}_{a,t}) - H^*\right] = \frac{d}{dt}H(\mathbf{x}_{a,t}),$$

we get

$$\frac{d}{dt}\left[\frac{1}{2}\|\varsigma_t\|^2\right] \leq -H(\mathbf{x}_{a,t}) - \mu_t^{-1}\frac{d}{dt}H(\mathbf{x}_{a,t}) - \partial H(\mathbf{x}_{a,t})^\top(\eta - \mu_t^{-1}\varepsilon_t).$$

Then, integrating both sides of this inequality on the interval $[t_0, t]$ and in view of the property $\varsigma_{t_0} = 0$, we get

$$\begin{aligned} \int_{\tau=t_0}^{t} H(\mathbf{x}_{a,\tau})d\tau &\leq -\frac{1}{2}\|\varsigma_t\|^2 - \mu_t^{-1}H(\mathbf{x}_{a,t})\,|_{t_0}^{t} \\ + \int_{\tau=t_0}^{t} H(\mathbf{x}_{a,\tau})\dot{\mu}_\tau^{-1}d\tau - \left[\int_{\tau=t_0}^{t}\partial^\top H(\mathbf{x}_{a,\tau})d\tau\right]^\top \eta - \\ \int_{\tau=t_0}^{t}\mu_\tau^{-1}\|\partial H(\mathbf{x}_{a,\tau})\|\|\varepsilon_\tau\|d\tau \end{aligned} \tag{10.43}$$

Since $\frac{d}{dt}\mu_t^{-1} = 1$, and $\|\partial H(\mathbf{x}_{a,t})\| \leq \rho$,the following relation can be obtained from the (10.43) yielding

$$\begin{gathered}\mu_t^{-1}H(\mathbf{x}_{a,t}) \leq \mu_{t_0}H(\mathbf{x}_{a,t_0}) - \frac{1}{2}\|\varsigma_t\|^2 + \varsigma_t^\top \eta \\ -\rho \int_{\tau=t_0}^{t} \mu_\tau \|\varepsilon_\tau\| d\tau = \\ \mu_{t_0}^{-1}H(\mathbf{x}_{a,t_0}) + \frac{1}{2}\|\eta\|^2 - \frac{1}{2}\left[\|\varsigma_t\|^2 - 2\varsigma_t^\top(\eta) + \|\eta\|^2\right] - \\ \rho \int_{\tau=t_0}^{t} \mu_\tau^{-1}\|\varepsilon_\tau\| d\tau\end{gathered}$$

Expanding the terms in the brackets, one has:

$$\begin{gathered}\mu_t^{-1}H(\mathbf{x}_{a,t}) \leq \mu_{t_0}H(\mathbf{x}_{a,t_0}) - \frac{1}{2}\|\varsigma_t - \eta\|^2 + \frac{1}{2}\|\eta\|^2 - \\ \rho \int_{\tau=t_0}^{t} \mu_\tau^{-1}\|\varepsilon_\tau\| d\tau \leq \\ \mu_{t_0}^{-1}H(\mathbf{x}_{a,t_0}) + \frac{1}{2}\|\eta\|^2 - \rho \int_{\tau=t_0}^{t} \mu_\tau^{-1}\|\varepsilon_\tau\| d\tau\end{gathered} \tag{10.44}$$

Taking ε_t as

$$\varepsilon_t = \frac{\varepsilon_0}{(t+\mu_0)^{1+\gamma}}, \quad \gamma, \varepsilon_0 > 0$$

the term last term in the expression (10.44) satisfies

$$\rho \int_{\tau=t_0}^{t} \mu_\tau^{-1}\|\varepsilon_\tau\| d\tau \leq \frac{\rho\varepsilon_0}{(1-\gamma)(t+\mu_0)^\gamma} \tag{10.45}$$

and in consequence, then the expression (10.44) can be expressed as

$$\mu_t^{-1}H(\mathbf{x}_{a,t}) \leq \mu_{t_0}^{-1}H(\mathbf{x}_{a,t_0}) + \frac{1}{2}\|\eta\|^2 - \frac{\rho\varepsilon_0}{(1-\gamma)(t+\mu_0)^\gamma} \tag{10.46}$$

The last inequality implies the result of Lemma 1.

In view of the three main theorems in chapter 6 following a similar structure and the tools needed for defining the main stability analysis are equivalent, this appendix presents a simplified form for developing all the proofs. Hence, the proofs are presented following a unified structure with the corresponding particularization for each surface.

Stability analysis of sliding surfaces $\mathbf{s}_{i,t}$ for $i = 1,2,3$. Given the dynamics structures described in the equations (7.1), (7.15) and (7.24), the proposed stability analysis in this section is applicable to demonstrate the stability of the sliding surfaces $\mathbf{s}_{i,t}$. Introducing a candidate of Lyapunov function as

$$V_{i,t}(\mathbf{s}_{i,t}) = \frac{1}{2}\left[\sqrt{\mathbf{s}_{i,t}^{\top} D_i \mathbf{s}_{i,t}} - \varepsilon_{i,t}\right]_+^2, \quad i = 1,2,3$$

where $D_1 = D_2 = I$, $D_3 = B^{-1}$, $\varepsilon_{i,t} > 0$, the function $[\cdot]_+$ satisfies $[\alpha]_+ = \begin{cases} \alpha & if \quad \alpha \geq 0 \\ 0 & if \quad \alpha < 0 \end{cases}$.
Notice that this definition implies that $\left([\alpha]_+\right)^2$ is differentiable. The full-time derivative of the Lyapunov function is given by

$$\dot{V}_{i,t}(\mathbf{s}_{i,t}) = \frac{\left[\sqrt{\mathbf{s}_{i,t}^{\top} D_i \mathbf{s}_{i,t}} - \varepsilon_{i,t}\right]_+}{\sqrt{\mathbf{s}_{i,t}^{\top} D_i \mathbf{s}_{i,t}}} \left(\mathbf{s}_{i,t}^{\top} D_i \dot{\mathbf{s}}_{i,t} - \sqrt{\mathbf{s}_{i,t}^{\top} D_i \mathbf{s}_{i,t}}\dot{\varepsilon}_{i,t}\right) \tag{10.47}$$

The time derivative of the proposed candidate Lyapunov function $V_{i,t}(\mathbf{s}_{i,t})$ is subjected to the dynamics of the sliding surfaces $\mathbf{s}_{i,t}$ given as

$$\dot{\mathbf{s}}_{i,t} = \dot{\Delta}_{2i-1,t} + \mu_t \left[+\partial H(\Delta_{2i,t}) - \Psi_{i,t}\right] - \mu_t^2 \left[\Delta_{2i,t} + \eta_i\right]. \tag{10.48}$$

Defining the auxiliary variable $\chi_{i,t} := \dfrac{\left[\sqrt{\mathbf{s}_{i,t}^{\top} D_i \mathbf{s}_{i,t}} - \varepsilon_{i,t}\right]_+}{\sqrt{\mathbf{s}_{i,t}^{\top} D_i \mathbf{s}_{i,t}}}$ the dynamic equation (10.47) can be expressed as

$$\dot{V}_{i,t}(\mathbf{s}_{i,t}) = \chi_{i,t} \mathbf{s}_{i,t}^{\top} D_i \left(M_{i,t} + \bar{\xi}_{i,t} - N_{i,t} + h_{0,i,t} - \frac{\mathbf{s}_{i,t}}{\|\mathbf{s}_{i,t}\|}\dot{\varepsilon}_{i,t}\right) \tag{10.49}$$

where the dynamics of Δ_{2i-1} given in (7.1), (7.15) and (7.25). In (10.49), the following definitions were used for each stage:

$$M_{1,t} = \Omega(\theta_t, \psi_t)\Gamma_t \qquad M_{2,t} = \begin{bmatrix} -\dfrac{d_{22} v_t}{m_{22}} \\ -\dfrac{d_{33} w_t}{m_{33}} \end{bmatrix} \qquad M_{3,t} = B^{-1}\mathbb{M}^{-1} f_{0,t} \tag{10.50}$$

$$N_{1,t} = H\left(\varsigma_t^*, t\right) \qquad N_{2,t} = \begin{bmatrix} \dot{v}_t^* \\ \dot{w}_t^* \end{bmatrix} - u_t M \begin{bmatrix} q_t \\ r_t \end{bmatrix} \qquad N_{3,t} = \mathring{k}_{3,t} + \mathring{k}_{3,0} \tag{10.51}$$

$$\bar{\xi}_{1,t} = \xi_{1,t} \qquad \bar{\xi}_{2,t} = \begin{bmatrix} \xi_{v,t} \\ \xi_{w,t} \end{bmatrix} \qquad \bar{\xi}_{3,t} = \beta^- \|\xi\| \tag{10.52}$$

The corresponding definitions for $h_{0,i,t}$ satisfy:

$$\begin{aligned} h_{0,1,t} &:= \mu_t \left[\Delta_{1,t} + \partial H(\Delta_{2,t}) - \Psi_{1,t}\right] - \mu_t^2 \left[\Delta_{2,t} + \eta_1\right] \\ h_{0,2,t} &:= \mu_t \left[\Delta_{3,t} + \partial H_2(\Delta_{4,t}) - \Psi_{2,t}\right] - \mu_t^2 \left[\Delta_{4,t} + \eta_2\right] \\ h_{0,3,t} &:= \beta^- \left[\mu_t \left[\Delta_{5,t} + \partial H(\Delta_{6,t}) - \Psi_{3,t}\right] - \mu_t^2 \left[\Delta_{6,t} + \eta_3\right]\right] \end{aligned} \tag{10.53}$$

Using the proposed control in equations (7.6), (7.17) and (7.26) for their corresponding $\mathbf{s}_{i,t}$, then the derivative of the Lyapunov function in (10.49) is defined by the following expression

$$\dot{V}_{i,t}(\mathbf{s}_{i,t}) = \varepsilon_{i,t} \mathbf{s}_{i,t}^\top D_i \left(-k_i \frac{\mathbf{s}_{i,t}}{\|\mathbf{s}_{i,t}\| + \varepsilon_{i,t}} + \xi_{i,t} - \frac{\mathbf{s}_{i,t}}{\|\mathbf{s}_{i,t}\| + \varepsilon_{i,t}} \frac{\varepsilon_{i,t}}{\|\mathbf{s}_{i,t}\|} \dot{\varepsilon}_{i,t} \right) \tag{10.54}$$

In view of the upper estimate presented in (2.10) yields and if $\varepsilon_{i,t}$ is monotonically non-increasing ($\dot{\varepsilon}_{i,t} \leq 0$), the expression (10.54) becomes

$$\dot{V}_{i,t}(\mathbf{s}_{i,t}) \leq -\chi_{i,t} \|\mathbf{s}_{i,t}\| \left(k_i \frac{\|\mathbf{s}_{i,t}\|}{\|\mathbf{s}_{i,t}\| + \varepsilon_{i,t}} - h_{i,1,t} \right) \tag{10.55}$$

where

$$h_{i,1,t} := \xi_i^+ + \frac{\varepsilon_{i,t=0}}{\varepsilon_{1,t=0} + \varepsilon_{i,t=0}} \left| \dot{\varepsilon}_{i,t=0} \right|$$

Since the inequality (10.55) is not trivial (only when $\chi_{i,t} = 1$) if $\|\mathbf{s}_{i,t}\| \geq \varepsilon_{i,t}$, which is a condition that is fulfilled if $\|\mathbf{s}_{i,t}\|$ satisfies $\|\mathbf{s}_{i,t}\| > \varepsilon_{i,t}$. Therefore, within the such region, one may get

$$\frac{\|\mathbf{s}_{i,t}\|}{\|\mathbf{s}_{i,t}\| + \varepsilon_t} \geq \frac{\varepsilon_{i,t}}{\varepsilon_{i,t} + \varepsilon_t} = \frac{1}{2} \tag{10.56}$$

The estimated lower bound in (10.56) justifies that the derivative of the suggested candidate Lyapunov function in (10.55) becomes

$$\dot{V}_{i,t}(\mathbf{s}_{i,t}) \leq -\|\mathbf{s}_{i,t}\| \left(\frac{1}{2} k_i - h_{i,1} \right). \tag{10.57}$$

The selection of k_i in (7.7) implies that the following inequality is valid then (10.57) becomes

$$\dot{V}_{i,t}(\mathbf{s}_{i,t}) \leq -\lambda_i \|\mathbf{s}_{i,t}\| \leq -\lambda_i \sqrt{2V_{i,t}(\mathbf{s}_{i,t})} \tag{10.58}$$

From (10.58), the finite time convergence of $V_{i,t}(\mathbf{s}_{i,t})$ to the origin when $\chi_{i,t} = 1$ follows. Indeed, for $\chi_{i,t} = 1$, it can be proven that

$$0 \leq \sqrt{V_{i,t}(\mathbf{s}_{i,t})} \leq \sqrt{V_{i,t}(\mathbf{s}_{i,0})} - \frac{\lambda_i}{\sqrt{2}} t \tag{10.59}$$

implying $V_{i,t}(\mathbf{s}_{i,t}) = 0$ for any $t \geq t_{reach,i} = \dfrac{i}{\lambda_i} \left\|\mathbf{s}_{i,0}\right\| = 0$. But taking $\mathbf{s}_{i,0} = 0$, one may get $t_{reach,i} = t_0 = 0$, which concludes the first part (Theorem 1) of the general proof of the main result attained in this study.

Following [41] and considering that the property (7.8) is satisfied, one has

$$\varsigma_{i,t} = \Delta_{2i-1,t} + \mu_t \left(\Delta_{2i,t} + \eta_i\right) + \Psi_{i,t} \tag{10.60}$$

Defining an auxiliary variable

$$\phi_{i,t} := \int_0^t -\partial H\left(\Delta_{2i,\tau}\right) d\tau \tag{10.61}$$

which is satisfying

$$\phi_{i,t} = \mu_t^{-1} \left[\Delta_{2i-1,t} - \varsigma_{i,t} + \mu_t \left(\Delta_{2i,t} + \eta_i\right)\right]. \tag{10.62}$$

Taking into consideration that

$$\frac{d}{dt}\left[\frac{1}{2}\left\|\phi_{i,t}\right\|^2 - \phi_{i,t}^\top \Delta_{2i}\right] = \phi_{i,t}^\top \dot{\phi}_{i,t} - \dot{\phi}_{i,t}^\top \Delta_{2i} \tag{10.63}$$

Using the expression for the derivative of $\phi_{i,t}$, the following equation is valid:

$$\begin{gathered}\frac{d}{dt}\left[\frac{1}{2}\left\|\phi_{i,t}\right\|^2 - \phi_{i,t}^\top \Delta_{2i}^*\right] = -\mu_t^{-1} \Delta_{i,t}^\top \partial H\left(\Delta_{2i,t}\right) - \\ \left[-\mu_t^{-1}\varsigma_{i,t} + \eta_i\right]^\top \partial H\left(\Delta_{2i,t}\right) - \partial H\left(\Delta_{2i,t}\right)^\top \left[\Delta_{2i,t} - \Delta_{2i}^*\right]\end{gathered} \tag{10.64}$$

Applying the Jensen's inequality to the term $\left(\Delta_{2i,t} - \Delta_{2i}^*\right)^\top \partial H\left(\Delta_{2i,t}\right)$ yields

$$\left(\Delta_{2i,t} - \Delta_{2i}^*\right)^\top \partial H\left(\Delta_{2i,t}\right) \geq H\left(\Delta_{2i,t}\right) - H\left(\Delta_{2i}^*\right) \tag{10.65}$$

Noticing that the term $\Delta_{i,t}^{\top}\partial H\left(\Delta_{2i,t}\right)$ admits the following equation

$$\Delta_{i,t}^{\top}\partial H\left(\Delta_{2i,t}\right)=\frac{d}{dt}H\left(\Delta_{2i,t}\right)=\frac{d}{dt}\left[H\left(\Delta_{2i,t}\right)-H\left(\Delta_{2i}^{*}\right)\right] \tag{10.66}$$

The substitution of (10.65) and (10.66) in (10.64) leads to:

$$\begin{gathered}\frac{d}{dt}\left[\frac{1}{2}\left\|\phi_{i,t}\right\|^{2}-\phi_{i,t}^{\top}\Delta_{2i}^{*}\right]\leq-\mu_{t}^{-1}\frac{d}{dt}\left[H\left(\Delta_{2i,t}\right)-H_{i}\left(\Delta_{2i}^{*}\right)\right]- \\ \left[-\mu_{t}^{-1}\varsigma_{i,t}+\eta_{i}\right]^{\top}\partial H\left(\Delta_{2i,t}\right)-\left[H\left(\Delta_{2i,t}\right)-H\left(\Delta_{2i}^{*}\right)\right]\end{gathered} \tag{10.67}$$

Taking the third term in the right of the inequality in (10.67) to the left side an integrating this inequality on the interval $[t_0,t]$ yields

$$\begin{gathered}\int_{\tau=t_0}^{t}\left[H\left(\Delta_{2i,\tau}\right)-H\left(\Delta_{2i}^{*}\right)\right]d\tau\leq \\ \left[\frac{1}{2}\left\|\phi_{i,\tau}\right\|^{2}-\phi_{i,\tau}^{\top}\Delta_{2i}^{*}\right]_{t_0}^{t}-\left(\mu_{\tau}^{-1}\left[H\left(\Delta_{2i,\tau}\right)-H\left(\Delta_{2i}^{*}\right)\right]\right)_{t_0}^{t}+ \\ \int_{\tau=t_0}^{t}\dot{\mu}_{\tau}^{-1}\left[H\left(\Delta_{2i,\tau}\right)-H\left(\Delta_{2i}^{*}\right)\right]d\tau-\left[\int_{\tau=t_0}^{t}\partial H\left(\Delta_{2i,\tau}\right)d\tau\right]\eta_{i}+ \\ \int_{\tau=t_0}^{t}\mu_{\tau}^{-1}\varsigma_{i,\tau}^{\top}\partial H\left(\Delta_{2i,\tau}\right)d\tau\end{gathered} \tag{10.68}$$

Given the following equation $\dot{\mu}_{\tau}^{-1}=1$, the following result can be obtained to get the uper bound for $\left(\mu_{t}^{-1}\left[H\left(\Delta_{2i,t}\right)-H\left(\Delta_{2i}^{*}\right)\right]\right)_{t_0}^{t}$:

$$\begin{gathered}\left(\mu_{t}^{-1}\left[H\left(\Delta_{2i,t}\right)-H\left(\Delta_{2i}^{*}\right)\right]\right)_{t_0}^{t}\leq\mu_{t_0}^{-1}\left[H\left(\Delta_{2i,t_0}\right)-H\left(\Delta_{2i}^{*}\right)\right]+ \\ \frac{1}{2}\left\|\phi_{i,t}-\left(\Delta_{2i}^{*}-\eta_{i}\right)\right\|^{2}-\frac{1}{2}\left\|\Delta_{2i}^{*}-\eta_{i}\right\|^{2}- \\ \frac{1}{2}\left\|\phi_{i,t_0}\right\|^{2}+\phi_{i,t_0}^{\top}\Delta_{2i}^{*}+\int_{\tau=t_0}^{t} \\ mu_{\tau}^{-1}\varepsilon_{i,\tau}\left\|\partial H\left(\Delta_{2i,\tau}\right)\right\|d\tau\end{gathered} \tag{10.69}$$

Taking into consideration the definition of $\Theta_{i,t}$, the inequality (10.69) admits the following upper bound:

$$\mu_{t}^{-1}\left[H\left(\Delta_{2i,t}\right)-H\left(\Delta_{2i}^{*}\right)\right]\leq\Theta_{i,t}+\int_{\tau=t_0}^{t}\mu_{\tau}^{-1}\varepsilon_{i,t}\left\|\partial H\left(\Delta_{2i,\tau}\right)\right\|d\tau \tag{10.70}$$

In view of the relationship for the gradient, $\left\|\partial H\left(\Delta_{2i,\tau}\right)\right\| \leq \sqrt{2}$, the inequality (10.70) satisfies

$$\mu_t\left[H\left(\Delta_{2i,t}\right) - H\left(\Delta_{2i}^*\right)\right] \leq \Theta_{i,t} + \sqrt{2}\int\limits_{\tau=t_0}^{t} \mu_\tau^{-1}\varepsilon_{i,\tau}d\tau \tag{10.71}$$

The lemma is proven.

Bibliography

[1] Juergen Ackermann and Vadim Utkin. Sliding mode control design based on ackermann's formula. *IEEE transactions on automatic control*, 43(2):234–237, 1998. 24

[2] Fadi Alyoussef and Ibrahim Kaya. A review on nonlinear control approaches: sliding mode control back-stepping control and feedback linearization control. In *International Engineering and Natural Sciences Conference (IENSC 2019)*, volume 2019, pages 608–619, 2019. 46, 48, 51

[3] Ahmad N Atassi and Hassan K Khalil. A separation principle for the stabilization of a class of nonlinear systems. *IEEE Transactions on Automatic Control*, 44(9):1672–1687, 1999. 74

[4] Mariana Felisa Ballesteros-Escamilla, David Cruz-Ortiz, Isaac Chairez, and Alberto Luviano-Juárez. Adaptive output control of a mobile manipulator hanging from a quadcopter unmanned vehicle. *ISA transactions*, 94:200–217, 2019. 15

[5] FJ Bejarano, L Fridman, and A Poznyak. Exact state estimation for linear systems with unknown inputs based on hierarchical super-twisting algorithm. *International Journal of Robust and Nonlinear Control: IFAC-Affiliated Journal*, 17(18):1734–1753, 2007. 24

[6] D Richard Blidberg. The development of autonomous underwater vehicles (auv); a brief summary. In *Ieee Icra*, volume 4, page 1. Citeseer, 2001. 75

[7] Luca Caracciolo, Alessandro De Luca, and Stefano Iannitti. Trajectory tracking control of a four-wheel differentially driven mobile robot. In *Proceedings 1999 IEEE international*

conference on robotics and automation (Cat. No. 99CH36288C), volume 4, pages 2632–2638. IEEE, 1999. 17

[8] Zhenzhong Chu and Daqi Zhu. Adaptive sliding mode heading control for autonomous underwater vehicle including actuator dynamics. In *OCEANS 2016-Shanghai*, pages 1–5. IEEE, 2016. 9

[9] Tayfun Cimen and Stephen P Banks. Nonlinear optimal tracking control with application to super-tankers for autopilot design. *Automatica*, 40(11):1845–1863, 2004. 2

[10] Jorge Estrela da Silva, Bruno Terra, Ricardo Martins, and Joao Borges de Sousa. Modeling and simulation of the lauv autonomous underwater vehicle. In *13th IEEE IFAC International Conference on Methods and Models in Automation and Robotics*, volume 1. Szczecin, Poland Szczecin, Poland, 2007. 76

[11] Jorge Davila, Leonid Fridman, and Arie Levant. Second-order sliding-mode observer for mechanical systems. *IEEE transactions on automatic control*, 50(11):1785–1789, 2005. 24

[12] John Joachim d'Azzo and Constantine Dino Houpis. *Linear control system analysis and design: conventional and modern*. McGraw-Hill Higher Education, 1995. 28

[13] Rui L Pedroso de Lima, Floris C Boogaard, and Rutger E de Graaf-van Dinther. Innovative water quality and ecology monitoring using underwater unmanned vehicles: field applications, challenges and feedback from water managers. *Water*, 12(4):1196, 2020. 1

[14] Sergey V Drakunov and Vadim I Utkin. Sliding mode control in dynamic systems. *International Journal of Control*, 55(4):1029–1037, 1992. 21, 22

[15] Kenan Ezal, Zigang Pan, and Petar V Kokotovic. Locally optimal and robust backstepping design. *IEEE transactions on automatic control*, 45(2):260–271, 2000. 85

[16] Thierry Floquet and Jean-Pierre Barbot. Super twisting algorithm-based step-by-step sliding mode observers for nonlinear systems with unknown inputs. *International journal of systems science*, 38(10):803–815, 2007. 24, 25

[17] Thor I Fossen et al. Guidance and control of ocean vehicles. *University of Trondheim, Norway, Printed by John Wiley & Sons, Chichester, England, ISBN: 0 471 94113 1, Doctors Thesis*, 1994. 8, 73

[18] Thor I Fossen and Tor A Johansen. A survey of control allocation methods for ships and underwater vehicles. In *2006 14th Mediterranean Conference on Control and Automation*, pages 1–6. IEEE, 2006. 12

[19] Rubén Alejandro Garrido Moctezua. *Drones: Modelado y control de cuadrotores*. Alfaomega Grupo Editor S.A. de C.V., first edition edition, October 2018. 8

[20] Shweta Gupte, Paul Infant Teenu Mohandas, and James M Conrad. A survey of quadrotor unmanned aerial vehicles. In *2012 Proceedings of IEEE Southeastcon*, pages 1–6. IEEE, 2012. 1

[21] Afiqah Ismail, A Rashid Ahmad Safuan, Radzuan Sa'ari, Mushairry Mustaffar, Rini Asnida Abdullah, Azman Kassim, Norbazlan Mohd Yusof, Norisam Abd Rahaman, Roohollah Kalatehjari, et al. Application of combined terrestrial laser scanning and unmanned aerial vehicle digital photogrammetry method in high rock slope stability analysis: A case study. *Measurement*, 195:111161, 2022. 1

[22] Hojjat A Izadi, Youmin Zhang, and Brandon W Gordon. Fault tolerant model predictive control of quad-rotor helicopters with actuator fault estimation. In *Proceedings of the 18th IFAC World Congress*, pages 6343–6348, 2011. 9

[23] Sarangapani Jagannathan and Pingan He. Neural-network-based state feedback control of a nonlinear discrete-time system in nonstrict feedback form. *IEEE Transactions on Neural Networks*, 19(12):2073–2087, 2008. 28

[24] Arash Kalantari and Matthew Spenko. Modeling and performance assessment of the hytaq, a hybrid terrestrial/aerial quadrotor. *IEEE Transactions on Robotics*, 30(5):1278–1285, 2014. 9

[25] Hassan K Khalil and Jessy W Grizzle. *Nonlinear systems*, volume 3. Prentice hall Upper Saddle River, NJ, 2002. 28

[26] Jinhyun Kim, Min-Sung Kang, and Sangdeok Park. Accurate modeling and robust hovering control for a quad-rotor vtol aircraft. In *Selected papers from the 2nd International Symposium on UAVs, Reno, Nevada, USA June 8–10, 2009*, pages 9–26. Springer, 2009. 8

[27] Minsung Kim, Hangil Joe, Jinwhan Kim, and Son-cheol Yu. Integral sliding mode controller for precise manoeuvring of autonomous underwater vehicle in the presence of unknown environmental disturbances. *International Journal of Control*, 88(10):2055–2065, 2015. 24

[28] Svetlana Anatol'evna Krasnova, Victor Anatol'evich Utkin, and Yu V Mikheev. Cascade design of state observers. *Automation and Remote Control*, 62(2):207–226, 2001. 85

[29] Burak Kürkçü, Coşku Kasnakoğlu, and Mehmet Önder Efe. Disturbance/uncertainty estimator based integral sliding-mode control. *IEEE Transactions on Automatic Control*, 63(11):3940–3947, 2018. 75

[30] Arie Levant. Sliding order and sliding accuracy in sliding mode control. *International journal of control*, 58(6):1247–1263, 1993. 24

[31] Arie Levant. Robust exact differentiation via sliding mode technique. *automatica*, 34(3):379–384, 1998. 24

[32] Arie Levant. Higher-order sliding modes, differentiation and output-feedback control. *International journal of Control*, 76(9-10):924–941, 2003. 70, 73

[33] Ruixia Liu, Ming Liu, and Yuan Liu. Nonlinear optimal tracking control of spacecraft formation flying with collision avoidance. *Transactions of the Institute of Measurement and Control*, 41(4):889–899, 2019. 2

[34] Ningsu Luo and M_ de la Sen. State feedback sliding mode control of a class of uncertain time delay systems. In *IEE Proceedings D (Control Theory and Applications)*, pages 261–274. IET, 1993. 28

[35] N Martínez-Fonseca, I Chairez, and A Poznyak. Uniform step-by-step observer for aerobic bioreactor based on super-twisting algorithm. *Bioprocess and biosystems engineering*, 37(12):2493–2503, 2014. 25

[36] Jaime A Moreno and Marisol Osorio. Strict lyapunov functions for the super-twisting algorithm. *IEEE transactions on automatic control*, 57(4):1035–1040, 2012. 70

[37] Kenichiro Nonaka and Hirokazu Sugizaki. Integral sliding mode altitude control for a small model helicopter with ground effect compensation. In *Proceedings of the 2011 american control conference*, pages 202–207. IEEE, 2011. 24

[38] Benjamas Panomrattanarug, Kohji Higuchi, and Félix Mora-Camino. Attitude control of a quadrotor aircraft using lqr state feedback controller with full order state observer. In *The SICE Annual Conference 2013*, pages 2041–2046. IEEE, 2013. 29

[39] Marco Piras, Glenda Taddia, Maria Gabriella Forno, Marco Gattiglio, Irene Aicardi, Paolo Dabove, S Lo Russo, and Alberto Lingua. Detailed geological mapping in mountain areas using an unmanned aerial vehicle: application to the rodoretto valley, nw italian alps. *Geomatics, Natural Hazards and Risk*, 8(1):137–149, 2017. 1

[40] Alessandro Pisano and Elio Usai. Sliding mode control: A survey with applications in math. *Mathematics and Computers in Simulation*, 81(5):954–979, 2011. 21, 22

[41] A. Poznyak, A. Nazin, and H. Alazki. Integral sliding mode convex optimization in uncertain lagrangian systems driven by pmdc motors: averaged subgradient approach. *IEEE Transactions on Automatic Control*, 66(9):4267–4273, 2021. 46, 49, 51, 86, 91, 149

[42] Geoff N Roberts and Robert Sutton. *Advances in unmanned marine vehicles*, volume 69. Iet, 2006. 1

[43] Shubhobrata Rudra, Ranjit Kumar Barai, and Madhubanti Maitra. *Block Backstepping Design of Nonlinear State Feedback Control Law for Underactuated Mechanical Systems*. Springer, 2017. 28

[44] Iván Salgado, Isaac Chairez, Bijnan Bandyopadhyay, Leonid Fridman, and Oscar Camacho. Discrete-time non-linear state observer based on a super twisting-like algorithm. *IET Control Theory & Applications*, 8(10):803–812, 2014. 25

[45] Angela P Schoellig, Fabian L Mueller, and Raffaello D'andrea. Optimization-based iterative learning for precise quadrocopter trajectory tracking. *Autonomous Robots*, 33(1):103–127, 2012. 2

[46] Ghazanfar Shahgholian and Pegah Shafaghi. State space modeling and eigenvalue analysis of the permanent magnet dc motor drive system. In *2010 2nd International Conference on Electronic Computer Technology*, pages 63–67. IEEE, 2010. 9

[47] Roland Siegwart, Illah Reza Nourbakhsh, and Davide Scaramuzza. *Introduction to autonomous mobile robots*. MIT press, 2011. 1

[48] Mark W Spong, Seth Hutchinson, and Mathukumalli Vidyasagar. *Robot modeling and control*. John Wiley & Sons, 2020. 8

[49] Guanghui Sun and Zhiqiang Ma. Practical tracking control of linear motor with adaptive fractional order terminal sliding mode control. *IEEE/ASME Transactions on Mechatronics*, 22(6):2643–2653, 2017. 75

[50] Jian Sun and GP Liu. State feedback and output feedback control of a class of nonlinear systems with delayed measurements. *Nonlinear Analysis: Theory, Methods & Applications*, 67(5):1623–1636, 2007. 28

[51] Zhijian Sun, Guoqing Zhang, Bowen Yi, and Weidong Zhang. Practical proportional integral sliding mode control for underactuated surface ships in the fields of marine practice. *Ocean Engineering*, 142:217–223, 2017. 75

[52] Siew-Chong Tan, YM Lai, and K Tse Chi. Indirect sliding mode control of power converters via double integral sliding surface. *IEEE Transactions on Power Electronics*, 23(2):600–611, 2008. 24

[53] Sylvain Thorel and Brigitte D'Andrea-Novel. Hybrid terrestrial and aerial quadrotor control. *IFAC Proceedings Volumes*, 47(3):9834–9839, 2014. 29

[54] Vadim Utkin, Jürgen Guldner, and Ma Shijun. *Sliding mode control in electro-mechanical systems*, volume 34. CRC press, 1999. 21, 22, 23, 24, 34, 46, 49, 51, 71, 86, 93

[55] Vadim Utkin and Jingxin Shi. Integral sliding mode in systems operating under uncertainty conditions. In *Proceedings of 35th IEEE conference on decision and control*, volume 4, pages 4591–4596. IEEE, 1996. 24

[56] Vadim I Utkin and Alex S Poznyak. Adaptive sliding mode control with application to super-twist algorithm: Equivalent control method. *Automatica*, 49(1):39–47, 2013. 24, 25

[57] Xinghuo Yu and Okyay Kaynak. Sliding-mode control with soft computing: A survey. *IEEE transactions on industrial electronics*, 56(9):3275–3285, 2009. 21

[58] Huan-Yin Zhou, Kai-Zhou Liu, and Xi-Sheng Feng. State feedback sliding mode control without chattering by constructing hurwitz matrix for auv movement. *International Journal of Automation and Computing*, 8(2):262–268, 2011. 28